EXPERIMENTAL AND NUMERICAL INVESTIGATION OF THE EVOLUTION OF PIPING AND RESULTING BREACH IN EARTH-FILL DAMS

A Thesis Submitted to
the Graduate School of Engineering and Sciences of
İzmir Institute of Technology
in Partial Fulfillment of the Requirements for Degree of

MASTER OF SCIENCE

In Civil Engineering

by
Emre DUMLU

December 2022
İZMİR

ACKNOWLEDGEMENTS

To begin with, I would like to thank The Scientific and Technological Research Council of Turkey (TUBITAK) for their financial support in the scope of project 119M609, since this support allowed the realization of the elaborate experimental and numerical studies.

I owe my special thanks to my advisor Prof. Dr. Gökmen TAYFUR, who gave me a chance to build my career and supported me throughout my master's. This thesis wouldn't be completed without his kind, supportive, patient guidance without giving up on me and his teaching skills. I would also like to thank him for allowing me to meet Prof. Dr. Şükrü GÜNEY.

I would like to state that I am pleased to have had the opportunity to work with Prof. Dr. GÜNEY, the coordinator of the TÜBİTAK 119M609 project, from the beginning to the end, as he trusted me in every part of the project and allowed me to express my creativity. I appreciate for allowing me to represent our project at national and international conferences many times. I learned from him how to find solutions when faced with a problem. He was the one who brought my guidance and engineering knowledge to the next level throughout the project, not only completing works but also including the concept of time in these works and educating me on time management.

Another Professor that Prof. GÜNEY allowed us to meet throughout the project is Prof. Gürkan ÖZDEN. I am proud to know that I am the only hydraulics student he has studied. I learned to study rationally and calmly, and steadily from him. I would like to thank him very much for being able to receive geotechnical and numerical analysis support and, for sharing his experiences even during his busy times.

I would also like to thank Merve OKAN, who was involved in the project, for her help and for having a chance to present and discuss a different perspective.

Also, I would like to thank İsmail KESKİN, who is a technician at the laboratory of the Izmir University of Economics, for getting support from him in the construction of the dams and for helping us under all circumstances.

Also, I like to be grateful to the management and dedicated teams of the Izmir University of Economics for their support during the project.

I would also show all my special respect to Prof. Dr. Şebnem ELÇİ for her support during my master's degree. We worked together on many studies apart from this thesis. She gave me a different and comprehensive perspective, improved my practical work, and broadened my horizons.

I would also like to thank Bahadır ÖZTÜRK, whom I met in the last period of my master's degree and received his ideas, helps, and offering good friendship during my thesis writing process.

I show my gratitude to my family, that we are a team within a team, Cevriye DUMLU, Emin DUMLU, Ecenur KURT, and Gökhan KURT who gave me all their unconditional support, endless love, and motivation throughout my life. Glad you are my family.

ABSTRACT

EXPERIMENTAL AND NUMERICAL INVESTIGATION OF THE EVOLUTION OF PIPING AND RESULTING BREACH IN EARTH-FILL DAMS

Earth-fill dams have been constructed for decades by compacting natural soil materials near the dam site. Piping is of the most important causes of their failure.

In the scope of this thesis, 2 m in length homogenous earth-fill dams were constructed in a rectangular flume in the laboratory of the Izmir University of Economics. The experimental and numerical investigations on a breach by generating piping were realized with different weak zone scenarios. Three experiments were performed by placing a weak layer cross-section 5x5 cm^2 at the dam bottom center. One scenario was performed by locating a weak layer of 2x2 cm^2, 28 cm above the bottom.

Temporal breach areas and the breach-wetted areas are evaluated on scaled screenshots by using Gauss's area formulation. The Temporal breach discharges were calculated from the continuity equation.

Furthermore, finite element analyses on the breaching of homogenous earth-fill dams in different scenarios were performed by comparing the hydraulic gradient with the critical value. In addition to the bottom and middle scenarios, two upper scenarios were also modeled. The water depths were used for each scenario to represent the experimental conditions, and some approaches were made for the weak zones. To simulate the breach mechanism with different loops, a python algorithm was integrated with the Jupyter console. As a result of the simulations, it has been observed that the findings obtained by simulations were in accord with the experimental studies, and the dams were exposed to backward piping starting from downstream towards upstream.

ÖZET

TOPRAK DOLGU BARAJLARDA BORULANMA VE BORULANMA NEDENLİ GEDİK OLUŞUMUNUN DENEYSEL VE SAYISAL ARAŞTIRILMASI

Toprak dolgu barajlar, onlarca yıldır baraj sahasının yakınında doğal toprak malzemelerinin sıkıştırılmasıyla inşa edilmiştir. Borulama, baraj yıkılmalarının en önemli nedenlerinden biridir.

Bu tez kapsamında, İzmir Ekonomi Üniversitesi laboratuvarında dikdörtgen bir kanal içine 2 m uzunluğunda homojen toprak dolgu barajları inşa edilmiştir. Farklı zayıf bölge senaryoları ile borulama oluşturularak bir gediklenmenin deneysel ve sayısal incelemeleri gerçekleştirilmiştir. Baraj tabanı ve ortasında 5x5 cm^2 en kesitinde bir zayıf bölge yerleştirilerek üç deney, tabandan 28 cm yukarıya 2x2 cm^2'lik bir zayıf bir bölge yerleştirilerek bir deney gerçekleştirildi.

Zamansal gedik alanları ve gedik-ıslak alanları Gauss alan formulasyonu kullanılarak ölçekli ekran görüntüleri üzerinde değerlendirildi. Zamansal gedik debileri ise süreklilik denkleminden hesaplandı.

Deneysel çalışmalara ilaveten, hidrolik eğim ile kritik eğim karşılaştırılarak farklı senaryolarda homojen toprak dolgu barajlarda borulanma üzerine sonlu elemanlar analizleri yapılmıştır. Alt ve orta senaryolara ilaveten, iki adet üst senaryo da modellenmiştir. Deneysel koşulları gerçekleştirmek etmek için her senaryoda zamana bağlı su derinlikleri kullanılmış ve zayıf bölgeler için bazı yaklaşımlar yapılmıştır. Gedik mekanizmasını farklı döngülerle simüle etmek için Jupyter konsoluna bir python algoritması geliştirildi. Simülasyonlar sonucunda simülasyonlarla elde edilen bulguların deneysel çalışmalarla uyumlu olduğu ve barajların mansaptan başlayarak membaya doğru geriye doğru borulamaya maruz kaldığı görülmüştür.

TABLE OF CONTENTS

LIST OF FIGURES

Figure **Page**

Figure **Page**

Figure **Page**

Figure **Page**

Figure **Page**

Figure **Page**

Figure **Page**

LIST OF TABLES

Table **Page**

CHAPTER 1

INTRODUCTION

1.1. Background

Dams are hydraulic structures having a variety of beneficial purposes such as flood control, irrigation, water supply, hydroelectric energy production, and reservoir water management. An earth-fill dam is a type of artificial water barrier that can be homogeneous or non-homogeneous (with a clay core or impervious layer) and is made up of a compacted mixture of soil (sand, clay, and silt or rock). Earth-fill dams were used for years, and they continue to be used nowadays. Some advantages of earth-fill dams are as follows (Okan, 2022):

- They can be easily built using soil materials that are readily available nearby.
- Their design is relatively easy by allowing a range of materials to be employed in their construction.
- They are economical to construct with locally available soil materials.
- Their compaction styles are suitable to be improved by technological developments.
- The earth-fill dams are environmentally friendly dam types because of consisting of natural and organic soil materials.

Although earth-fill dams have some advantages, there are some disadvantages, as well:

- It is possible to occur miscalculations in the project or construction stages caused by human factors, machines, or due to environmental factors such.
- Before the construction stages, laboratory tests needed to be performed that means, compared to concrete gravity dams, it has additional labor costs.
- They may have unexpected behavior in the case of choosing improper soil material.

- After the construction, they need to be maintained, controlled, and observed since one of the most common problems is internal erosion caused by improper soil material or lack of maintenance.
- The seismic activities may result in liquefaction within the dam body, creating stability issues that could eventually lead to seepage and failure.

In the literature, there are many tragic examples. One of the most prominent is the Teton dam. Teton earth-fill dam was constructed on Teton river, Idaho with a geometry of 93 m in height, 940 m in length, and 520 m in bottom width. After the construction of the dam in November 1975, the reservoir started to be filled 30 cm per day. One month later, the filling process was increased up to 1.2 m per day, due to the groundwater flow being greater than expected (Perrow, 1984). When the reservoir was nearly full-on June 3 and 4, 1976, three minor leaks were seen on the dam's downstream side. A wet spot was observed at the downstream side of the dam on June 5, 1976. Then, the downstream soil material started to erode, while seepage discharges were measured at less than 1 m^3 per second. On the same day, the breach developed toward the upstream sides and a sudden failure occurred with an estimated discharge of about 57,000 m^3/s that resulted in the sediment being reached more than 10 km from the dam location (*No Finger in the Dike Could Have Stopped It!*, 2018). The failure resulted in up to $2 billion in losses (Reisner, 1993).

New Orleans levee failure (Sills et al., 2008), the Horse Creek Dam (Hinderlider, 1914), Davis Reservoir Dam (Justin, 1932), Lyman Dam (Babb, 1968), Baldwin Hills Dam (Sharma et al., 2013), Tunbridge Dam (Fisher et al., 2017) and Sparmos Dam (Tournier et al., 2019) are some known and documented dam failures.

Internal erosion is one of the major causes of dam failures and incidents, accounting for 28% of earthen embankment failures (Costa, 1985).

Foster et al. (2000a) concluded that homogenous earth-fill dams built before 1900 tend to fail roughly ten times higher than dams built after 1950.

According to Chen et al (2019), piping was the cause of more than 30% of dam failures that occurred between 1954 and 2018.

1.2. Problem Statement

As a result of being washed out of the soil by the effects of the groundwater, voids are created in the dam body (Van Beek et al., 2015). Backward erosion causes the soil particles to be transported out of the structure by forming a pipe or tunnel shape. Backward erosion piping might occur because of cracks, soil properties, environmental factors, and practical failures. Some studies show that initiation and progression may take several days or weeks.

The parameters that cause piping are not yet fully understood due to the behavior of the cohesive soil used in the dam body and many environmental factors. The investigations are limited because the development of the piping mechanism is difficult to visualize and its progress in the structure can not be accurately followed by experimental and numerical studies.

Although there have been few studies, piping is one of the major reasons that earthen dams fail. Since the initiation of piping cannot be parameterized individually, the most dominant and complex factors are geotechnical and hydraulic parameters, such as geometry and type of structure, erodibility of the soil, water level, compaction densities, reservoir volume, particle size distribution, sample aspect ratio, friction coefficients, hydraulic gradient, groundwater flow, permeability, void ratio, porosity, unit weights of soil, cohesion, internal friction, specific gravity, and others.

The dominant factors governing the mechanism of erosion are influenced by different geotechnical characteristics of the soil (Sharif, 2013). Cohesive soil mixtures used in dam bodies consist of fine or very fine materials such as sand or clay and silt, which play an important role in the behavior of piping and breach according to the compaction rate and water content. Therefore, it is important to fully understand the determination of geotechnical parameters to predict piping erosion mechanisms.

1.3. Research Objectives

Dam failures not only jeopardize public safety but also have the potential to cost the economy millions of dollars. Dam failures not only affect the dam site but also have

the potential to degrade several other facilities, including roads, bridges, and water systems.

The objective of this research is to conduct experiments at the Hydraulic Laboratory of Izmir University of Economics (IEU) by generating piping via weak layers at two different locations and dimensions of the homogenous earth-fill dams.

In addition, this research involves the realization of numerical analyses and the comparison of the numerical results with experimental findings. The numerical analyses were performed by using a commercial software, PLAXIS 3D by integrating a python algorithm with the Jupyter console. The so-integrated python algorithm searches for the hydraulic gradient within the dam body and compares it with the critical hydraulic gradient (threshold). Once the hydraulic gradient reached the threshold, the breached soil volumes were defined in that region by considering that the piping was initiated.

1.4. Dissertation Outline

In the scope of this thesis, The piping mechanism resulting in a breach in the homogenous earth-fill dams is investigated by creating a weak zone at different locations. This thesis is composed of 7 chapters in total.

In Chapter 1, the description of the earth-fill dams, their purposes, advantages, and shortcomings are discussed. The problem definition was stated by giving historical cases and statistical information about the dam failures due to piping.

The previous relevant studies are summarized in Chapter 2.

Chapter 3 contains the description of the experimental setup and the soil mechanics tests performed before the piping experiments.

The different scenarios are presented in Chapter 4, together with construction and experimental procedures.

Experimental findings are presented in Chapter 5.

Chapter 6 involves numerical investigations.

Conclusions and recommendations are given in Chapter 7.

CHAPTER 2

LITERATURE REVIEW

The literature reviews are composed of two sections. The first section focuses on experimental studies on piping and its mechanism while the second focuses on numerical studies on piping and breach mechanism initiation.

2.1. Experimental Studies

There has been a lot of research on dam failures, especially about overtopping. However, because it is very challenging the monitoring the erosion and carry out experiments, there have only been a few surveys on piping and breach mechanism: (Khilar et al. 1985; Ojha et al. 2003; Okeke et al. 2012; Richards and Reddy 2012; Sharif 2013; Borragan 2014; Elkholy et al. 2015; Sharif et al. 2015b; Zhenzhen 2015; Chen et al. 2019; Shin et al. 2019; Al-Janabi et al. 2020; Ke and Takahashi, 2022).

Khilar et al. (1985) created a capillary model of plugging as a result of their experimental observations to predict the piping in what conditions are likely to occur.

Ojha et al. (2003) developed an analytical model to estimate critical heads obtained from their laboratory test. They found that the length of the structure, soil types, and fluid properties affect the critical head.

Okeke et al. (2012) carried out twelve experiments on a homogenous dam by triggering the piping by using a horizontal pipe with different lengths and positions. They build a homogenous dam with a height ranging from 20 cm to 35 cm, a constant width of 45 cm, and various side slopes of 35º to 45º in a 5º degree slope rectangular flume with 2 m long, 0.45 m high, and 0.45 m wide. They observed four failure processes in their backward erosion piping experimental study, including forming a wet spot, continuation, progression, and breach. Once erosion reached the downstream face, wet spot formation was apparent to such an extent that pipe enlargement, progression, and breach occurred consequently. They assumed that the erosion started when the wet spot appeared at the

downstream face of the dam (Figure 2.1 (a)). It took an early decrease in the water level with the enlargement of the erosion due to piping (Figure 2.1 (b)). Water levels continue to decrease during piping progress in terms of downstream slope angle, reservoir, and dam volume (Figure 2.1 (c)). After the piping progression, the breach results in the collapse of the roof of the dam. Consequently, the presence of the removal soil did not allow enough water to flow through the dam, the water level increased (Figure 2.1 (d)) and the breach became its final form (Figure 2.1 (e)).

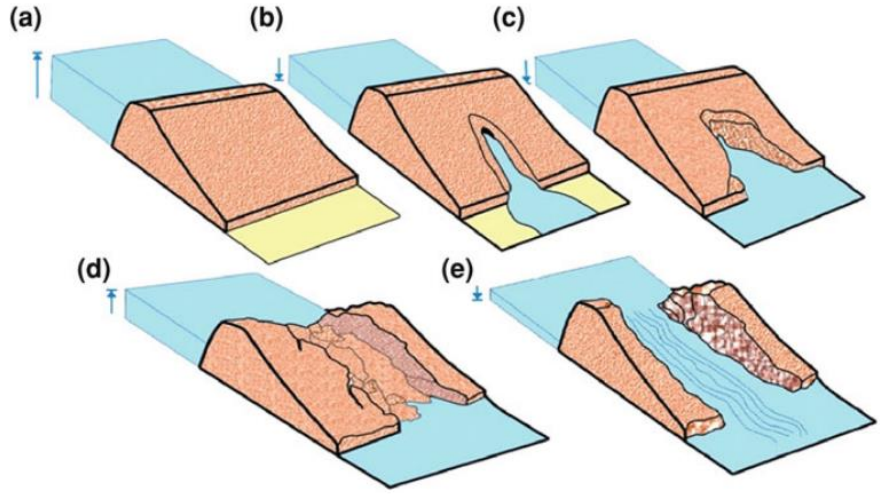

Figure 2.1. Piping failure processes resulted in a breach, a) initiation, b) continuation, c) progression, d) the collapsing of the dam roof, e) final breach formation (Okeke et al, 2012)

Richards and Reddy (2012) conducted experiments on field and laboratory mixed soils in a new true-triaxial test apparatus to observe the factors influencing piping initiation in non-cohesive and cohesive soils.

Sharif (2013) and Elkholy et al. (2015) used different compositions of mixture which consists of sand, silt, and clay with various rates of compaction by constructing a 15 cm high dam in a laboratory flume to investigate the erosion process.

Borragan (2014) studied the failure mechanisms of an embankment dam to validate the reliability of a risk analysis upon a dam breach.

In the research of Sharif et al. (2015b), the behavior of soil material changed during internal erosion, and they stated that the characteristics of soil have a significant impact on earth-fill dam failure, the proper compaction being the major component.

Zhenzhen (2015) defined backward erosion as the erosion induced by washing soil particles out and she defined erosion as the erosion caused by a concentrated leak where a pipe is formed due to a fracture, hollow, or void.

Chen et al. (2019) performed a sensitivity study on soil erodibility by different initial pipe positions. They found that soil erodibility can have an impact on breach evolution.

Shin et al. (2019) performed experiments by creating a weak zone in the middle of the earthen dam model to characterize temporal changes in sub-surfaces via a sandbox.

Al-Janabi et al. (2020) investigated seepage through a homogenous earth-fill dam with toe drains in different positions.

Ke and Takahashi (2022) performed a series of seepage tests on different soil compositions, densities, and hydraulic gradients by executing the cone penetration test. They found that the internal erosion affected the void ratio and the permeability resulting in a decrease in soil strength.

2.2. Theoretical and Numerical Studies

Different numerical methods such as finite element methods (FEM), discrete element methods (DEM), material point methods (MPM), finite difference methods (FDM), and computational fluid dynamics (CFD) are used to investigate the piping phenomenon:

Greco et al. (2008) simulated a 2D depth-averaged numerical model to investigate breach evolution in an earthen dam.

Lachouette et al. (2008) performed a numerical analysis to show that the particle concentration can be a significant factor at the beginning of the erosion process, resulting in the enlargement of the hole at the exit.

Gattinoni and Francani (2009) considered the phenomenon of backward piping evolution in the analysis of a slope, where for each simulation the corresponding hydraulic gradient in the nearby area was increased.

Kermani and Barani (2012) used a five-point approximation technique and compared it with the finite difference method.

Xu and Zhang (2013) used a physical-based numerical model for simulating piping in earth dams due to concentrated leak erosion.

Vandenboer et al. (2014) demonstrated and discussed a numerical methodology using the 3D finite element method for the groundwater flow that results in backward erosion piping.

Athani et al. (2015) used finite element analysis to investigate the seepage and stability with different withdrawal water level effects on the earth-fill dam to obtain the water head levels within the dam body.

Sazzad et al. (2015); Aslan and Temel (2022) used both analytical and numerical methods to analyze seepage discharge rates at different dam bodies.

Tao and Tao (2017) performed a numerical investigation to understand the factors of the piping resistance by using both coupled computational fluid dynamics (CFD) and the discrete element method (DEM). Additionally, they considered the equilibrium of a soil column at various soil properties such as hydraulic critical states, soil specific gravity, initial void ratio, particle size distribution, and friction coefficients, a concise model of piping resistance.

Zhong et al. (2018) performed a numerical simulation to improve the prediction of breach hydrograph and evaluate the breach morphology during the breaching

Chen et al. (2019) developed a numerical model by assuming the bottom, the top, and the channel of the pipe are an arch, rectangular, and a semicircle.

Saliba et al. (2019) performed finite element analysis to observe the piping path in steady conditions by using an iterative approach based on the simulated hydraulic gradient exceeding or reaching the threshold value

Al-Janabi et al. (2020) performed a series of finite element analyses with different types of toe drains to prevent seepage flow within both homogenous and clay-core earth-fill dams.

Al-Mansori et al. (2020) performed a seepage analysis to determine the quantity of seepage through the earth-fill dam by using the combination of the finite element method and artificial neural network.

Li et al. (2021) performed a combination of discrete element method (DEM) and computational fluid dynamics (CFD) analyses to investigate the longitudinal breach process of landslide dams.

Ghonim et al. (2022) performed computational fluid dynamics analyses (CFD) to investigate and compare the effects of initial artificial breach dimensions and locations on the peak outflow through the earth-fill dam.

Foster and Fell (1999) described how soil erosion might happen through an embankment, a foundation, or from an embankment to a foundation in earth structures, notably in earth dams and levees. He defined the processes as initiation, continuation, progression, and breach formation.

Bonelli (2013) described the four key mechanisms which initiate the backward erosion piping in earth-fill dams: concentrated leak erosion, backward erosion, contact erosion, and suffusion.

According to ICOLD (2017), suffusion can happen when seepage flow causes fine soil particle movements through the pores of coarse soil particles, whereas contact erosion happens when soil gradations come into contact and fine soils are washed away by the action of the water to the coarse particles.

Insufficient compaction of soil, different settings in the dam body, seismic hazards, and cracks caused by trees and animals also cause the piping (Hanson et al. 2010).

CHAPTER 3

SOIL MECHANICS TESTS AND EXPERIMENTAL SETUP

Before constructing the dam, soil mechanics tests were conducted. The ASTM requirements were followed during the realization of the soil mechanics tests. The required soil parameters were determined from specific weight tests, hydrometer analyses, wet sieve analyses, permeability tests, direct shear tests, consolidation tests as well as the standard proctor tests.

3.1. Soil Mechanics Tests

Mixture 1 consisted of 85 % (0-1 mm) sand-15 % clay while mixture 2 consisted of 85 % (0-0.4 mm) sand-15 % clay. Figure 3.1 shows distributions of grain sizes for two mixtures as determined by the wet sieve and hydrometer analyses.

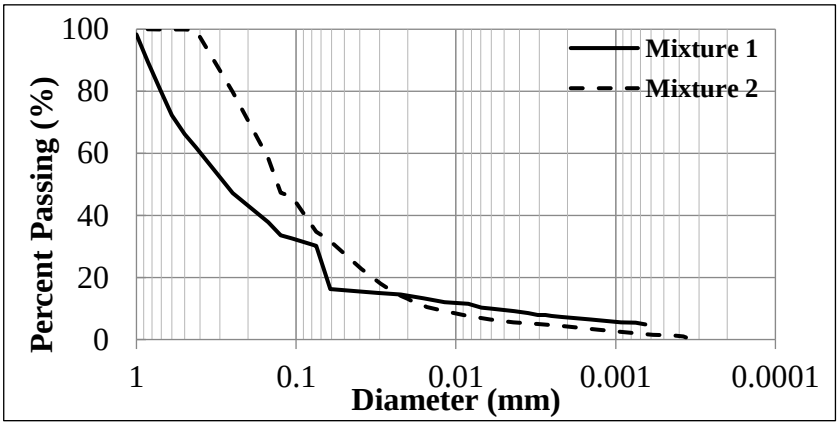

Figure 3.1. The distributions of grain size of the mixtures

From Figure 3.1, for mixture 1, D_{10}= 0.006 mm, D_{30}= 0.075 mm, D_{50}= 0.3 mm, and D_{60}= 0.4 mm. The coefficient of uniformity, C_u, and the coefficient of curvature, C_c, are found to be 66.7 and 2.34, respectively.

According to Figure 3.1, for mixture 2, D_{10}= 0.078 mm, D_{30}= 0.13 mm, D_{50}= 0.17 mm, and D_{60}= 0.21 mm. The coefficient of uniformity, C_u, and the coefficient of curvature, C_c, are found to be 2.69 and 1.03, respectively.

From Figure 3.1, for mixture 1, D_{10}= 0.006 mm, D_{30}= 0.075 mm, D_{50}= 0.3 mm, and D_{60}= 0.4 mm. The coefficient of uniformity, C_u, and the coefficient of curvature, C_c, are found to be 66.7 and 2.34, respectively.

According to Figure 3.1, for mixture 2, D_{10}= 0.078 mm, D_{30}= 0.13 mm, D_{50}= 0.17 mm, and D_{60}= 0.21 mm. The coefficient of uniformity, C_u, and the coefficient of curvature, C_c, are found to be 2.69 and 1.03, respectively.

The ASTM D854-14 test was applied to obtain the specific weights of the mixtures, as G_{s1}= 2.63 and G_{s2}= 2.67.

In order to facilitate the piping process, the standard proctor test (ASTM-698) was used, by reducing the applied energy by 50 % (13 blows instead of 25). The obtained curves mixture 1 and mixture 2 are given in Figure 3.2 and Figure 3.3, respectively.

From Figure 3.2, the maximum dry density was found to be 1.79 g/cm^3 at w_{opt}=12.5% for mixture 1.

From Figure 3.3, the maximum dry density was found to be 1.65 g/cm^3 at w_{opt}=15.4% for mixture 2.

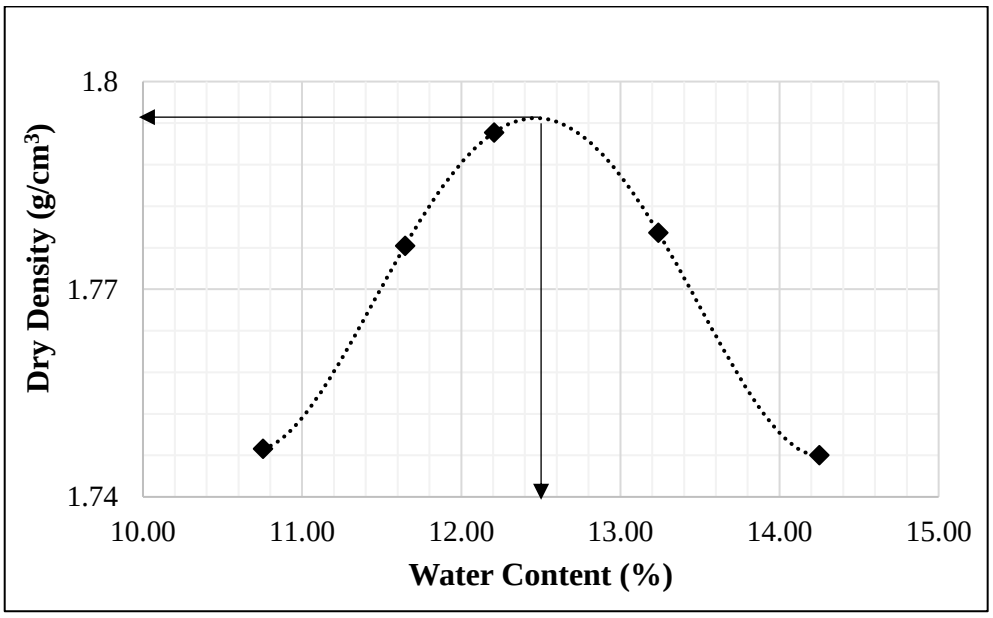

Figure 3.2. 13 blows proctor test curve for mixture 1

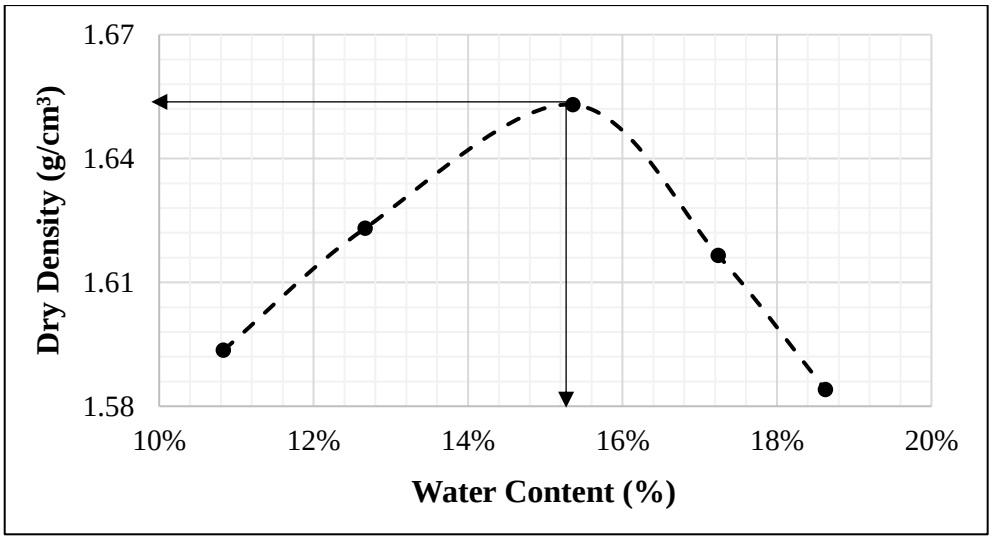

Figure 3.3. 13 blows proctor test curve for mixture 2

The permeability was obtained from the falling head permeability test. The soil parameters used in different experiments are given Table 3.1.

Table 3.1. The soil parameters used in different experiments

Experiment	Dry Density (ρ_{dry}) (g/cm^3)	Water Content w(%)	Bulk density $\rho_{bulk} = \rho_{dry} \cdot (1 + \frac{w}{100})$ (g/cm^3)	Void ratio $e = (\frac{Gs}{\rho_{dry}} - 1)$	Permeability (k) (m/s)
First and Second Experiments	1.79	12.5	2.0	0.47	$4.66 \cdot 10^{-7}$
Third Experiment	1.50	12.5	1.7	0.75	$6.24 \cdot 10^{-6}$
Fourth Experiment	1.79	12.5	2.0	0.49	$1.18 \cdot 10^{-6}$

Although the first two experiments were conducted by using mixture 1, the dam heights differed from each other.

The third experiment was conducted with lower density, while the fourth experiment was carried out by mixture 2.

The direct shear test was applied by satisfying the requirements of ASTM D3080, and the so obtained internal friction angle (φ^o) and cohesion (c') parameters for different conducted experiments are given in Table 3.2.

Table 3.2. Direct shear test results

Experiment	Internal Friction Angle (φ^o)	Cohesion (c') kN/m^2
First and Second Experiments	33.9	15.3
Third Experiment	28.4	12.8
Fourth Experiment	39.8	11.7

The consolidation test results by following ASTM D2435 standards are given in Table 3.3.

Table 3.3. Consolidation test results

Experiment	Eodemetric Modulus (Eoed) kN/m^2	Swelling Index (C_s)	Recompression Index (C_r)	Compression Index (C_c)
First and Second Experiments	35,700	0.01	0.01	0.1
Third Experiment	26,700	0.02	0.03	0.18
Fourth Experiment	13,800	0.02	0.02	0.13

3.2. Experimental Setup

Experiments were conducted in the rectangular flume 1 m wide and consisting of two channels. The dams are built in the upper channel, and the lower channel contains the required water pumped by means of a centrifugal pump.

The upper channel is 5.44 m long, and 0.81 m high. A double honeycomb and a mini tank were set to tranquil the water.

An electromagnetic sensor was placed to provide a constant water level. Tempered glass of 2 cm thickness was used on the side walls.

The sinking pool and water tank are divided with a 0.6 m high obstacle to avoid mixing the fresh water and collected sediment as much as possible.

The transmission line involves a pump, a check valve, a regulating valve, and a magnetic flowmeter. The experimental setup is given in Figure 3.4.

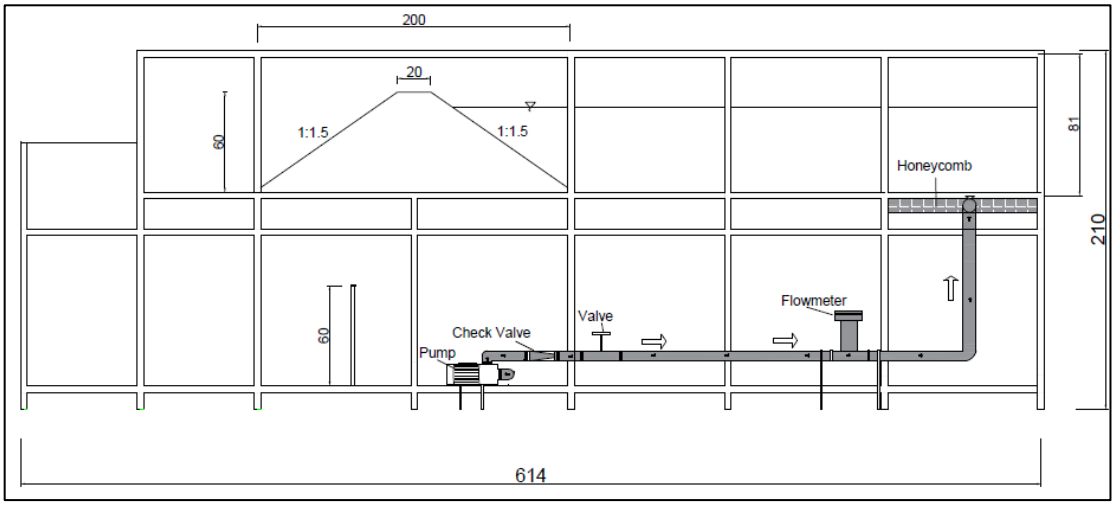

(a)

(b) (c)

Figure 3.4. The experimental setup (a) schematic longitudinal view (b) Upper channel (c) Transmission line

CHAPTER 4

EXPERIMENTAL PROCEDURE

4.1. Construction Procedure

Before preparing the dry mixture of the earth-fill dams, the soil mixture amounts for each 10 cm layer were determined for different bulk densities considering the dam heights.

The dry mixtures were mixed by using the concrete machine for 10 minutes to be sure the sand and clay particles are mixed uniformly (Figure 4.1 (a)). Then the dry mixture was poured into a wheelbarrow.

After adding 12.5 % water to the dry mixture, the wetted soil mixture was prepared by using shovels so that any dry part does not exist (Figure 4.1 (b)).

The dam body was constructed by layers of 10 cm. Since the compaction of the 10 cm layers may bring up homogeneity problems, each layer was built in four sub-layers of 2.5 cm thick.

After the construction of the first two sub-layers was completed, the 5x5 cm^2 area on the dam bottom center axis was dug up and the rock salt was poured to create the weak zone (Figure 4.1 (b) and Figure 4.2 (c)).

The surfaces of the compacted sub-layers were scraped by means of a brush (Figure 4.1 (e)).

The constructed third layer is given in Figure 4.1 (f). The construction of the fourth layer is given in Figure 4.1 (g). The pouring and grinding procedure at the fifth layer is given in Figure 4.1 (h). The compaction of the sixth layer is given in Figure 4.1 (i). The constructed dam body before trimming is given in Figure 4.1 (j).

The same construction procedures were followed for the middle-middle scenario. After the construction of the first three layers, a 2x2 cm^2 area was dug up along the dam center axis at 28 cm above the bottom. Then the area was filled with rock salt and the construction was continued. The final dams are 2 m in length, 1 m in width, and 0.6 m and 0.65 m in height, respectively.

(a)

(b)

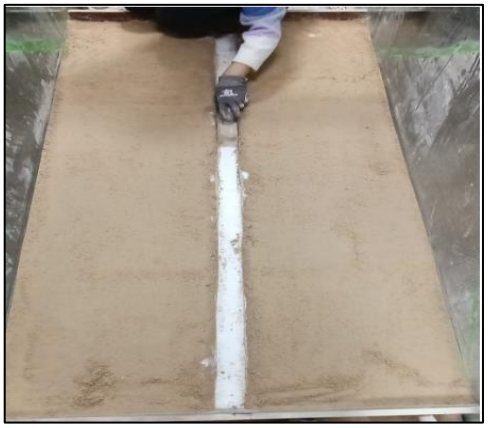

(c)

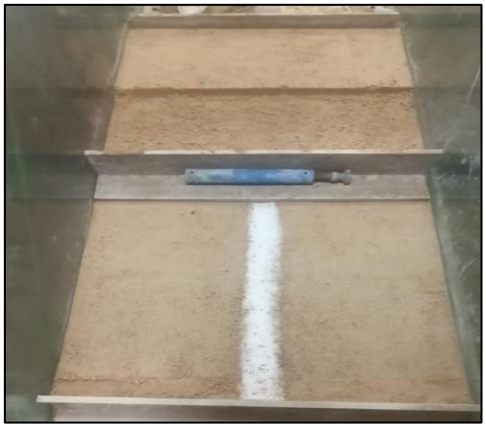

(d)

(e)

(f)

Figure 4.1. The construction process (a) dry mixing, (b) preparation of soil mixture, (c) creating the weak zone, (d) construction of the first 10 cm layer, (e) scraping the second layer, (f) the constructed third layer, (g) construction in the fourth layer, (h) pouring and grinding at the fifth layer, (i) compaction at the sixth layer, (j) before the trimming

(cont. on next page)

(g)

(h)

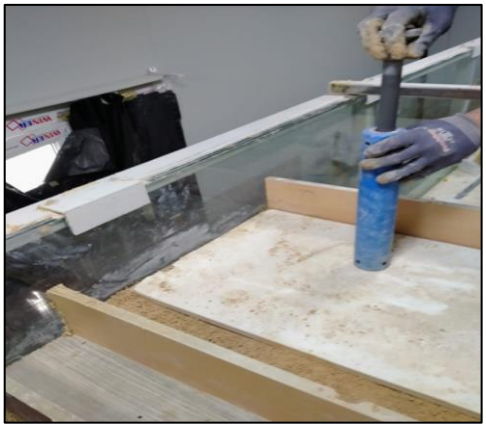

(i)

(j)

Figure 4.1. (cont.)

Green spray paint was used for both sides to prevent the reservoir from appearing turbidity.

While filling the reservoir, a trowel was placed at the exit of the weak zone, once the reservoir reached the desired level the trowel was withdrawn, and experiments started.

4.2. Evaluation of the Experiments

The experiments were conducted in the laboratory of Izmir University of Economics by using the soil mixture of 85% sand and 15% clay with different weak zone scenarios in the rectangular flume 81 cm high, 614 cm long, and 100 cm wide. The downstream and upstream slopes are the same at 1: vertical to 1.5: horizontal (Figure 3.4).

Six cameras placed at various locations monitored the progression of the breach.

An electromagnetic sensor was located in the channel to make start the pump when the initial water level decreases by 1.5 cm.

The temporal breach discharges, the time-dependent flow velocities, time-varied wetted areas, and temporal breach developments were calculated.

The temporal discharges through the breach were calculated by using the continuity equation which is given in Equation (4.1).

$$\Delta S=(Q_{pump}-Q_{breach})\cdot\Delta t \tag{4.1}$$

where Q_{pump} is the pump flow rate, Q_{breach} is the temporal breach discharges, ΔS is the storage in the channel during the time interval Δt.

The velocity V at the entrance and exit of the breach were approximately calculated by using Equation 4.2.

$$V=\frac{Q_{breach}}{A} \tag{4.2}$$

where *A* denotes the wetted area at the entrance or exit of the breach.

The experimental findings were recorded by means of high-resolution cameras. To obtain flatted recordings, the software Hitfilm Express v.2021.2 was used by selecting suitable preset options and rotation in the z-direction for each recording until the real boundaries fit the scale. Then, the flatted recording was used to obtain the changes in channel water level.

The Get-Data Graph Digitizer 2.26 software was used to evaluate the breach areas and wetted areas. The software can scale each recording by defining the dam boundaries at both the upstream and downstream sides.

Gauss's area Formulation was used to obtain the coordinates of the breach and its wetted areas.

The cartesian coordinates of all vertices are required to use the formula for cross multiplication (Figure 4.2).

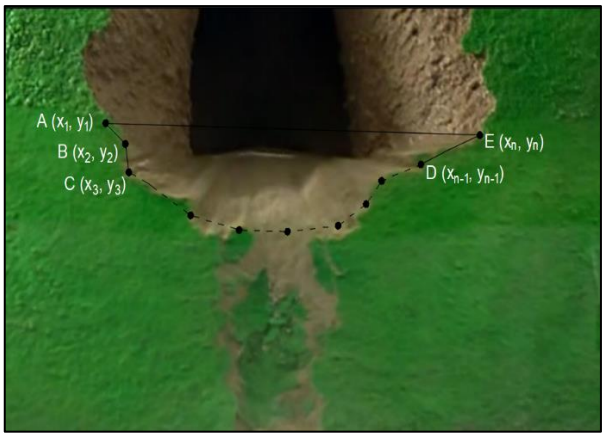

Figure 4.2. n-sided polygons on Get-data Graph Digitizer 2.26

Gauss's area formula also known as the Shoelace formula (Dahlke, 2017), calculates the area of a polygon whose vertices are specified by their cartesian coordinates. The formulation was described by Albrecht Ludwig Friedrich Meister in 1769 (Meister,1769) as follows:

The expressions of n-sided polygons area (x_1, y_1), (x_2, y_2), (x_3, y_3), …. (x_n, y_n) in Gauss's area formula is given in Equation 4.3.

$$Area = \frac{1}{2}|(x_1y_{2-}x_2y_{1+}\, x_2y_{3-}x_3y_{2+} \dots \dots . + x_ny_1 - x_1y_n)| \tag{4.3}$$

The formula can be written briefly,

$$Area = \frac{1}{2}\sum_{i=1}^{n} x_i\,(y_{i+1-}y_{i-1}) \tag{4.4}$$

or

$$Area = \frac{1}{2}\sum_{i=1}^{n} y_i\,(x_{i-1-}x_{i+1}) \tag{4.5}$$

where n is the number of the coordinates, x_i and y_i are abscissa and ordinate.

CHAPTER 5

EXPERIMENTAL FINDINGS

The experiments were performed with different high dams and various bulk densities. The details of different experiments are given in Table 5.1. All the weak zones consisted of rock salt.

Table 5.1. The details of different experiments

Experiment	Weak Zone Dimensions (cm^2)	Mixture Types	The bulk density (g/cm^3)	Dam Heights (cm)	Water Level (cm)	Input Discharge (m^3/h)
1	5x5	Mixture 1	2.0	60	55.5	9.0
2	5x5	Mixture 1	2.0	65	61	29.6
3	5x5	Mixture 1	1.7	65	61	6.2
4	2x2	Mixture 2	2.0	65	61	2.5

5.1. First Experiment

The final views of the constructed 60 cm high dam, the bulk density of 2 g/cm^3, and the weak zone of 5x5 cm^2 located at the bottom are given in Figure 5.1.

After the dam was constructed, the reservoir was filled with water via the pump until the electromagnetic sensor was activated at 55.5 cm.

Figures 5.2 shows the downstream temporal breach developments before the breach appeared at the upstream face (until the time t=192 hours).

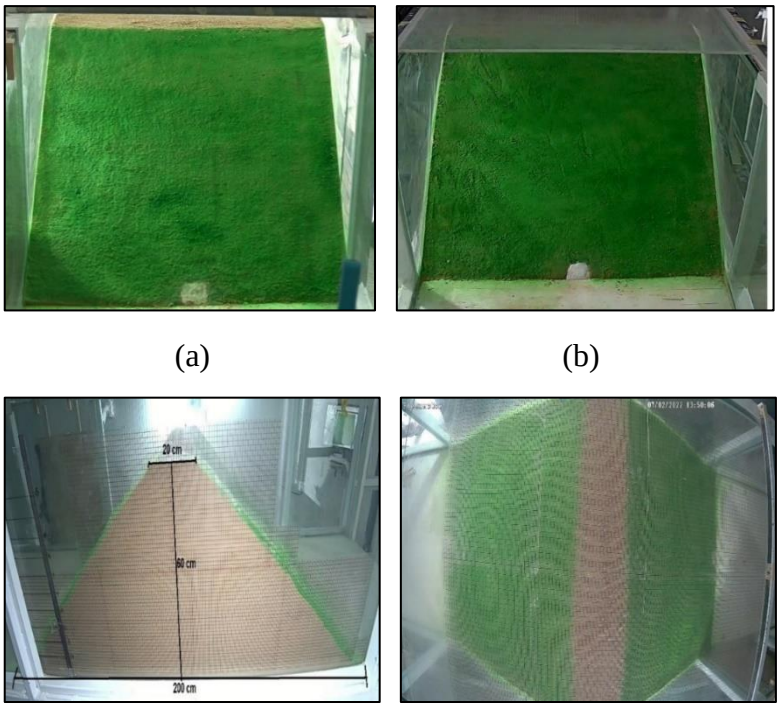

(a) (b)

(c) (d)

Figure 5.1. View of the dam from (a) upstream, (b) downstream, (c) side, (d) top

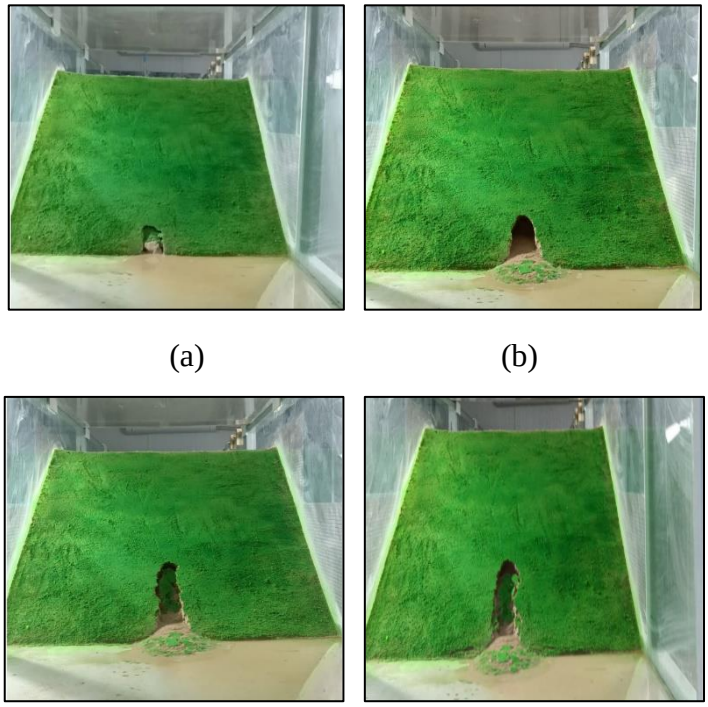

(a) (b)

(c) (d)

Figure 5.2. The downstream temporal breach developments a) t=0 h, b) t=24 h, c) t= 48 h, d) t= 192 h

With the removal of the eroded soil material from the dam boundary, the surface area of the breach did not change significantly, but it gained length backward.

When t=193 h, it was seen that the exit of the breach was filled again with the eroded soil material coming from inside (Figure 5.3 (a)). The length of the breach was measured at 26 cm.

When t=194 h, with the removal of the eroded soil material, it was observed that the surface area of the breach was not changed, and the length of the pipe was measured as 34 cm (Figure 5.3 (b)).

(a) (b)

Figure 5.3. Downstream breach surfaces at (a) t=193 h (b) t=194 h

When t=196 h, although there was not significant eroded soil material, the material coming from the breach was piled on top of each other (Figure 5.4).

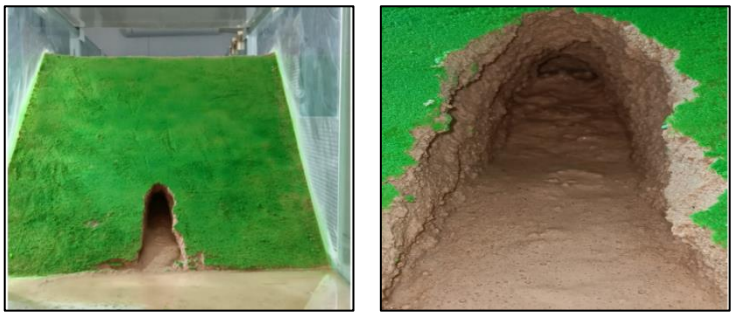

(a) (b)

Figure 5.4. Downstream breach surfaces at t=196 h (a) downstream view, (b) close-up view of the breach

A slight increase in the length of the breach was observed as shown in Figure 5.4 (a), while the change in the surface area was limited. The close-up view of the breach is given in Figure 5.4 (b). The length of the breach was measured as 39 cm.

When t =208 h, the eroded soil material accumulated in front of the dam continued to be removed without disturbing the breach. The breach length was measured by a laser meter, and it became 65 cm. The view of the breach at t=208 h is given in Figure 5.5.

(a) (b)

Figure 5.5. Downstream breach surfaces at t=208 h (a) downstream view, (b) close-up view of the breach

At t=216 h, not a significant change in the breach area was observed. The breach length was measured as 91 cm. Downstream views of the breach are given in Figure 5.6.

(a) (b) (c)

Figure 5.6. Downstream breach surfaces at t= 216 h (a) downstream view, (b) close-up view of the breach (c) eroded and transported soil materials due to the seepage

At t=230 h (12 minutes before the breach reached the upstream face), although there was not a significant difference in the breach surface area, the seepage discharge was measured as 6.3 cm^3/s. The length of the breach was measured as 119.9 cm.

12 minutes later, the breach reached the upstream side of the dam as shown in Figure 5.7.

The time-dependent discharge values corresponding to the interval at which the breach reached the upstream face are given in Figure 5.8.

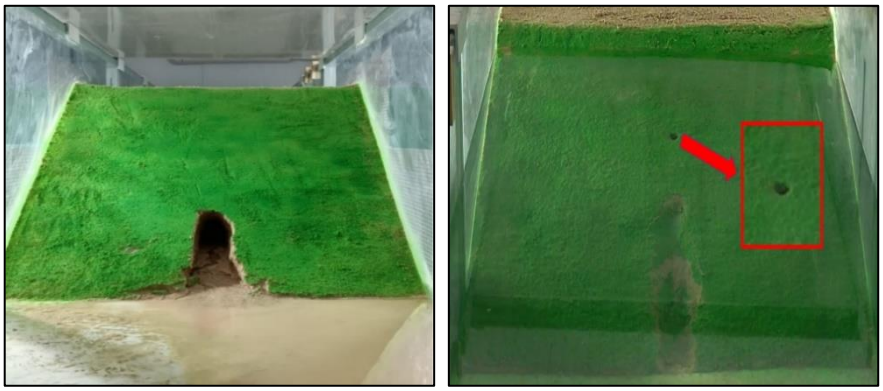

(a) (b)

Figure 5.7. The breach developments at t= 230 h (a) downstream, (b) upstream

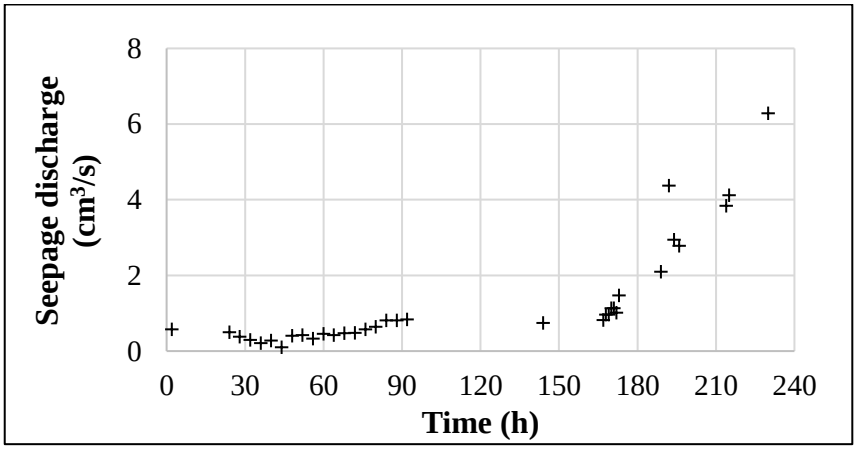

Figure 5.8. The seepage discharges before the breach did not reach the upstream face.

The breach views corresponding to different times are given from Figure 5.9 to Figure 5.11. The time t=0 represents when the breach appeared upstream.

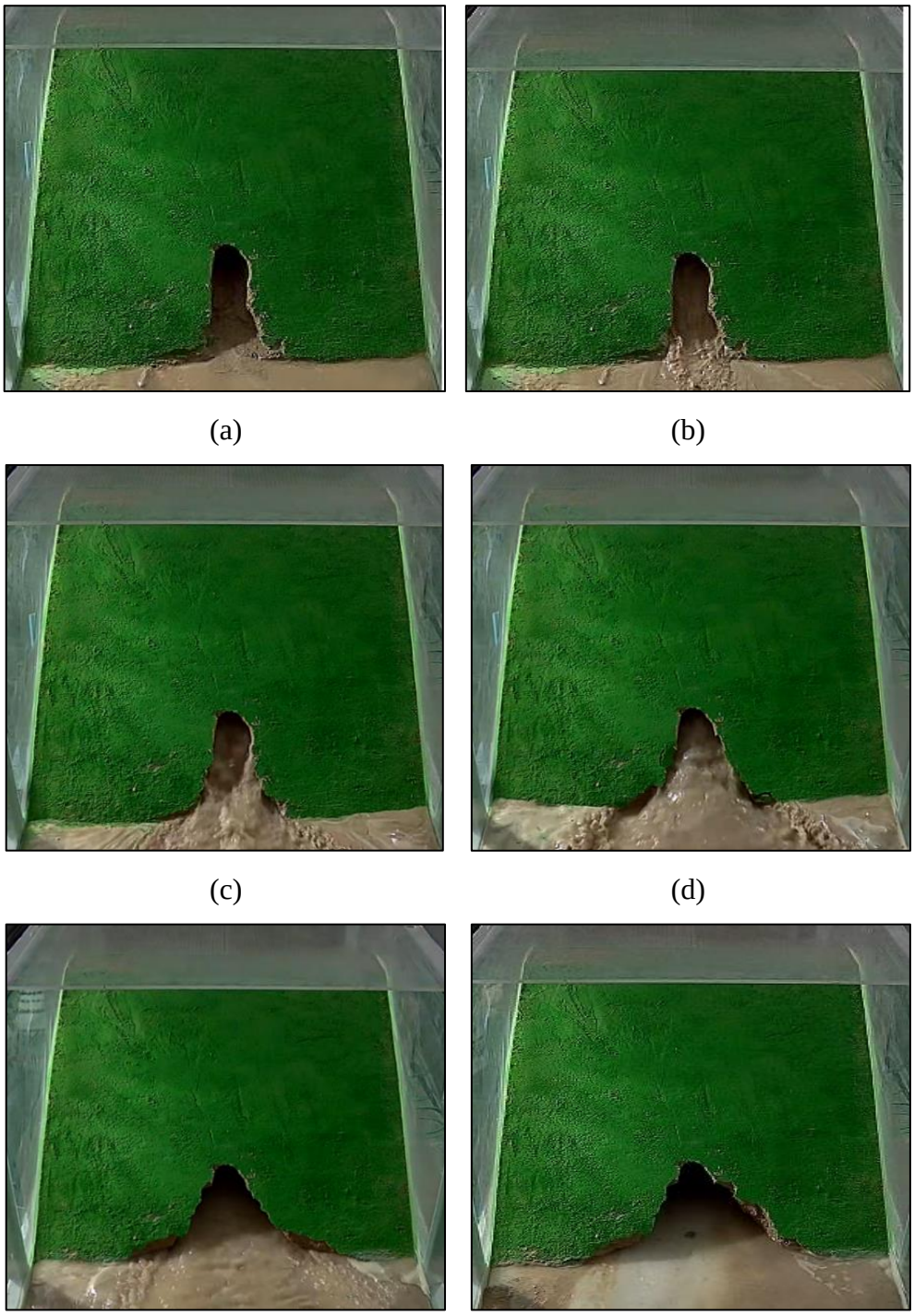

Figure 5.9. The breach views from downstream (a) t=0 s, (b) t=5 s, (c) t=10 s, (d) t=20 s, (e) t=50 s, (f) t=315 s

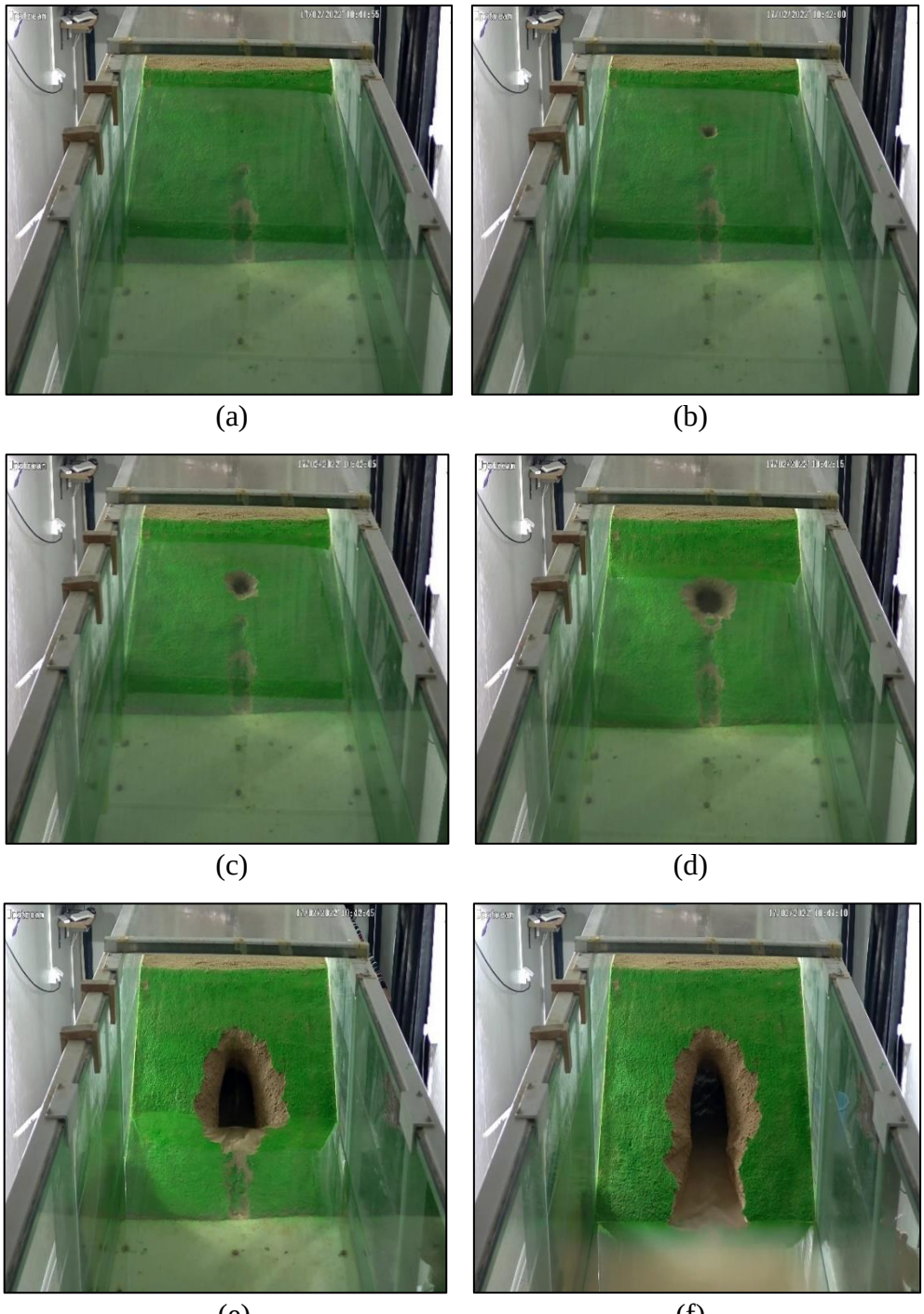

Figure 5.10. The breach views from upstream (a) t=0 s, (b) t=5 s, (c) t=10 s, (d) t=20 s, (e) t=50 s, (f) t=315 s

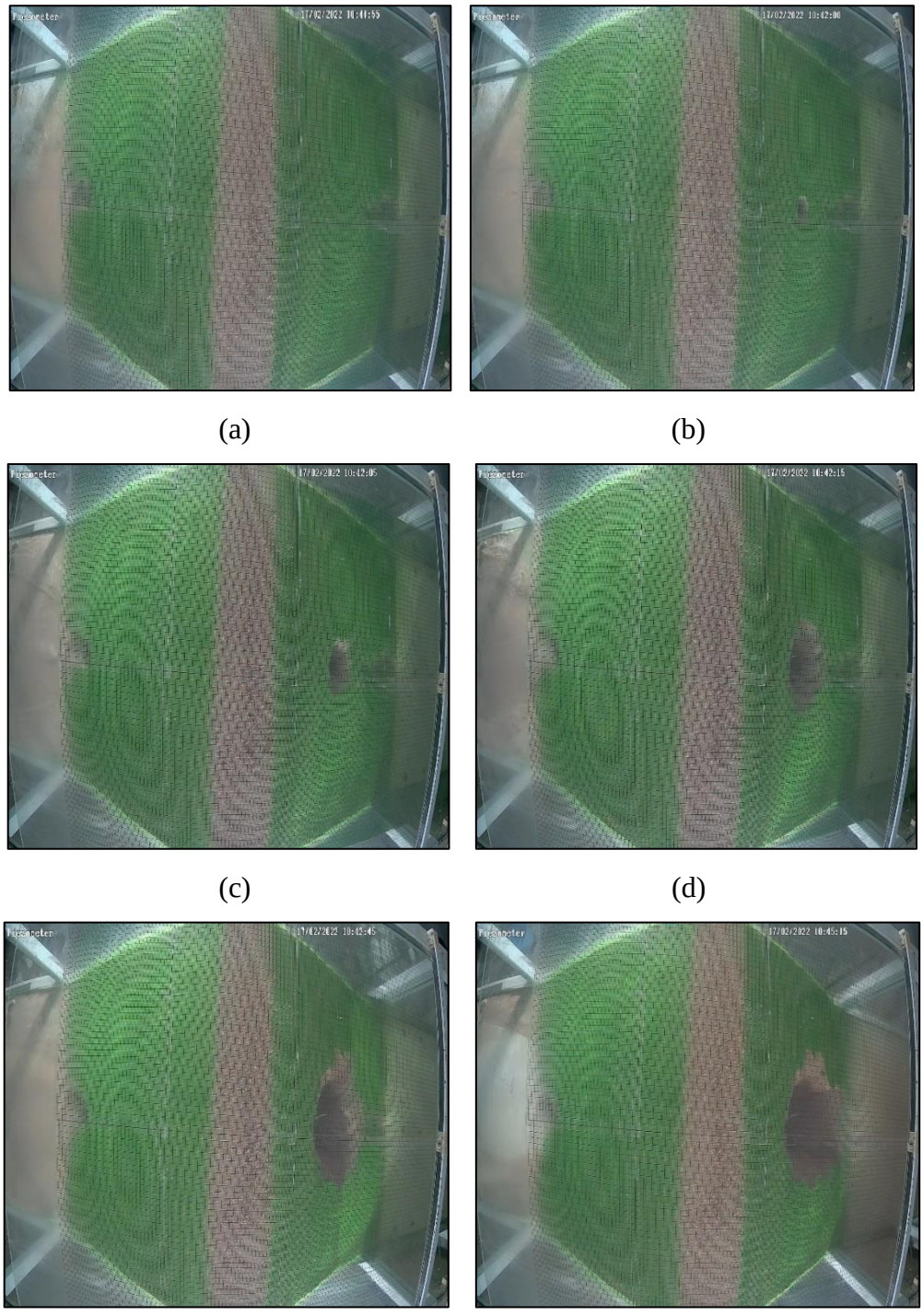

(a) (b)

(c) (d)

(e) (f)

Figure 5.11. The breach views from top (a) t=0 s, (b) t=5 s, (c) t=10 s, (d) t=20 s, (e) t=50 s, (f) t=315 s

The temporal changes in water depth during the experiment are shown in Figure 5.12

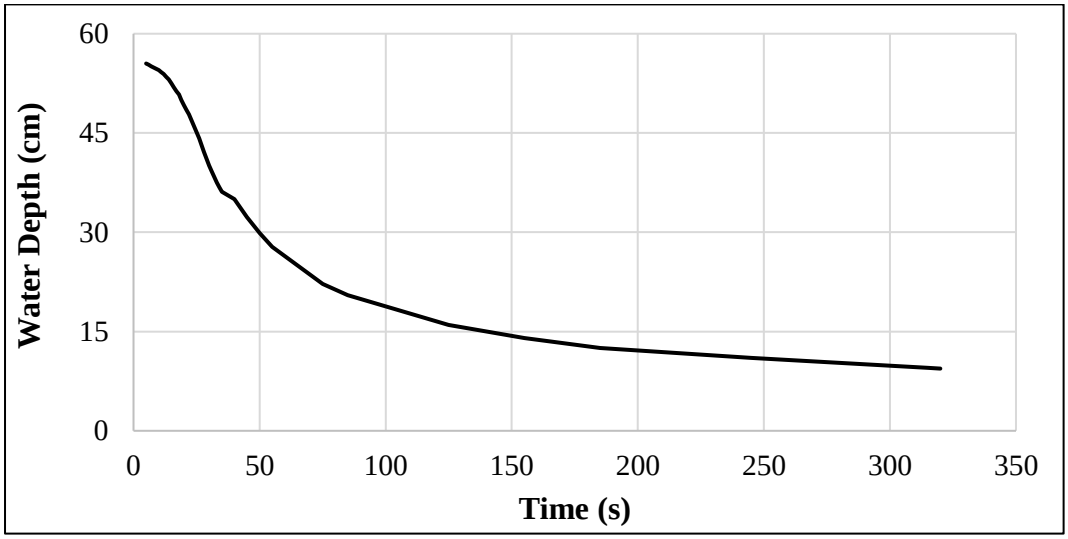

Figure 5.12. Temporal changes in water depths in the channel

The temporal breach developments at both sides are given together in Figure 5.13.

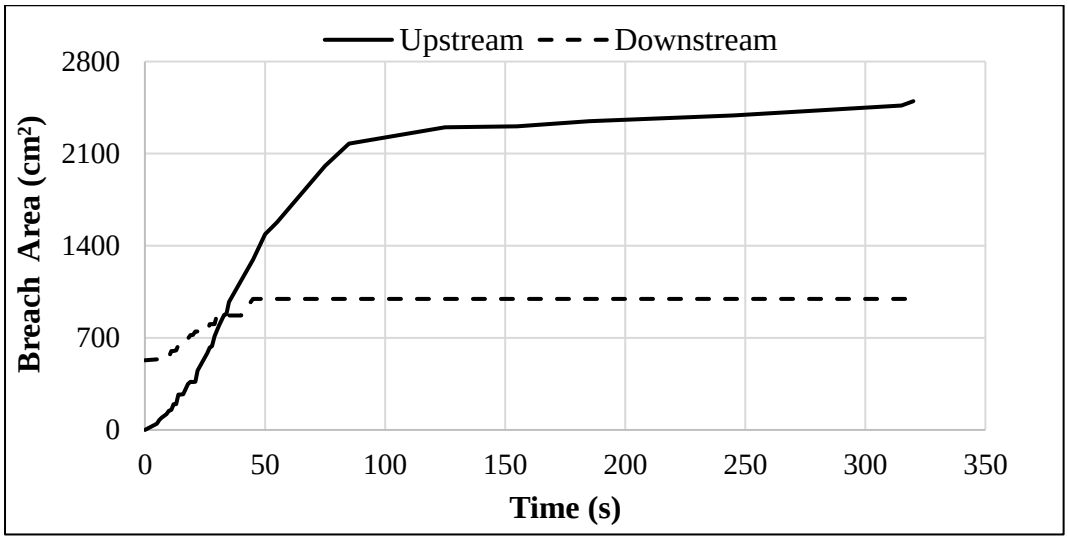

Figure 5.13. The upstream and downstream temporal breach developments

The temporal variations of the breach-wetted areas at upstream and downstream are shown in Figure 5.14.

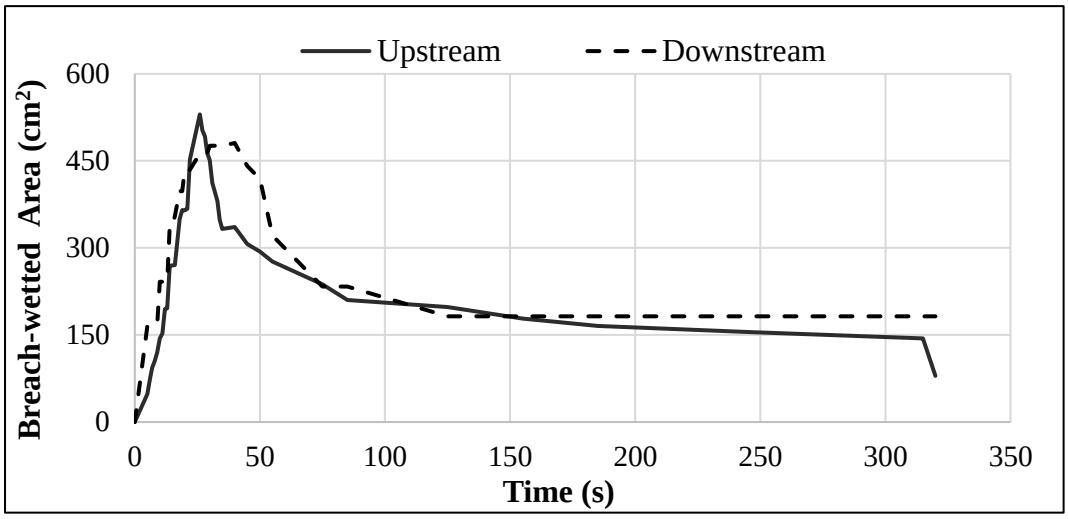

Figure 5.14. The upstream and downstream temporal variations of the breach-wetted areas

The temporal breach discharges calculated from Equation (4.1) are presented in Figure 5.15.

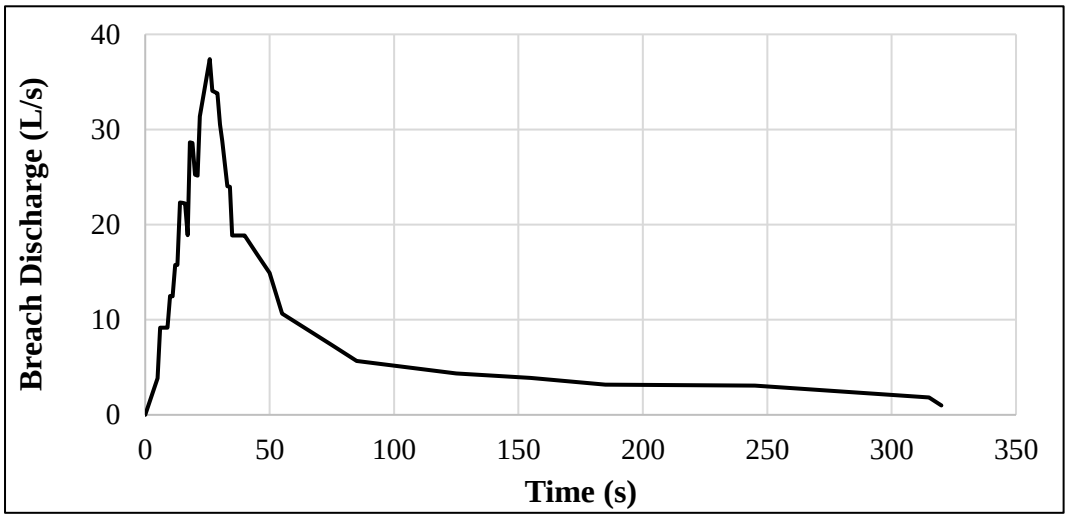

Figure 5.15. Temporal breach discharges

The time-varied upstream and downstream breach velocities, calculated by using Equation 4.2, are shown in Figure 5.16.

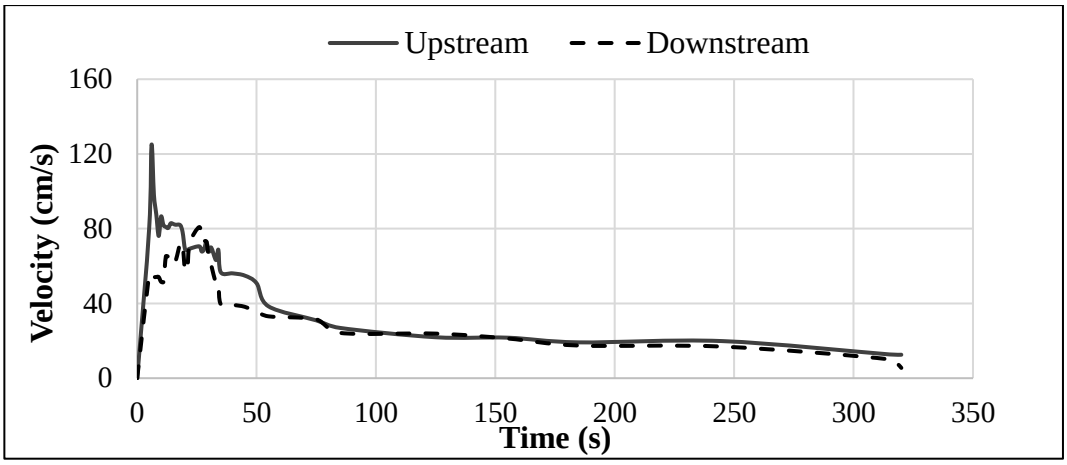

Figure 5.16. The time-varied upstream and downstream breach velocities

5.2. Second Experiment

The final views of the second experiment are given in Figure 5.17.

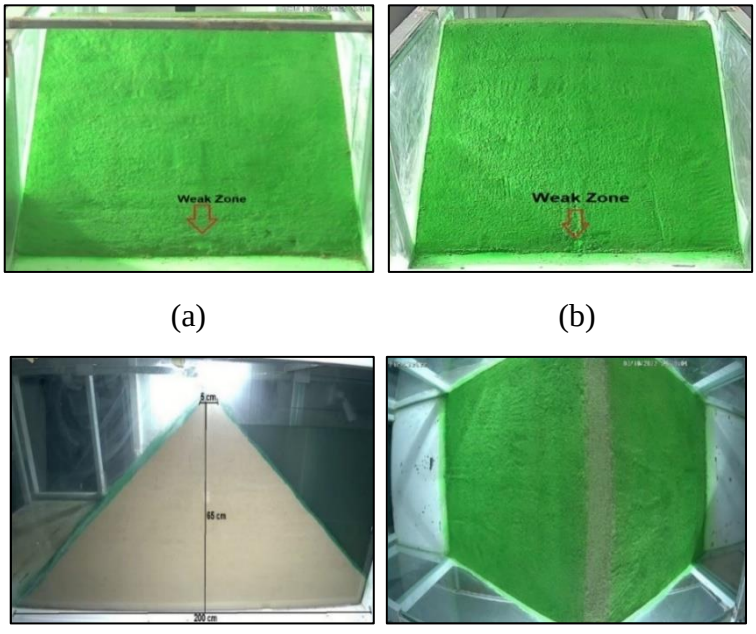

(a) (b)

(c) (d)

Figure 5.17. The final views of the second experiment, (a) upstream, (b) downstream, (c) left side, (d) top side

The breach views from the downstream and top are given in Figure 5.18 and Figure 5.19 for the downstream and top sides, separately. The time t=0 s represents the seepage initiation.

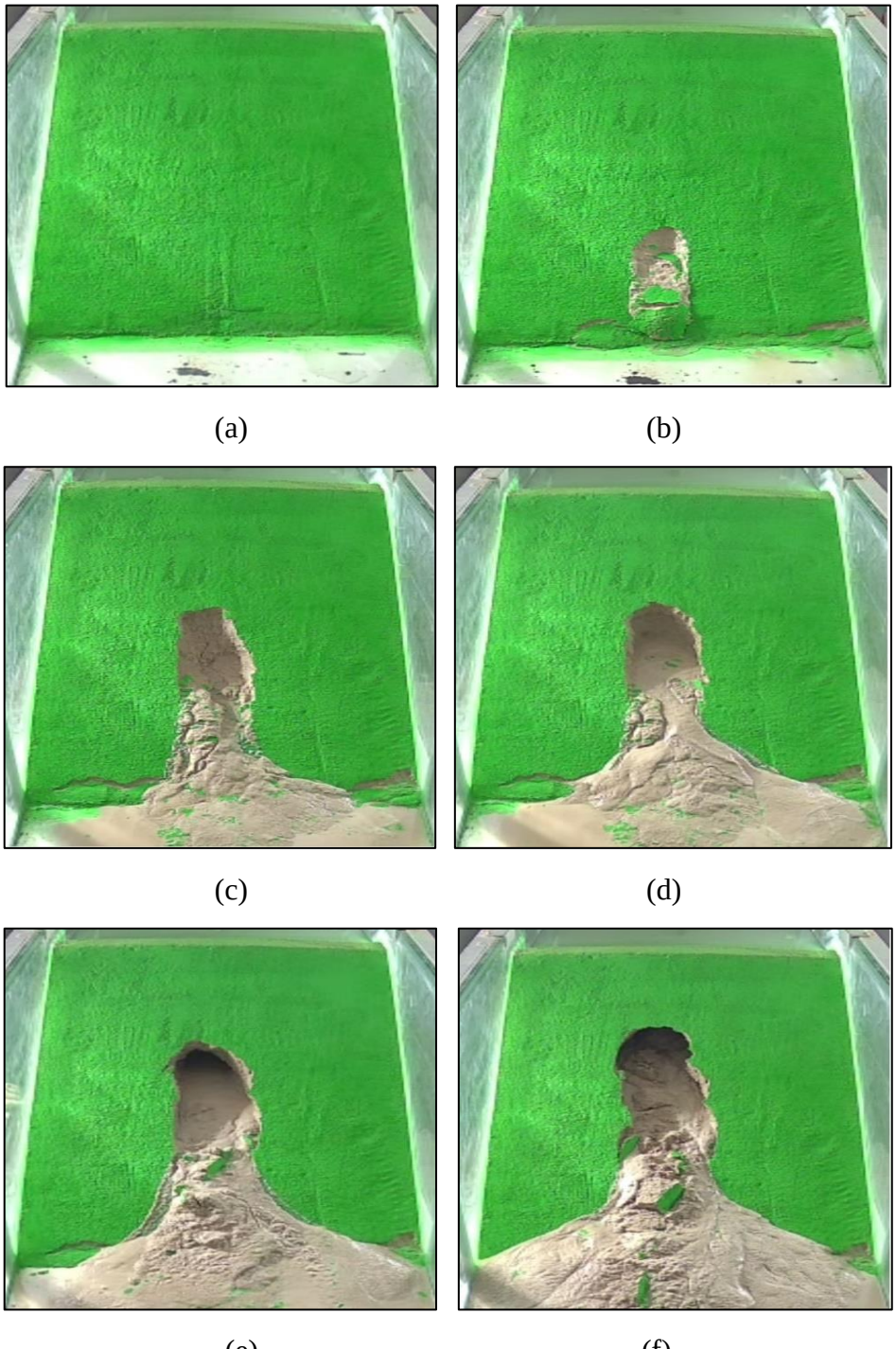

(a) (b)

(c) (d)

(e) (f)

Figure 5.18. The breach views from downstream (a) t=0 h, (b) t=1.1 h, (c) t=2 h, (d) t=3 h, (e) t=4 h, (f) t=4.8 h

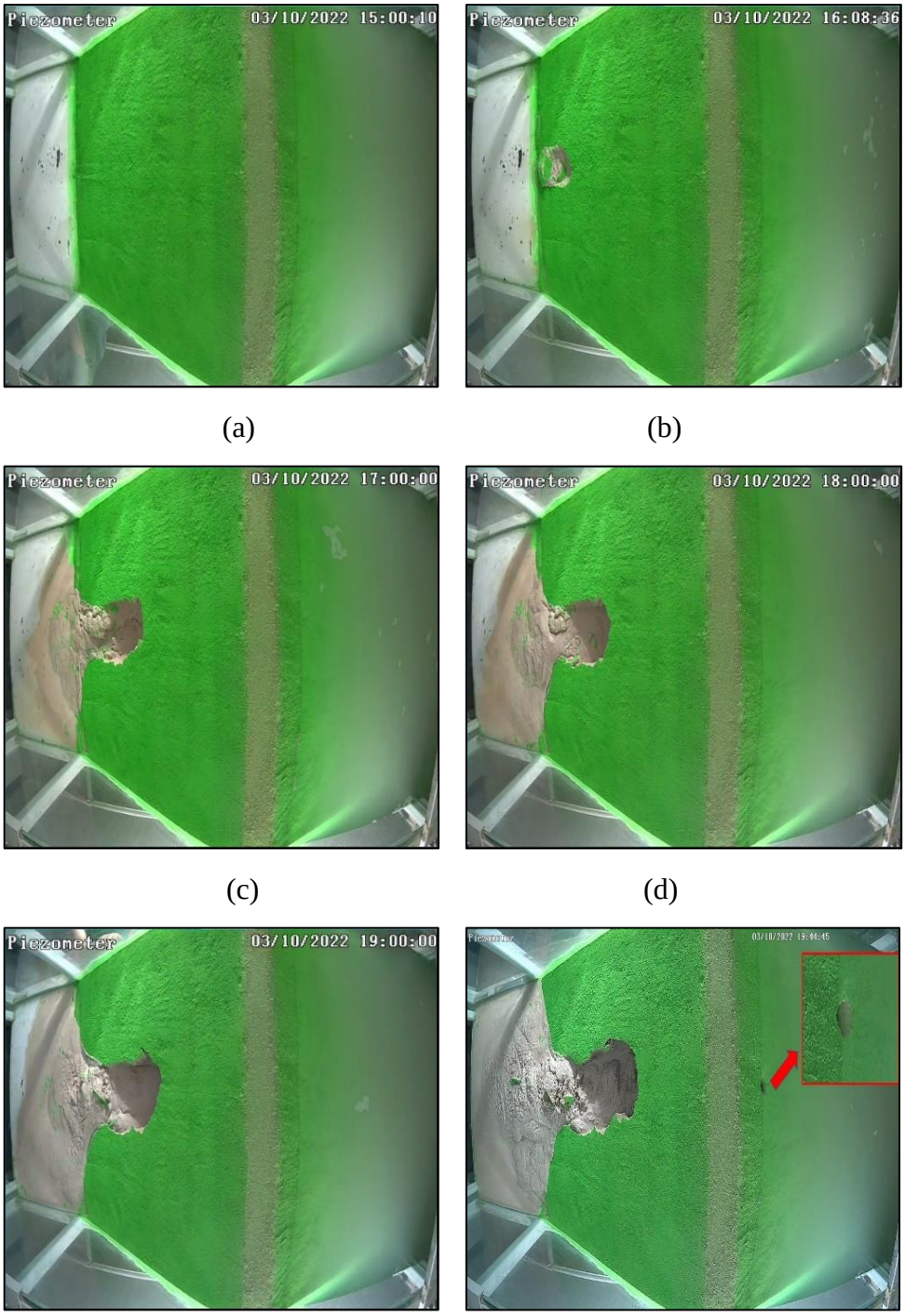

Figure 5.19. The breach views from the top (a) t=0 h, (b) t=1.1 h, (c) t=2 h, (d) t=3 h, (e) t=4 h, (f) t=4.8 h

The breach views corresponding to different times are given from Figure 5.20 to Figure 5.22. The time t=0 represents when the breach appeared upstream side.

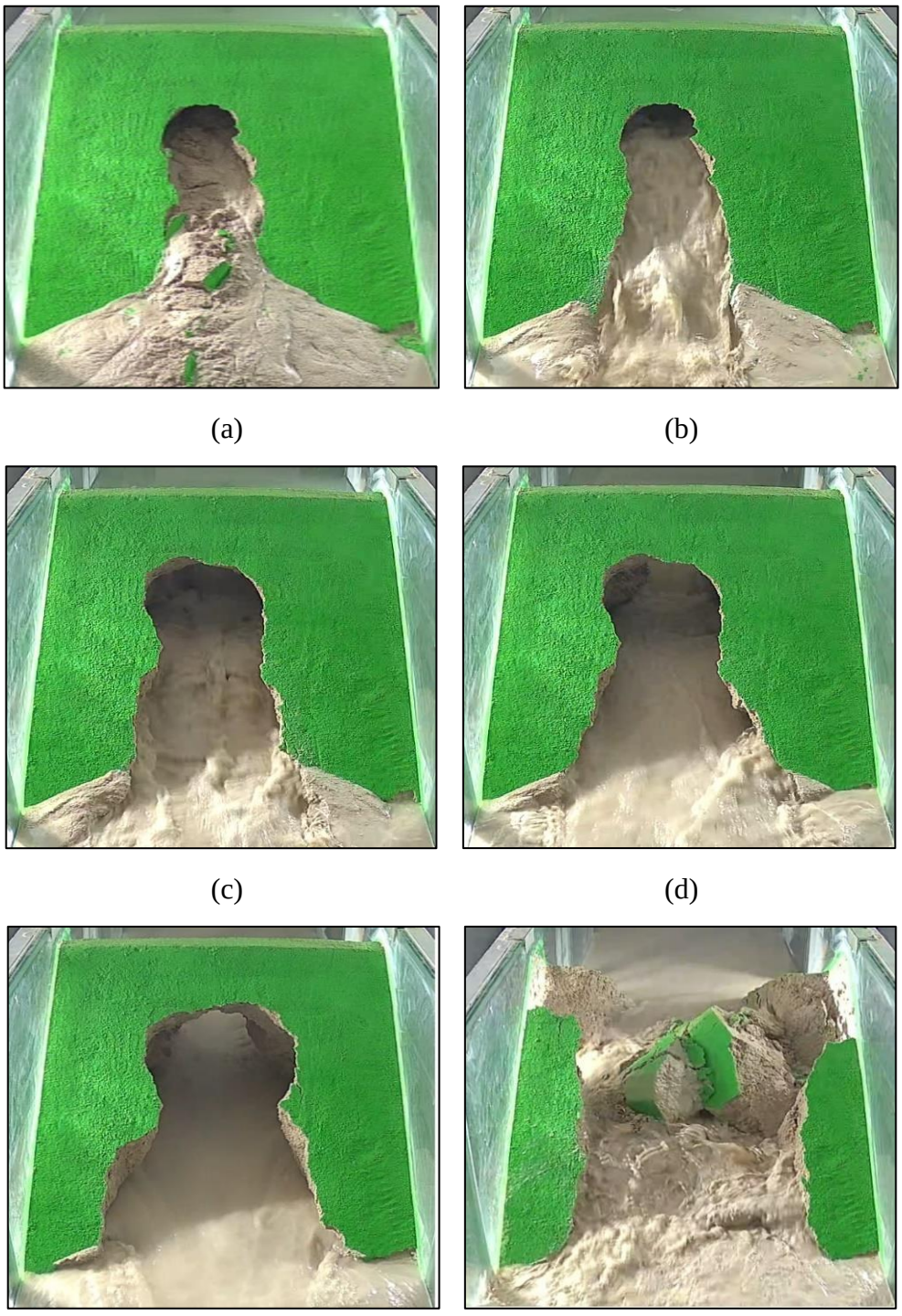

Figure 5.20. The breach views from downstream a) t=0 s, b) t=20 s, c) t=60 s, d) t=80 s, e) t=120 s, f) t=150 s

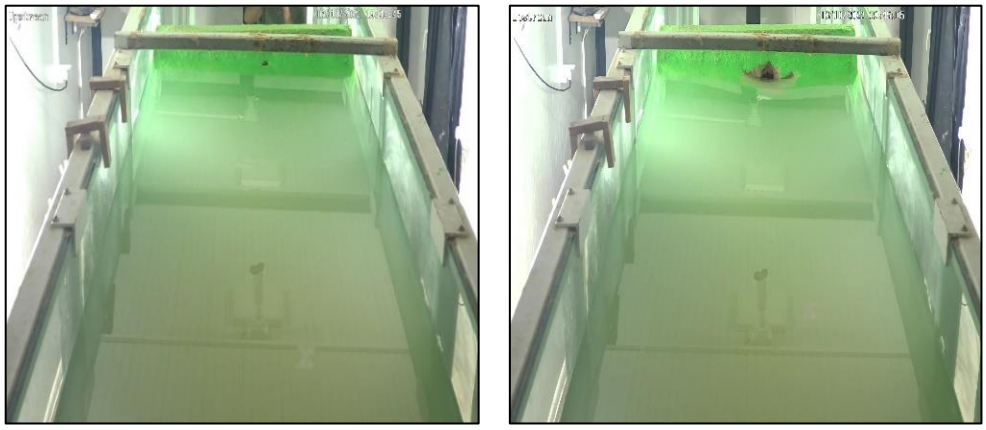

(a) (b)

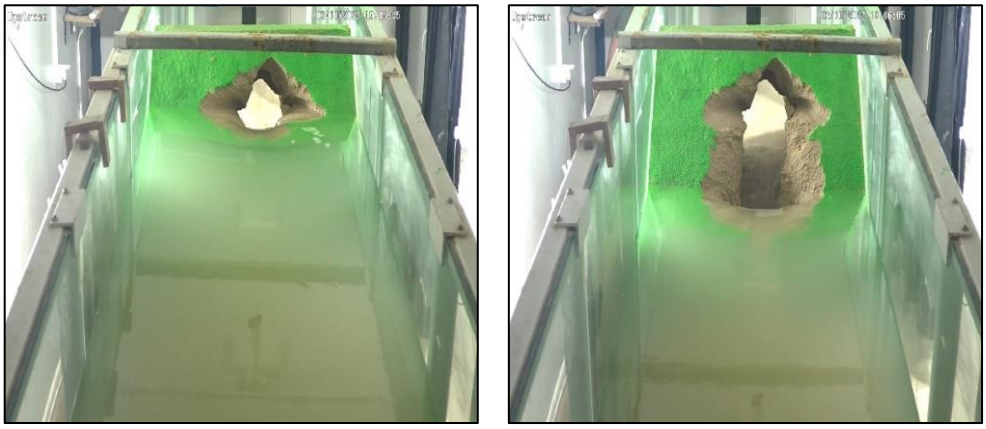

(c) (d)

(e) (f)

Figure 5.21. The breach views from upstream a) t=0 s, b) t=20 s, c) t=60 s, d) t=80 s, e) t=120 s, f) t=150 s

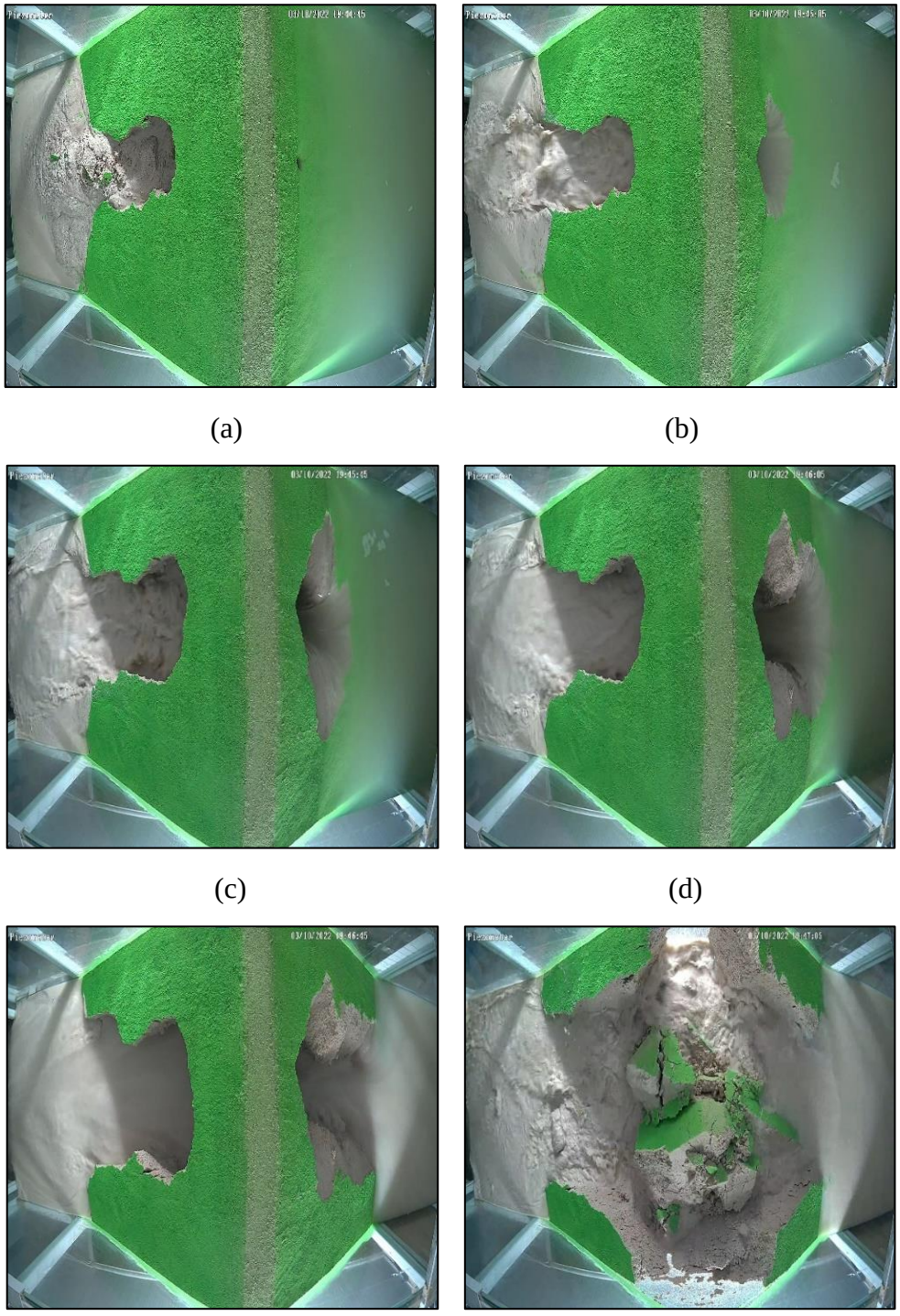

(a) (b)

(c) (d)

(e) (f)

Figure 5.22. The breach views from top a) t=0 s, b) t=20 s, c) t=60 s, d) t=80 s, e) t=120 s, f) t=150 s

The temporal changes in water depth during the experiment are shown in Figure 5.23.

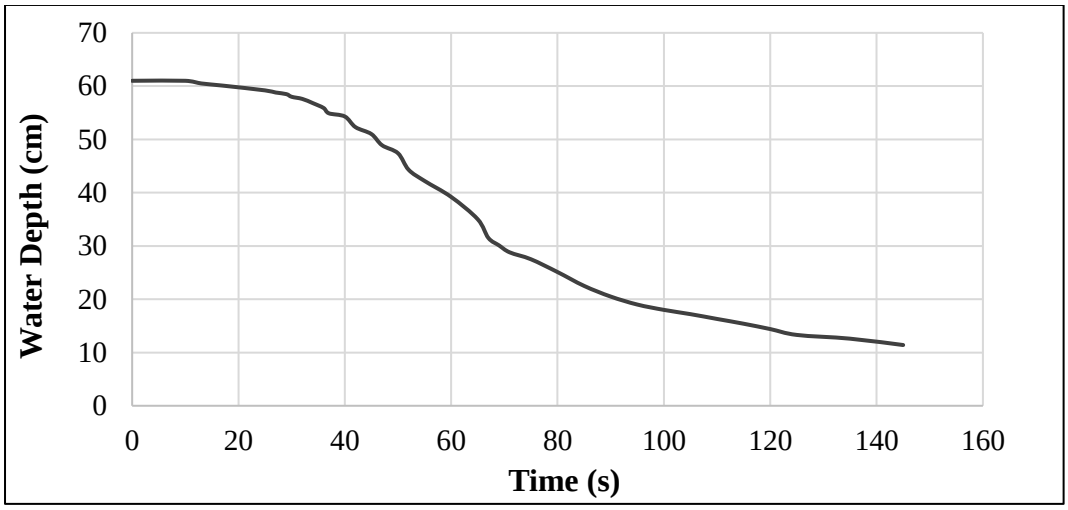

Figure 5.23. Temporal changes in water depths in the channel

The temporal breach developments at both sides are given together in Figure 5.24.

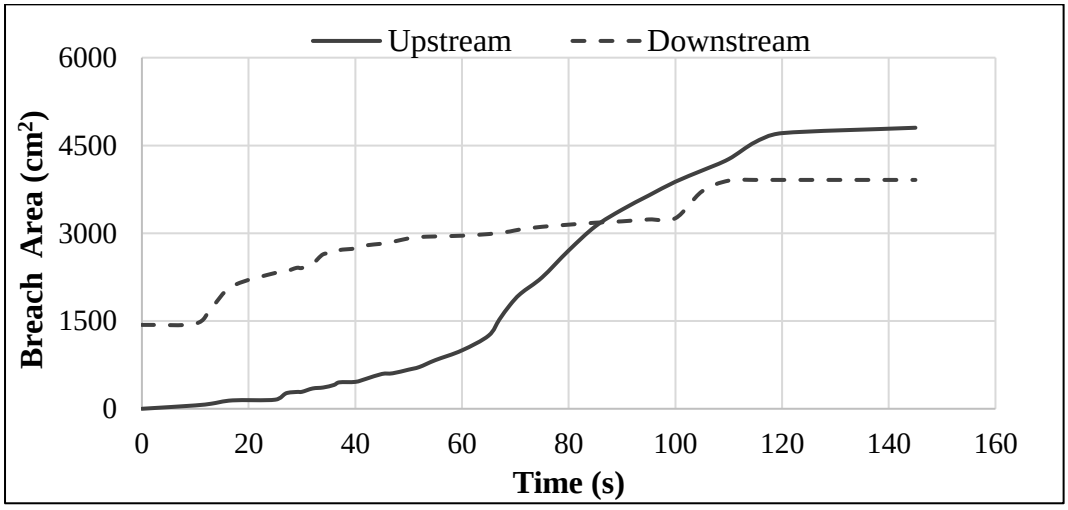

Figure 5.24. The upstream and downstream temporal breach developments

The temporal variations of the breach-wetted areas at upstream and downstream are shown in Figure 5.25.

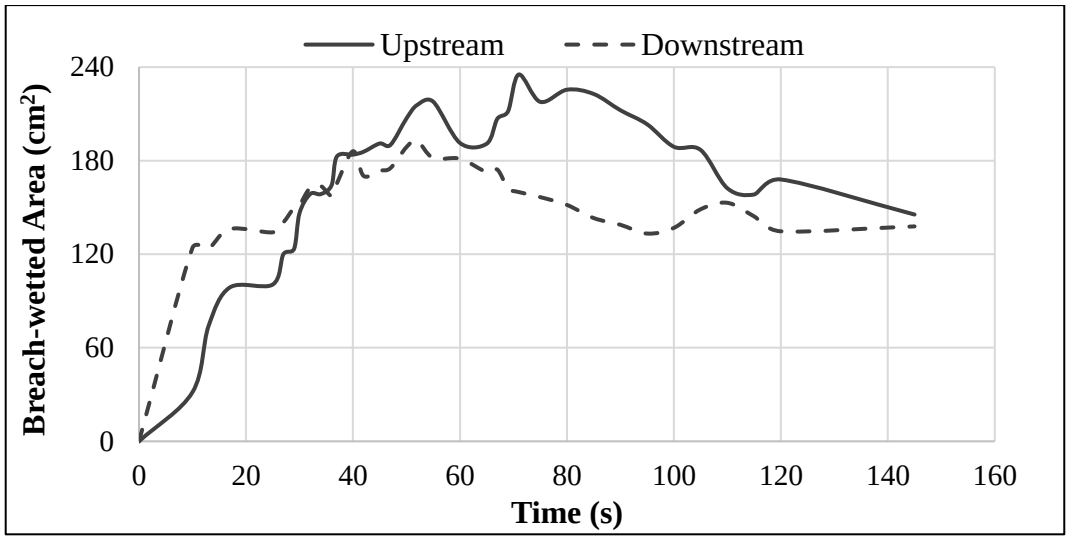

Figure 5.25. The upstream and downstream temporal variations of the breach-wetted areas

The temporal breach discharges calculated from Equation (4.1) are presented in Figure 5.26.

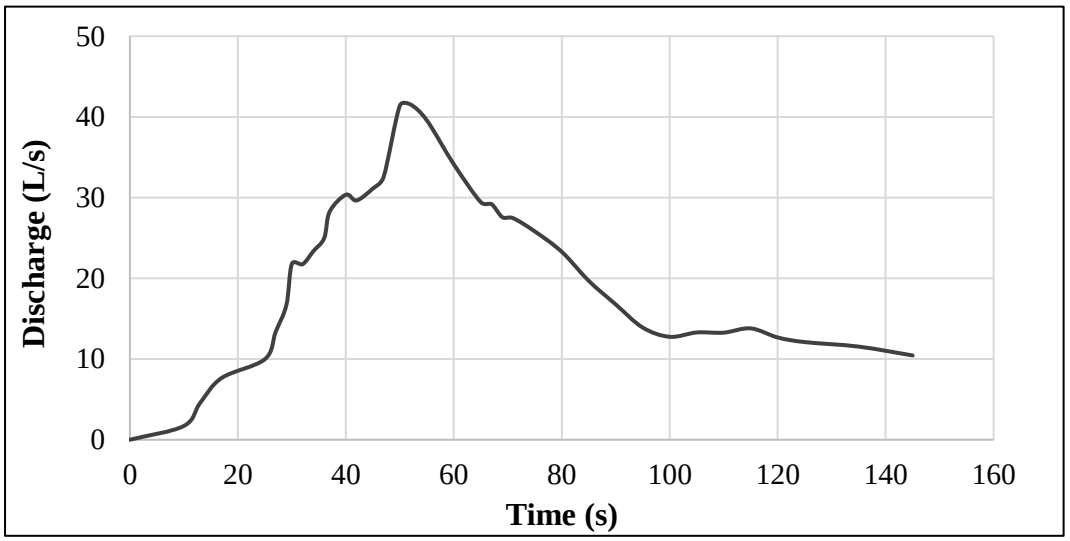

Figure 5.26.Temporal breach discharges

The time-varied upstream and downstream breach velocities, calculated by using Equation 4.2 are shown in Figure 5.27.

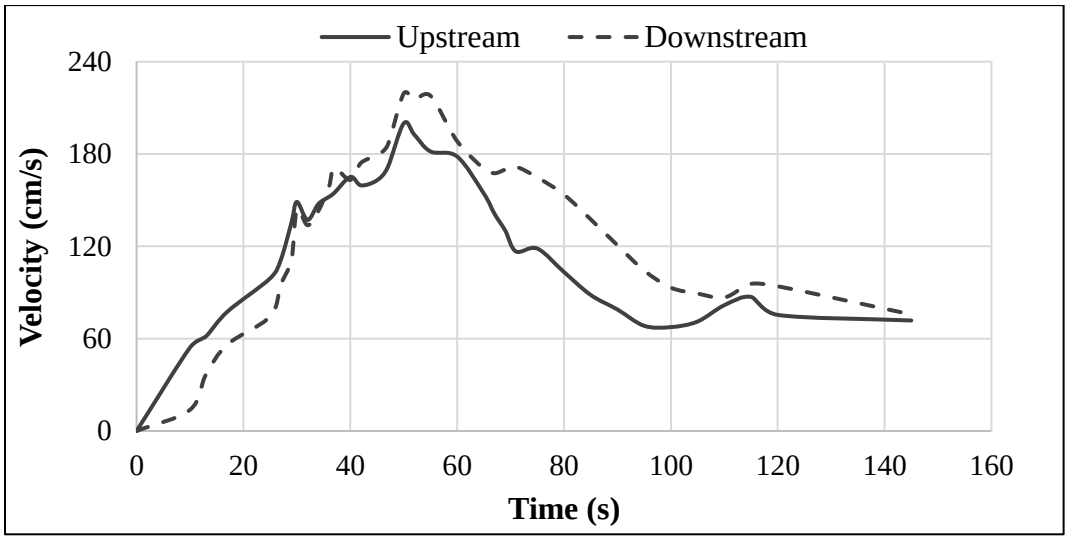

Figure 5.27. The time-varied upstream and downstream breach velocities

5.3. Third Experiment

In the third scenario, the dam height was 65 cm, and the water level was 61 cm. The bulk density, ρ_{bulk}, is 1.7 g/cm^3. The final view of the third experiment is given in Figure 5.28.

Figure 5.28. The final view of the dam

The breach views from downstream and top corresponding to different times are given in Figure 5.29 and Figure 5.30, respectively. The time t=0 represents when the breach appeared upstream.

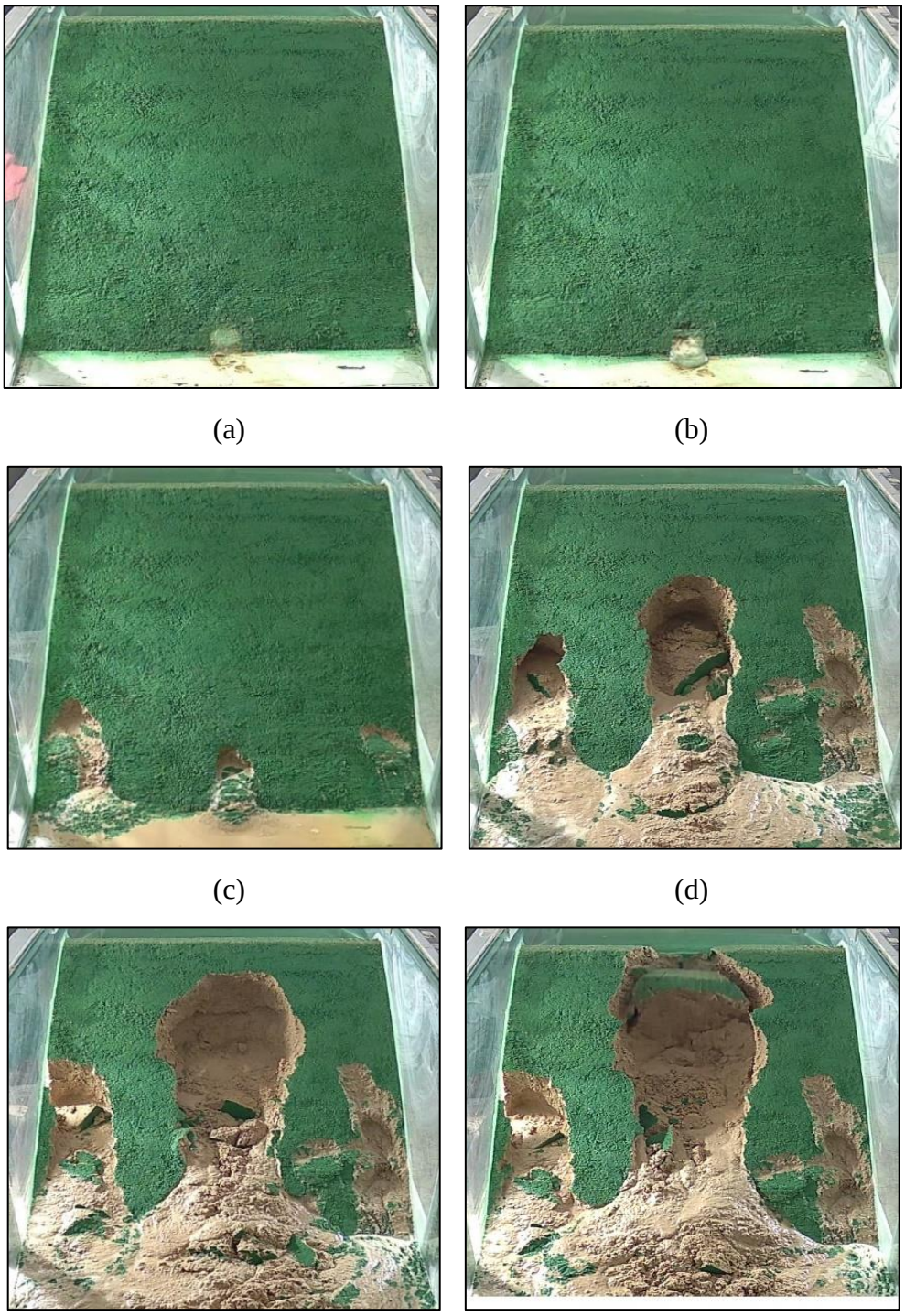

Figure 5.29. The breach views from downstream a) t=0 s, b) t=50 s, c) t=1710 s, d) t=2230 s, e) t=2410 s, f) t=2485 s

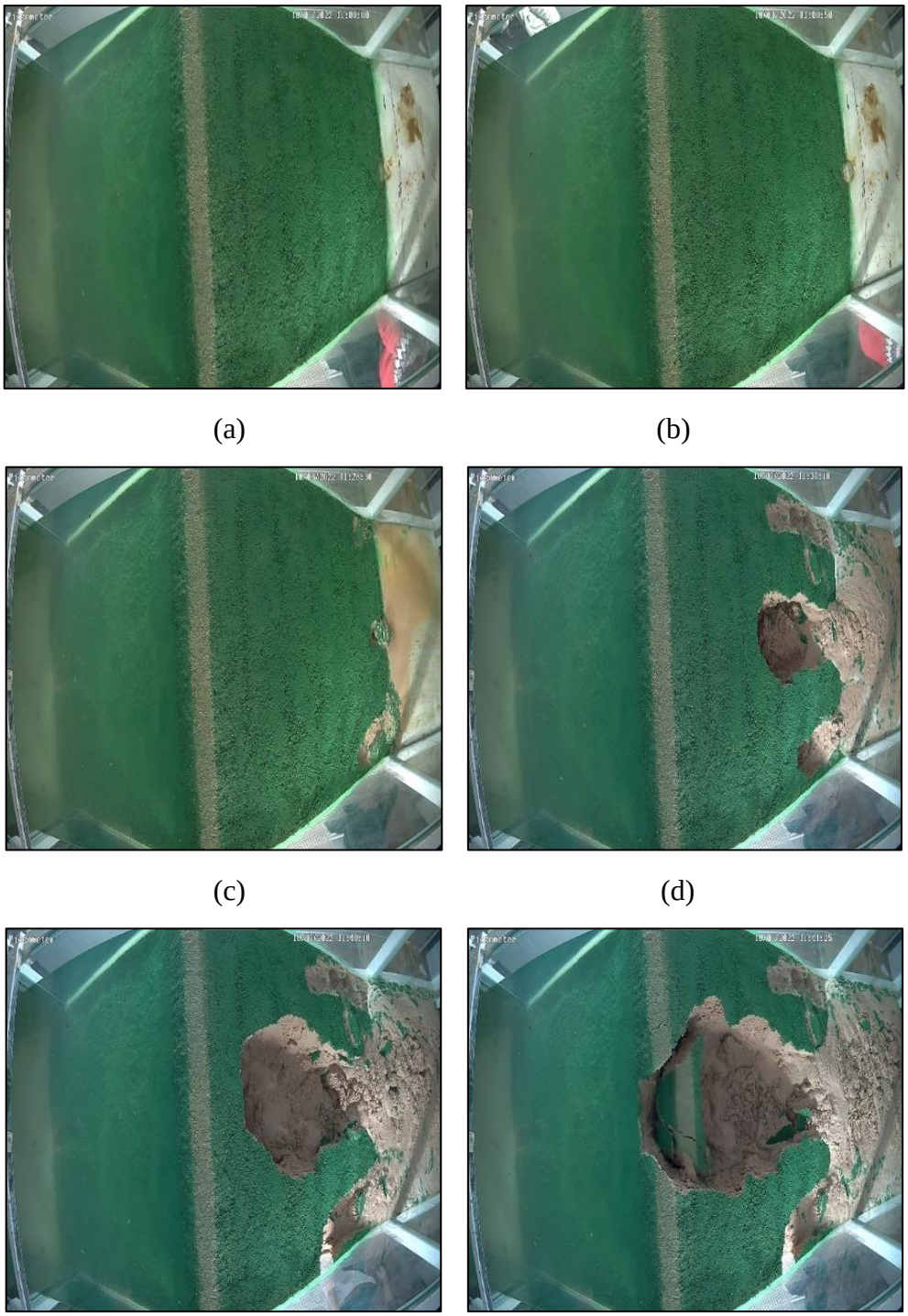

(a) (b)

(c) (d)

(e) (f)

Figure 5.30. The breach views from top a) t=0 s, b) t=50 s, c) t=1710 s, d) t=2230 s, e) t=2410 s, f) t=2485 s

At the time t=0, the seepage started from the weak area and turned into a breach, then reached the upstream side in less than 1 hour. For the evaluation of the experimental findings, when the breach reached the upstream was taken t=0 s. The breach views

corresponding to different times are given from Figure 5.31 to Figure 5.33. The time t=0 represents when the breach appeared upstream.

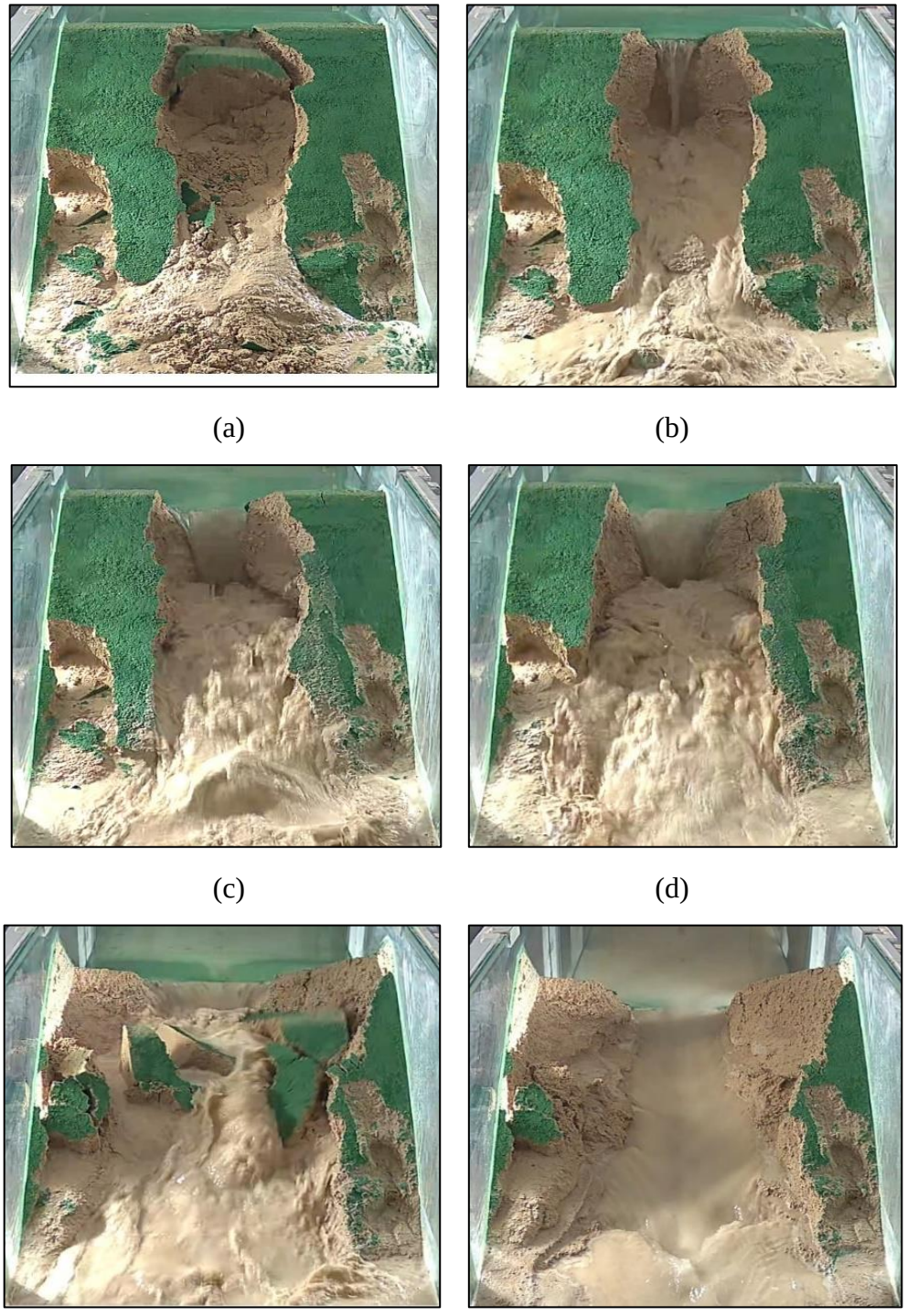

(a) (b)

(c) (d)

(e) (f)

Figure 5.31. The breach views from downstream a) t=0 s, b) t=10 s, c) t=30 s, d) t=40 s, e) t=60 s, f) t=150 s

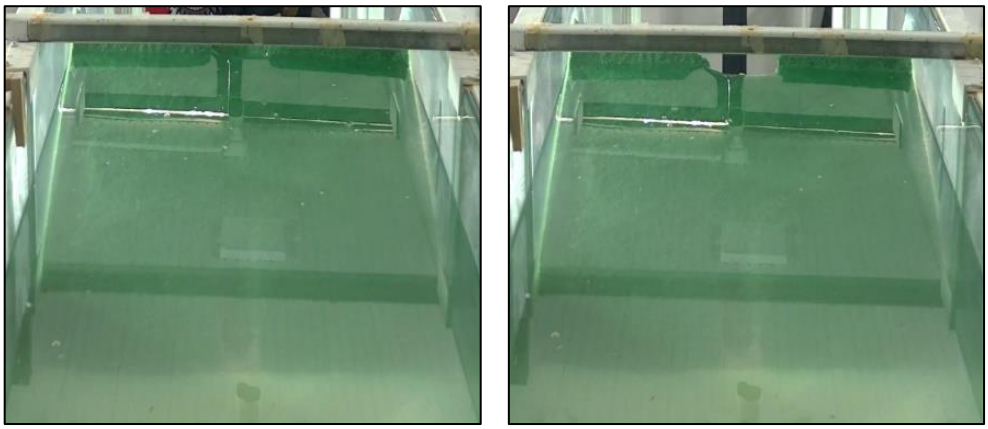

(a) (b)

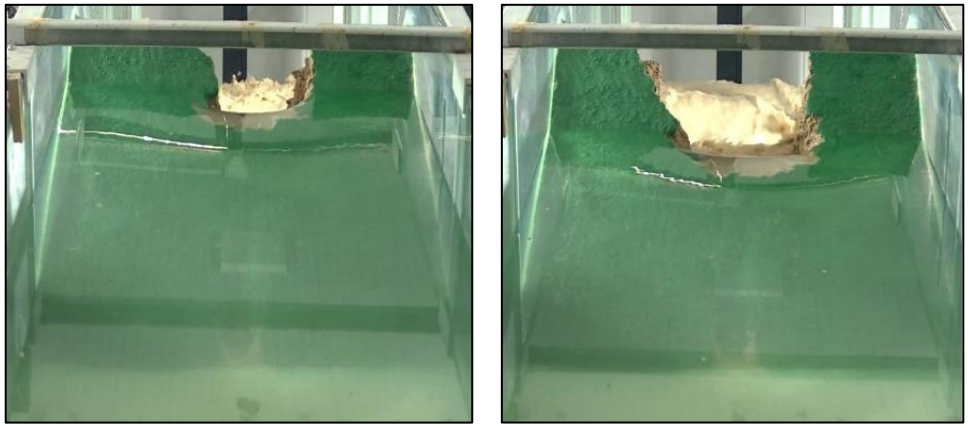

(c) (d)

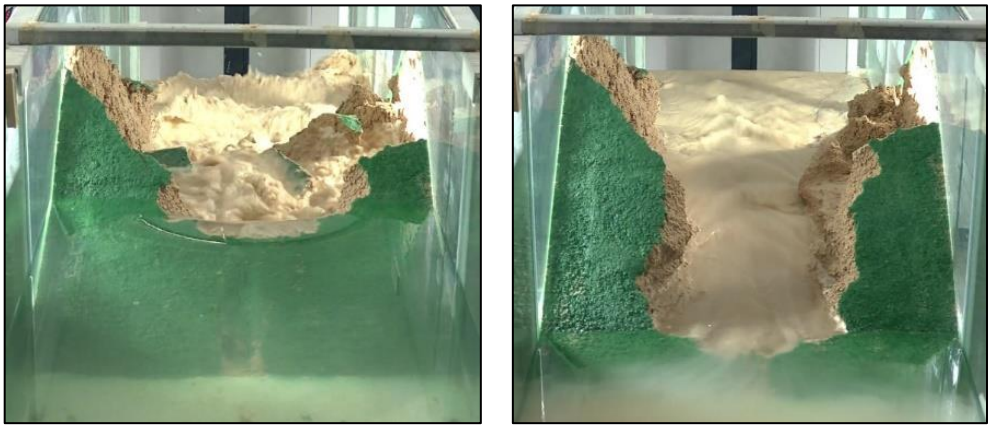

(e) (f)

Figure 5.32. The breach views from upstream a) t=0 s, b) t=10 s, c) t=30 s, d) t=40 s, e) t=60 s, f) t=150 s

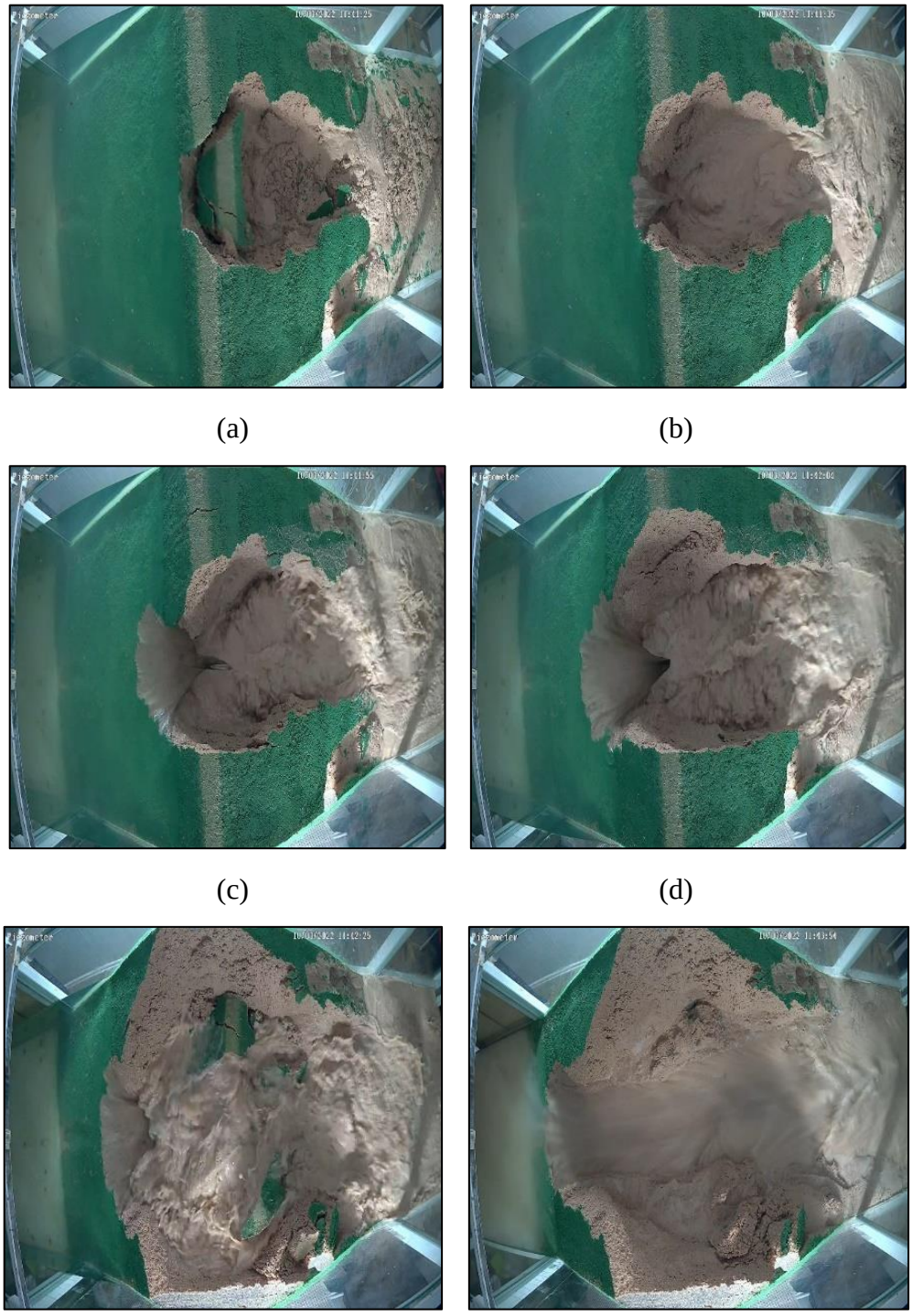

(a) (b)

(c) (d)

(e) (f)

Figure 5.33. The breach views from top a) t=0 s, b) t=10 s, c) t=30 s, d) t=40 s, e) t=60 s, f) t=150 s

The temporal changes in water depth during the experiment are shown in Figure 5.34.

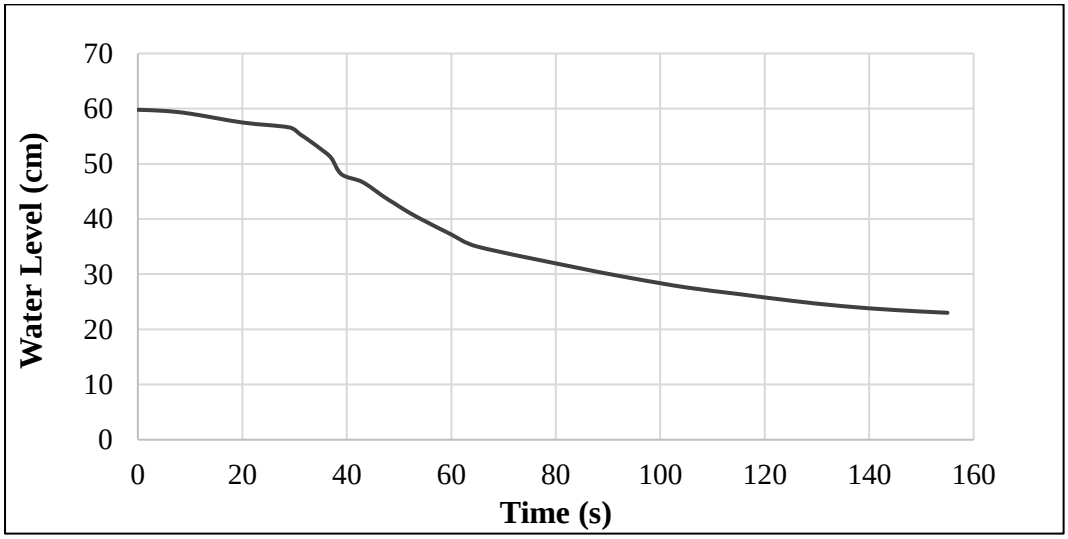

Figure 5.34. Temporal changes in water depths in the channel

The upstream temporal breach developments are given in Figure 5.35.

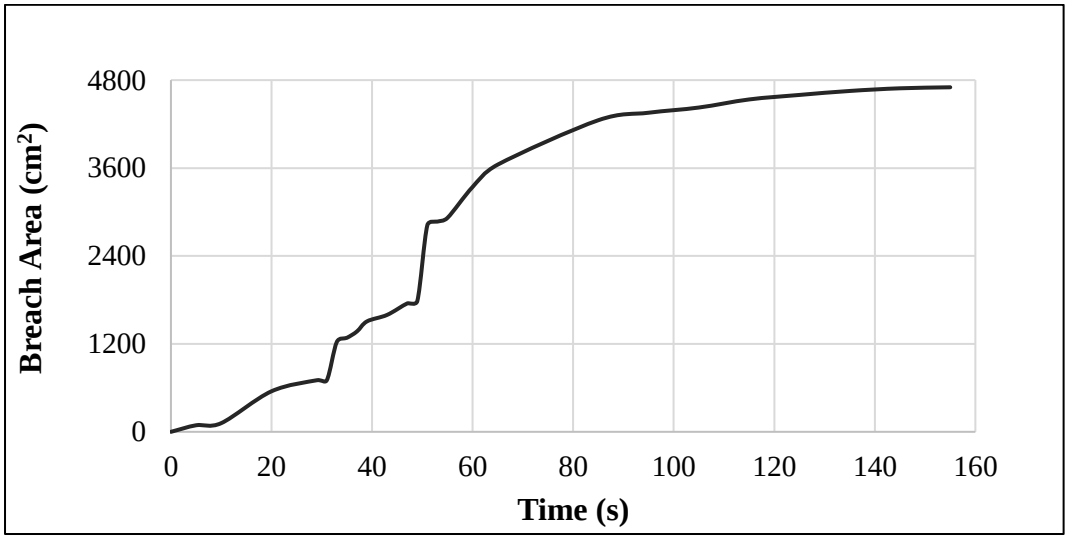

Figure 5.35. The upstream temporal breach developments

The upstream temporal variations of the breach-wetted areas are presented in Figure 5.36

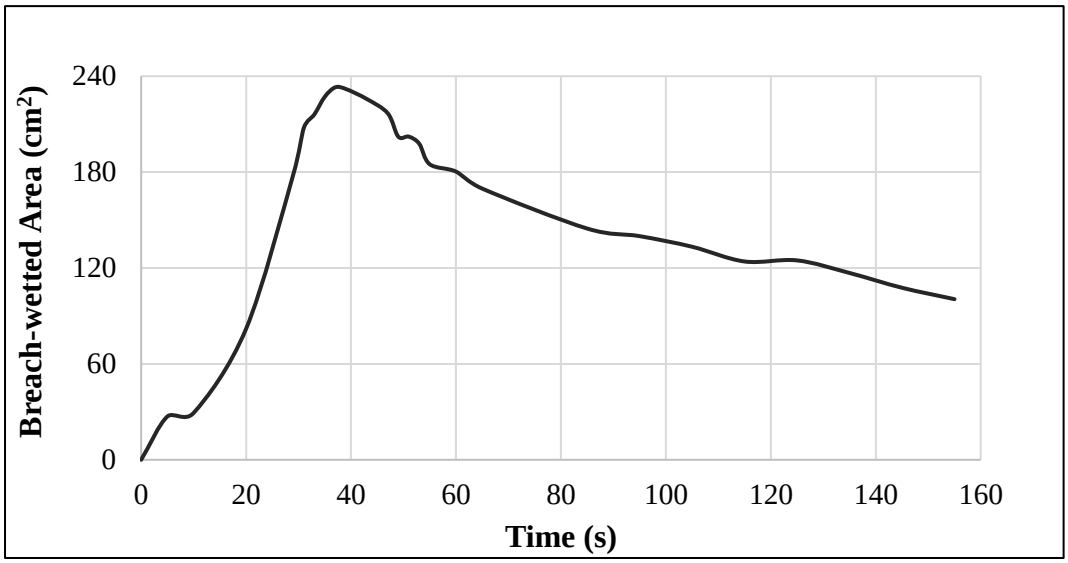

Figure 5.36. The upstream temporal variations of the breach-wetted areas

The temporal breach discharges calculated from Equation (4.1) are presented in Figure 5.37.

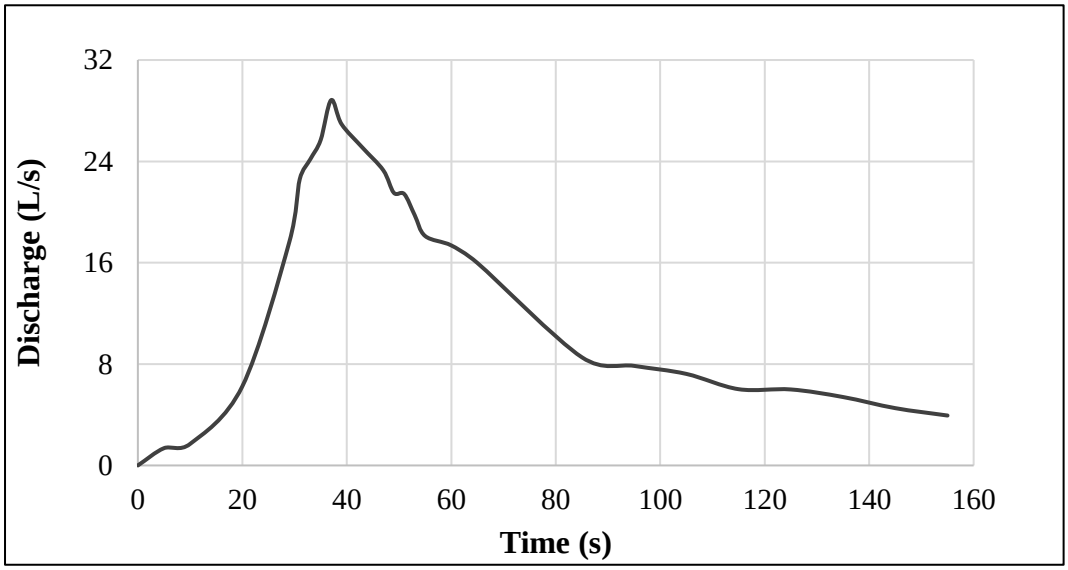

Figure 5.37. Temporal breach discharges

The time-varied upstream and downstream breach velocities, calculated by using Equation 4.2, are shown in Figure 5.38.

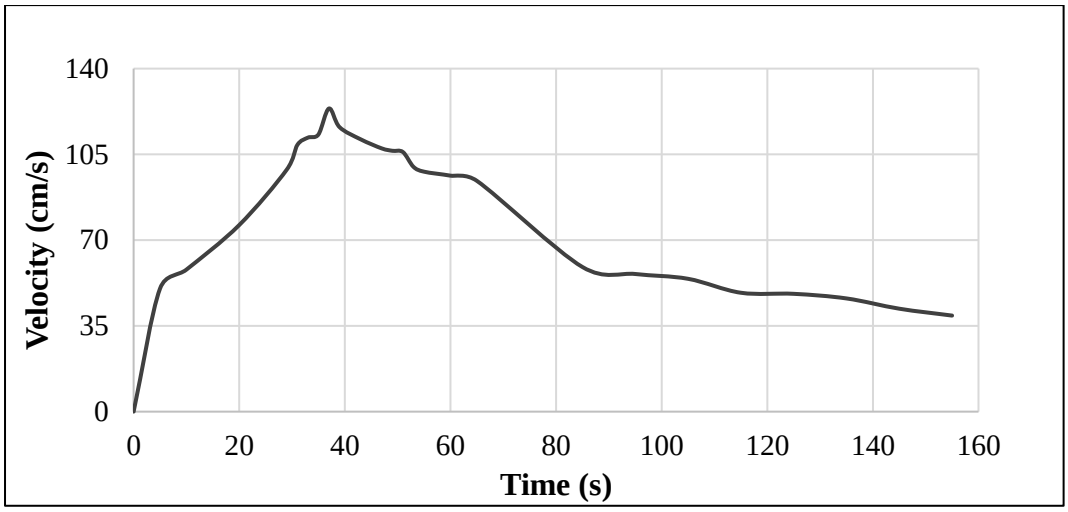

Figure 5.38. The time-varied upstream breach velocities

5.4. Fourth Experiment

In the fourth experiment, the dam high was 65 cm, and the water level was 61 cm. The bulk density, ρ_{bulk}, is 2 g/cm^3. The dam was constructed by mixture 2 and created 2x2 cm^2 weak layer at 28 cm above the bottom. The final views are given in Figure 5.39.

(a) (b)

Figure 5.39. The final view of the dam from (a) top (b) downstream

The breach views corresponding to different times are given from Figure 5.40 to Figure 5.46. The time t=0 represents when the breach appeared upstream.

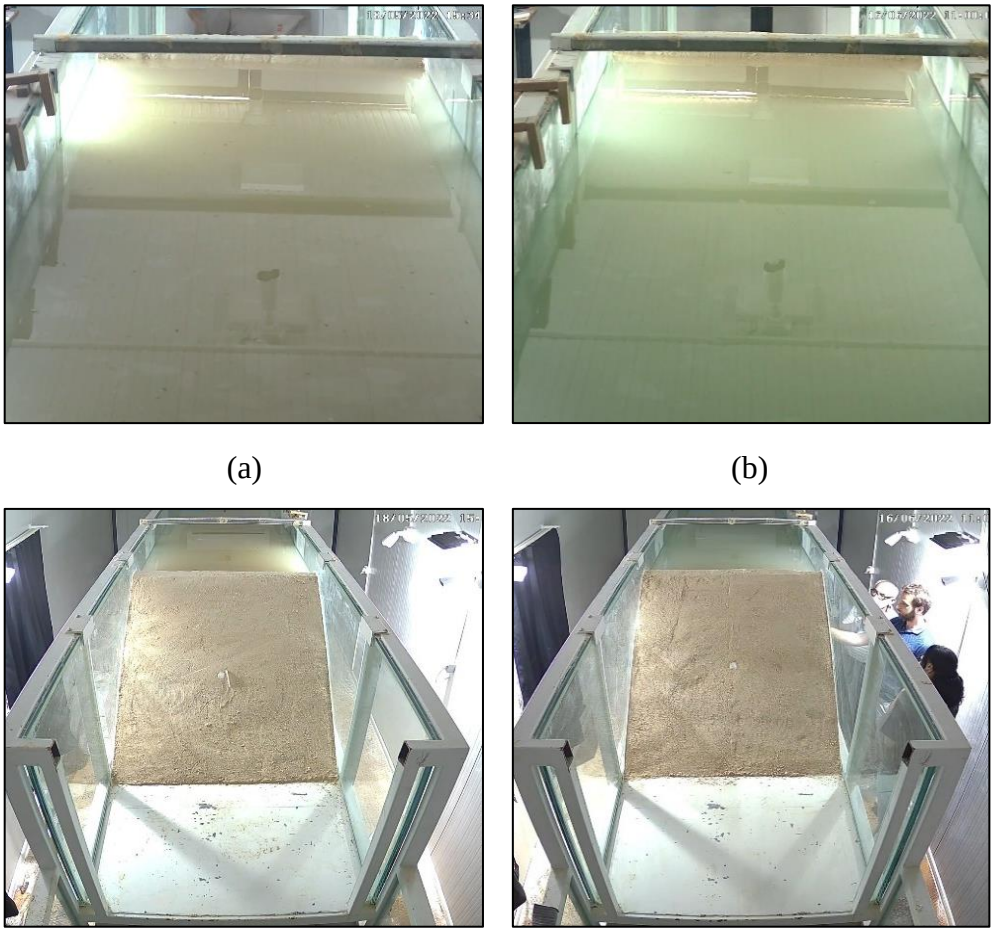

(a) (b)

(c) (d)

Figure 5.40. The breach views at t=0 s a) upstream of the first dam, b) upstream of the second dam, c) downstream of the first dam, d) downstream of the second dam

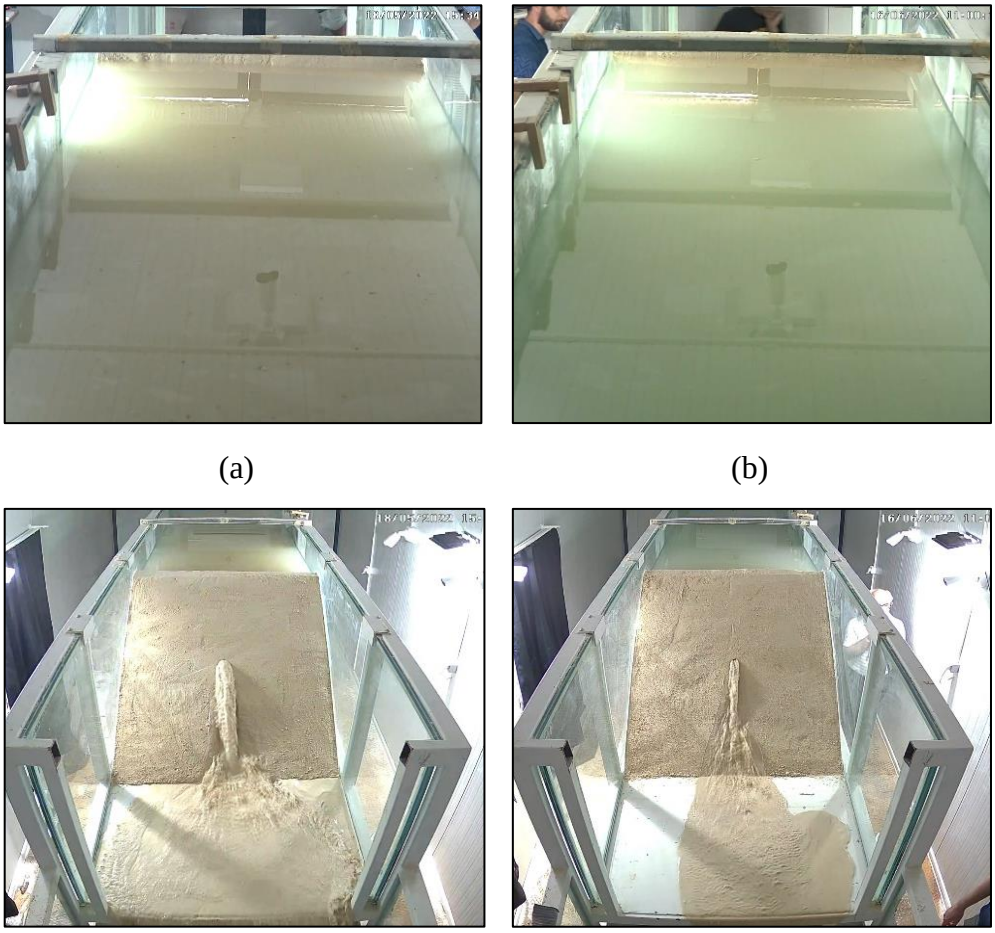

(a) (b)

(c) (d)

Figure 5.41. The breach views at t=15 s a) upstream of the first dam, b) upstream of the second dam, c) downstream of the first dam, d) downstream of the second dam

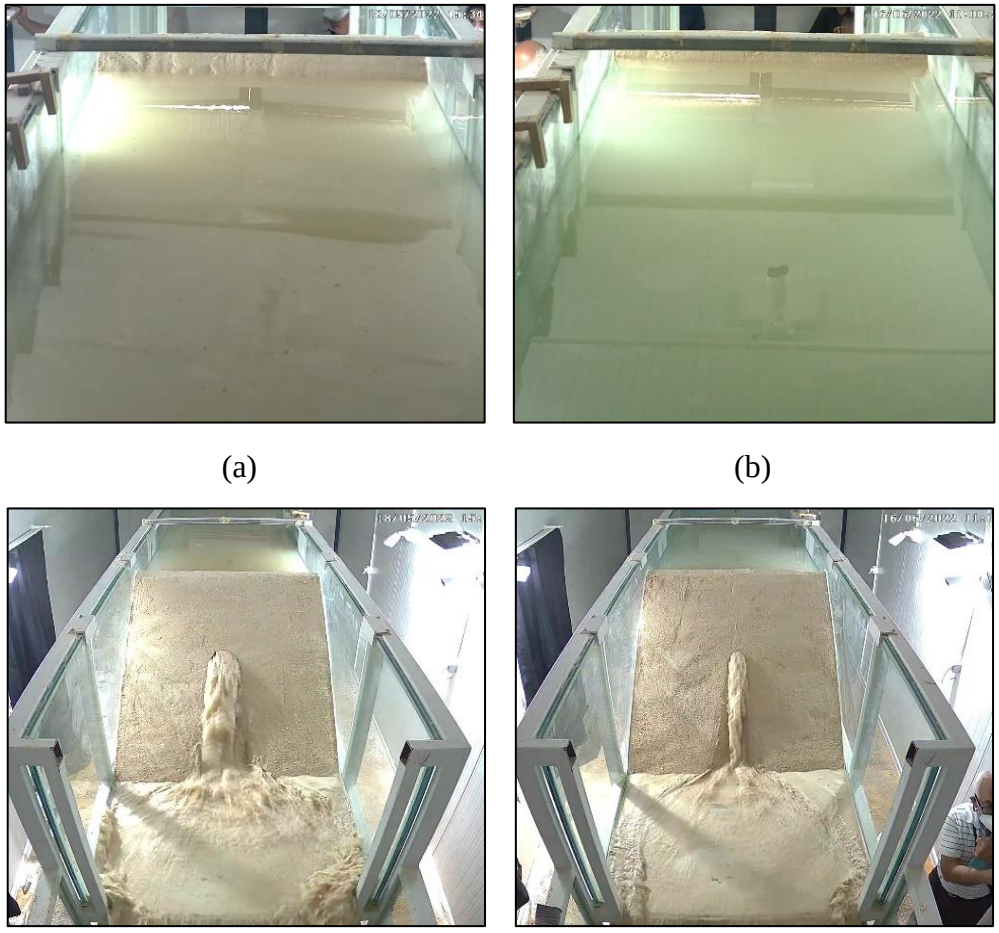

(a) (b)

(c) (d)

Figure 5.42. The breach views at t=25 s a) upstream of the first dam, b) upstream of the second dam, c) downstream of the first dam, d) downstream of the second dam

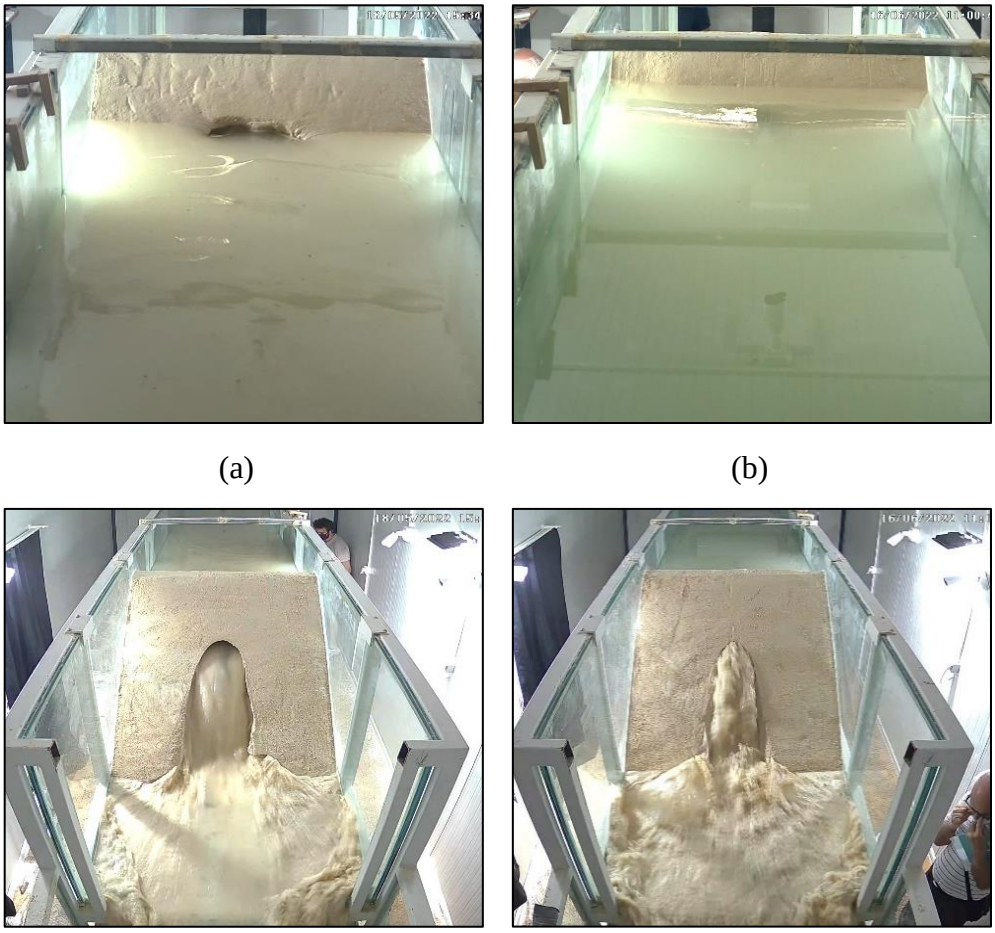

(a) (b)

(c) (d)

Figure 5.43. The breach views at t=40 s a) upstream of the first dam, b) upstream of the second dam, c) downstream of the first dam, d) downstream of the second dam

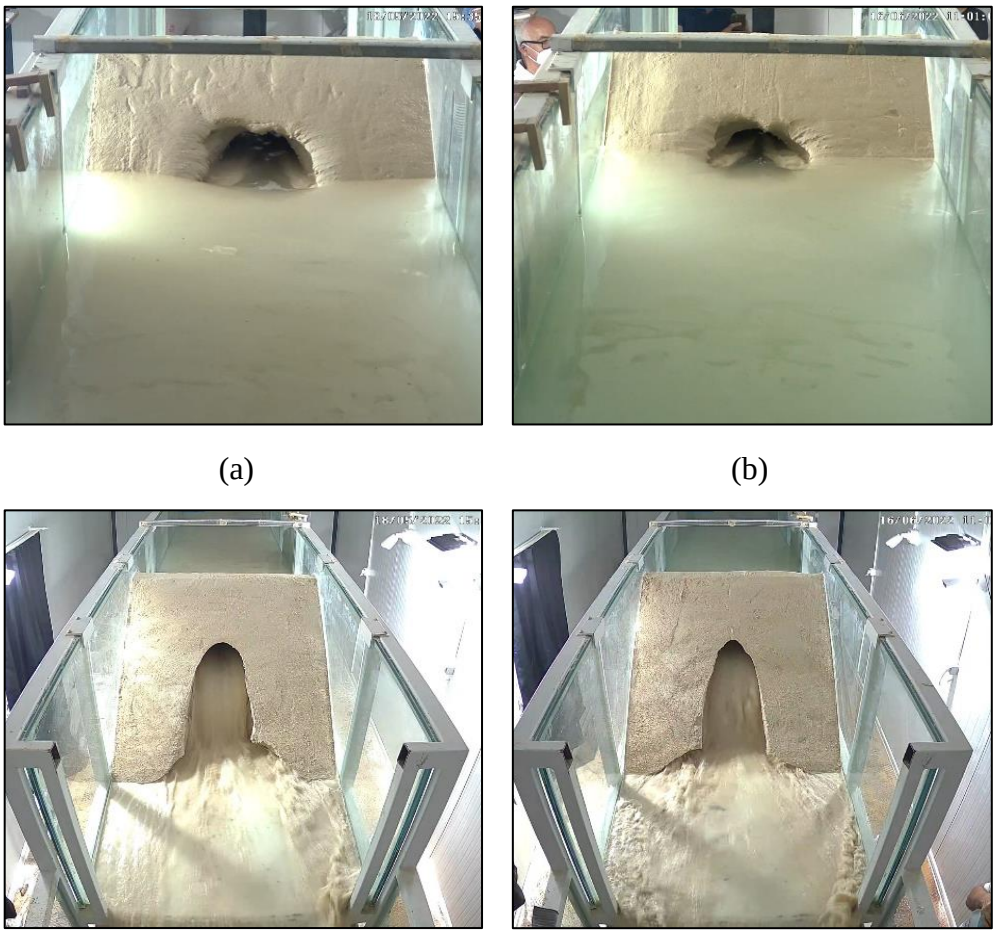

(a) (b)

(c) (d)

Figure 5.44. The breach views at t=60 s a) upstream of the first dam, b) upstream of the second dam, c) downstream of the first dam, d) downstream of the second dam

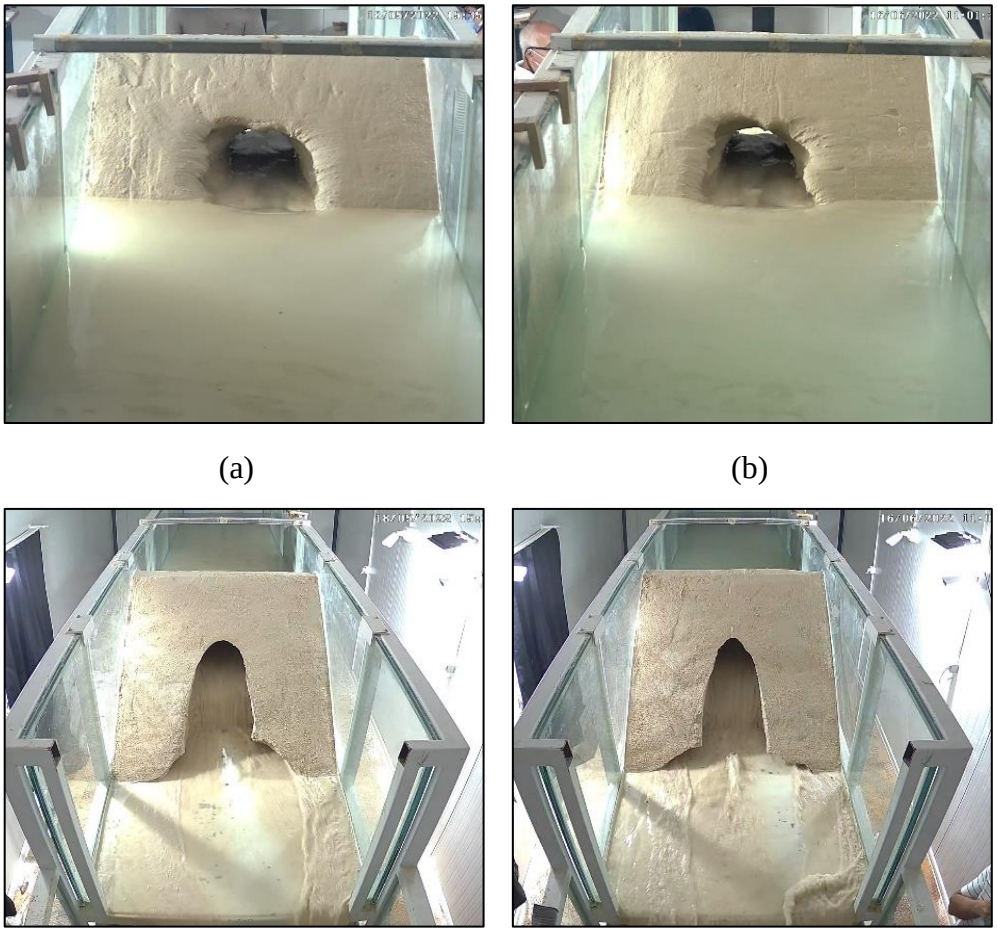

(a) (b)

(c) (d)

Figure 5.45. The breach views at t=90 s a) upstream of the first dam, b) upstream of the second dam, c) downstream of the first dam, d) downstream of the second dam

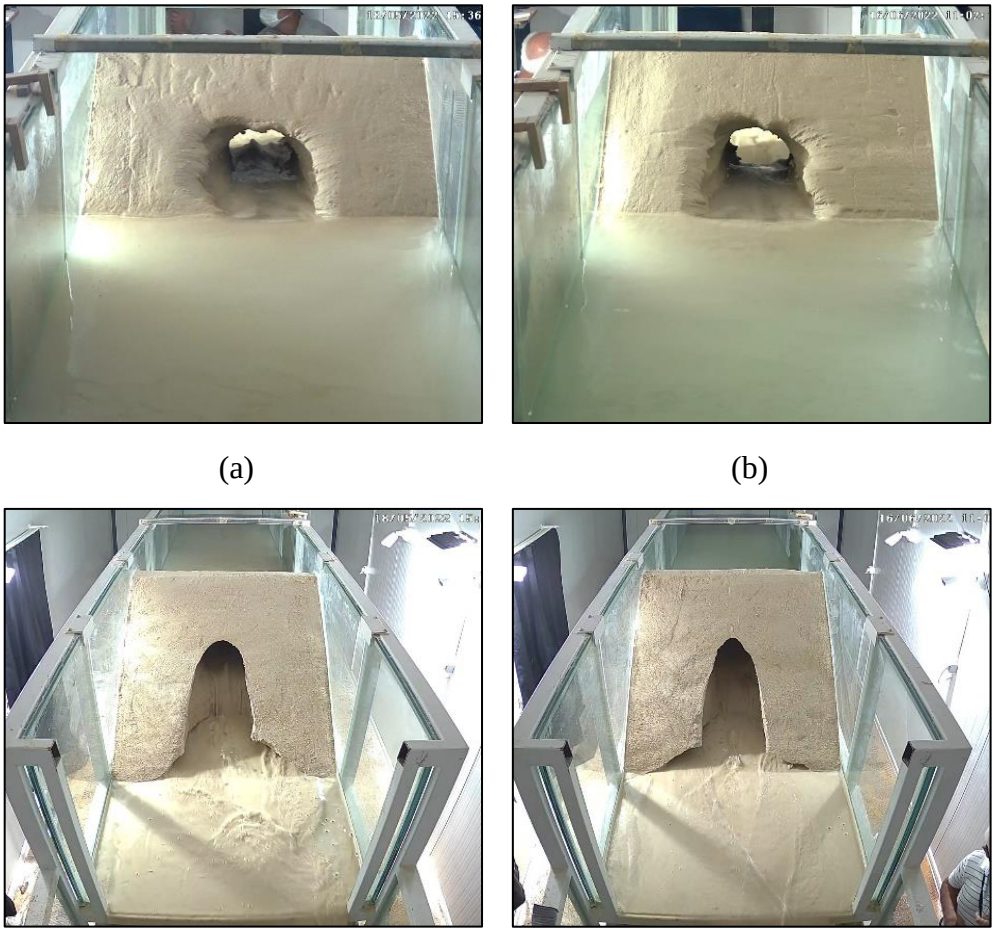

(a) (b)

(c) (d)

Figure 5.46. The breach views at t=134 s a) upstream of the first dam, b) upstream of the second dam, c) downstream of the first dam, d) downstream of the second dam

The temporal changes in water depth during the experiment are shown in Figure 5.47.

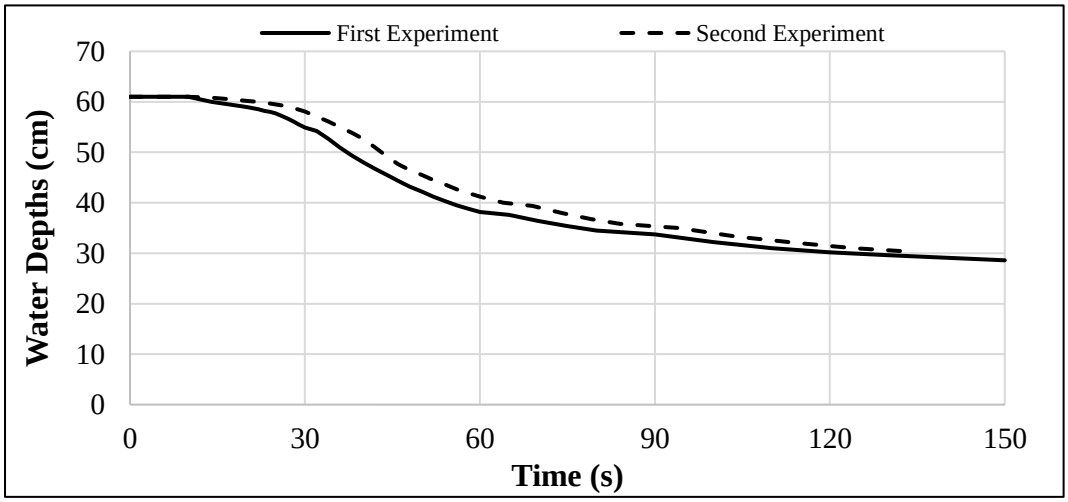

Figure 5.47. Temporal changes in water depths in the channel

The temporal breach developments at downstream and upstream sides together with the first and second experiment are given in Figure 5.48 and Figure 5.49, respectively.

The temporal variations of the breach-wetted areas at downstream and upstream are shown in Figure 5.50 and Figure 5.51, respectively.

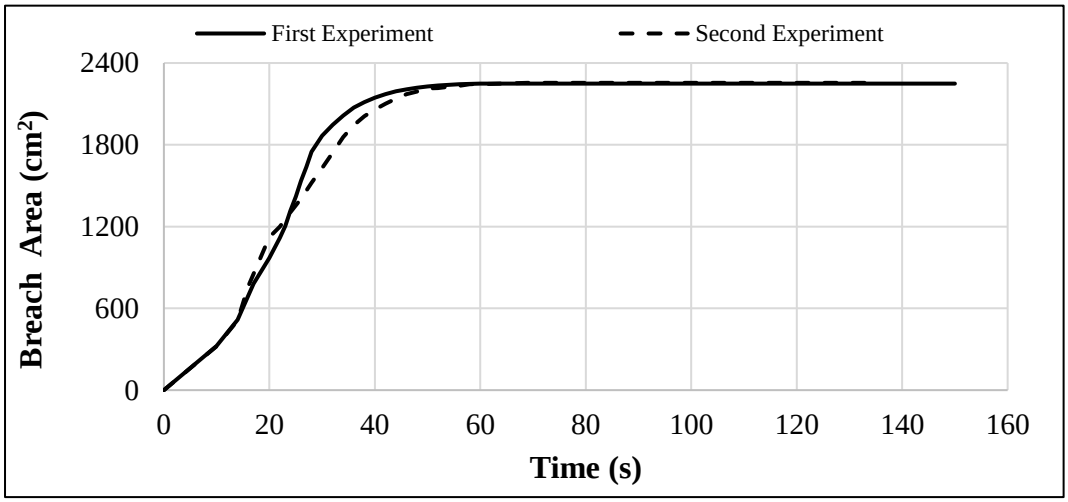

Figure 5.48. The downstream temporal breach developments

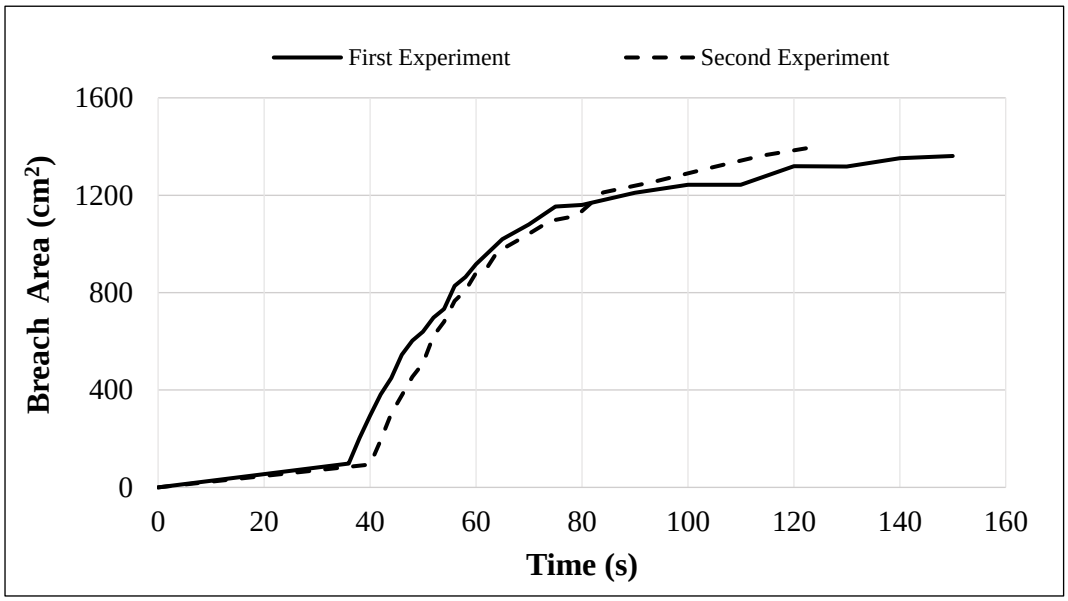

Figure 5.49. The upstream temporal breach developments

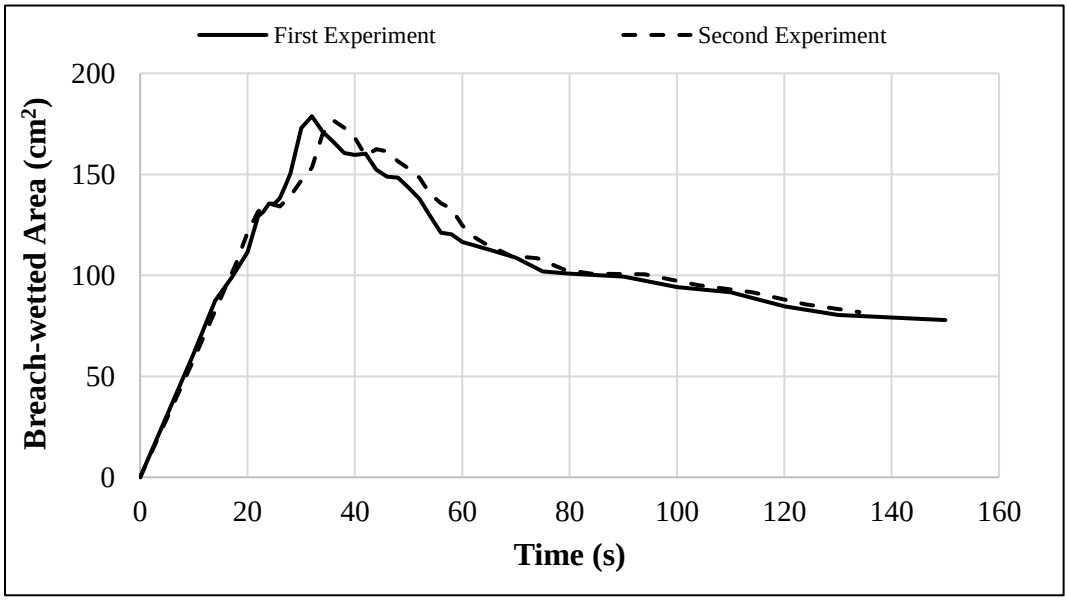

Figure 5.50. The temporal variations of the breach-wetted areas at downstream

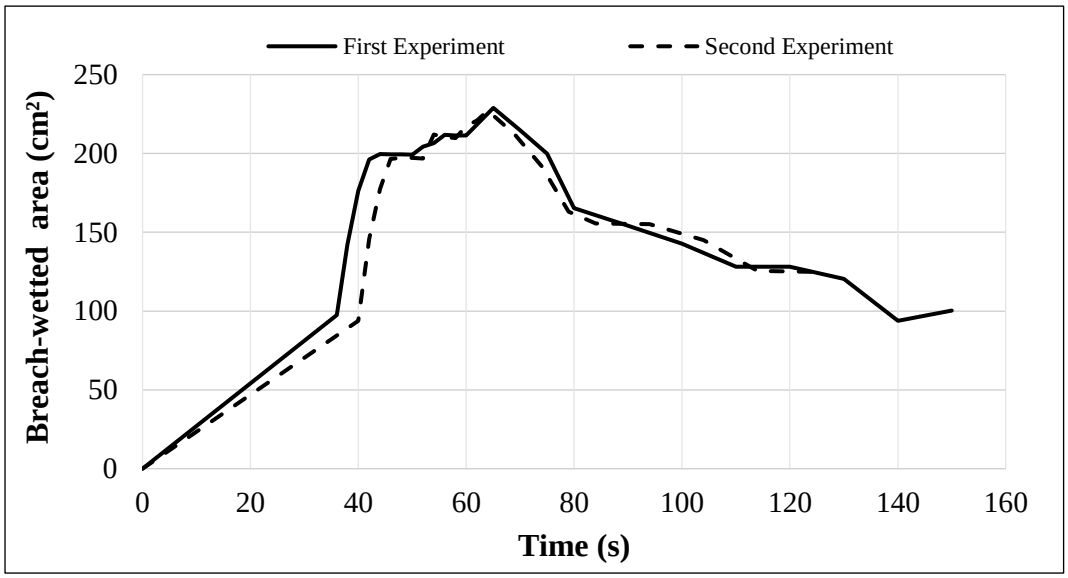

Figure 5.51. The temporal variations of the breach-wetted areas at upstream

The temporal breach discharges calculated from Equation (4.1) are presented in Figure 5.52.

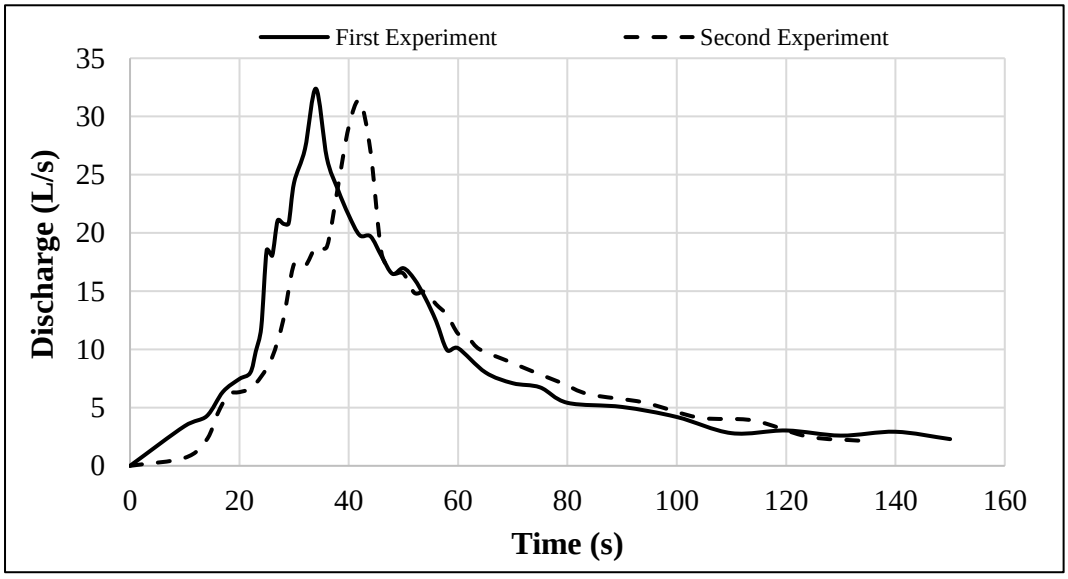

Figure 5.52. Temporal breach discharges

The time-varied downstream and upstream breach velocities, calculated by using Equation 4.2, are shown in Figure 5.53 and Figure 5.54, respectively.

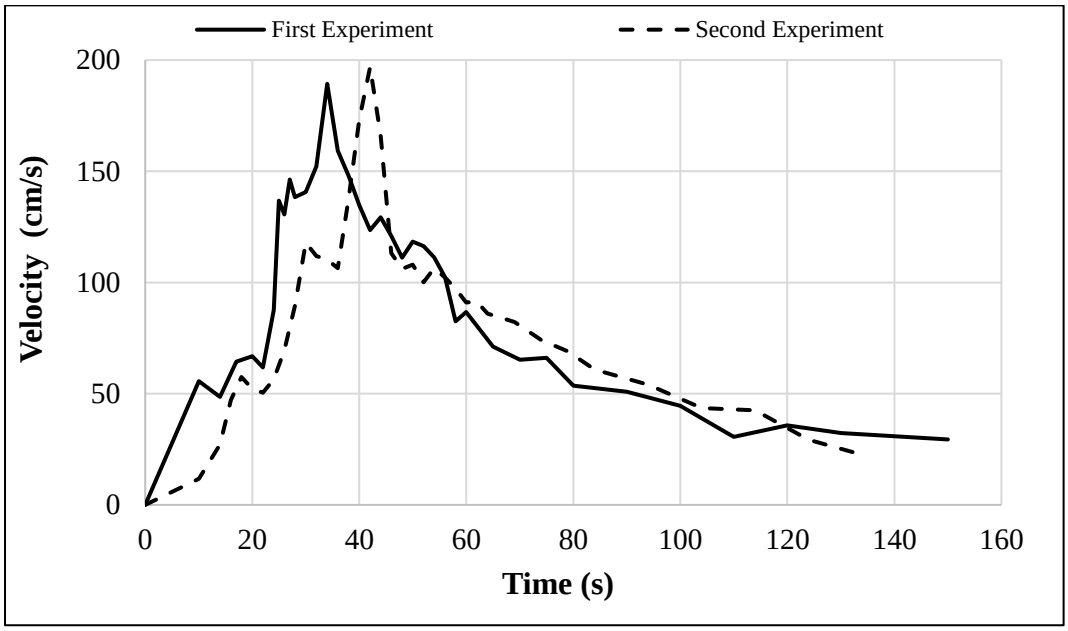

Figure 5.53. The time-varied downstream breach velocities

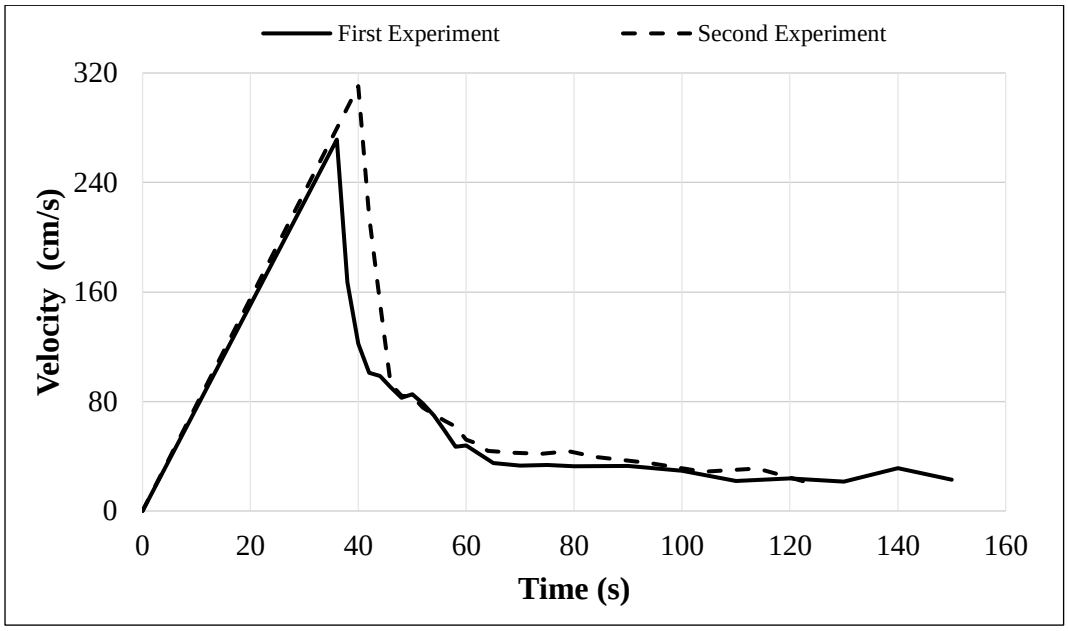

Figure 5.54. The time-varied upstream breach velocities

5.5. The compaction density effects

The experiments were conducted in the Izmir University of Economics laboratory by using mixture 1. For investigating the compaction density effect on the piping mechanism, the second and the third scenarios were compared to each other for the first t=37 s. Both dams have the same geometry, 65 cm height, and the same reservoir level, 61 cm. The second experiment (Chapter 6.2) was constructed with 26 proctor hammer blows to obtain a 2.5 cm sub-layer by providing the bulk density, ρ_{bulk}, 2.0 g/cm^3 (higher density) while the third experiment (Chapter 6.3) was conducted with 9 proctor hammer blows to obtain a 2.5 cm sub-layer by, ρ_{bulk}, 1.7 g/cm^3 (lower density) after pouring the soil material in the same volume.

Each dam has a 5x5 cm^2 weak zone which consists of rock salt along the dam axis. The slopes of the downstream and upstream of the scenarios are 1 vertical to 1.5 horizontal. Once the water reached the desired levels, the experiments were started.

The experiments were conducted by arranging the input discharges of 29.6 m^3/h for the higher-density dam body, and 6.2 m^3/h for the lower-density dam body.

The temporal changes in water depths in the channel together with lower and higher density dams during the experiments are shown in Figure 5.55.

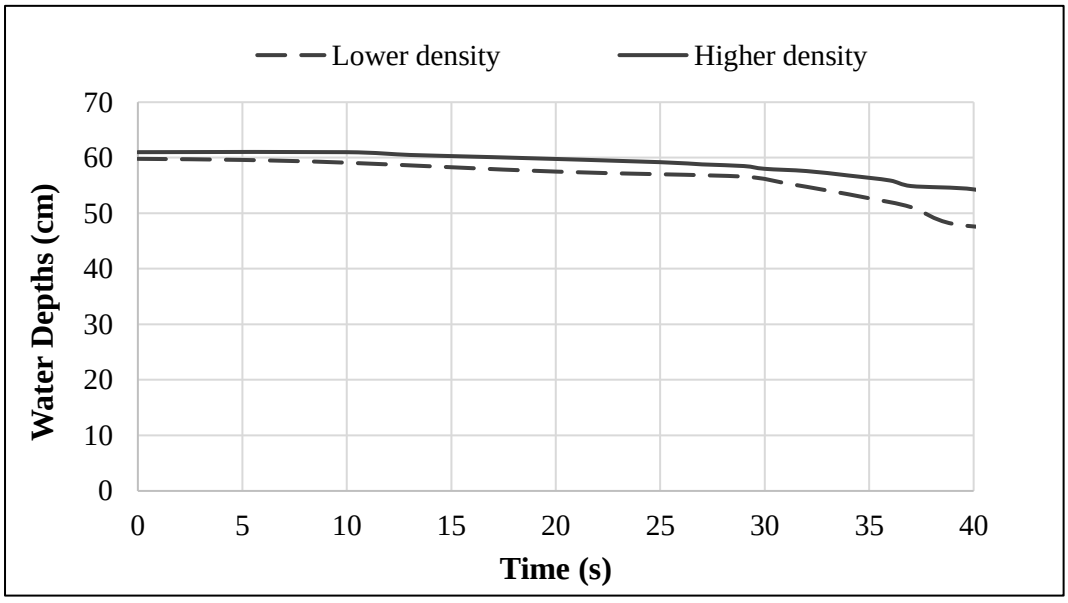

Figure 5.55. Temporal changes in water depths in the channel together with lower and higher density dams

The temporal breach developments at upstream together with the lower density and higher density dams are given in Figure 5.56.

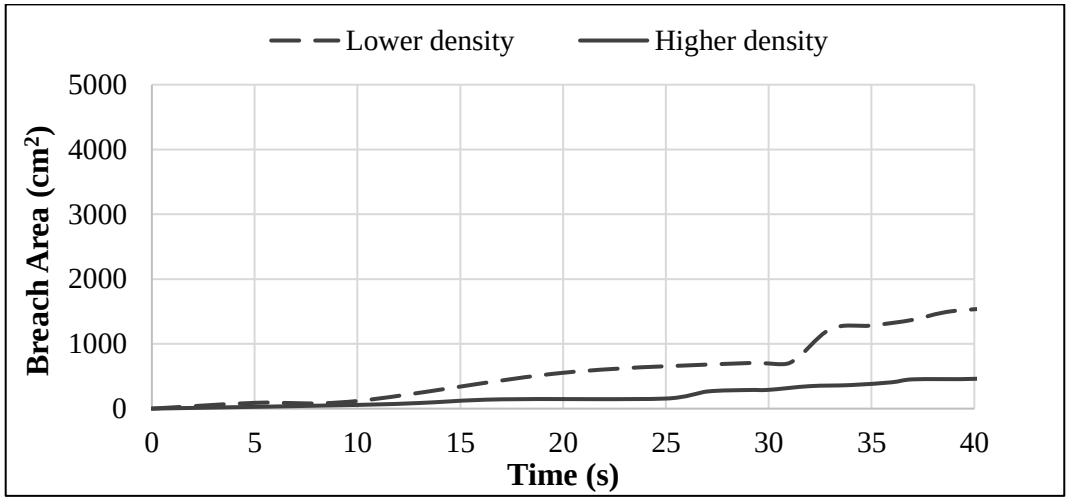

Figure 5.56. The temporal breach developments at upstream together with the lower density and higher density dams

The temporal variations of the breach-wetted areas at upstream together with the lower density and higher density dams are given in Figure 5.57.

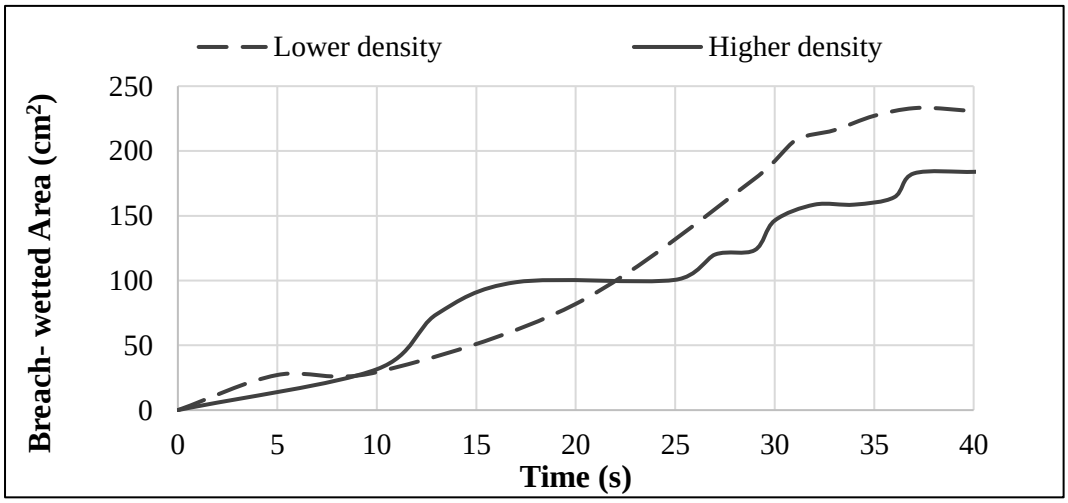

Figure 5.57. The temporal variations of the breach-wetted areas at upstream together with the lower density and higher density dams

The temporal breach discharges calculated from Equation (4.1) together with the lower density and higher density dams are presented in Figure 5.58.

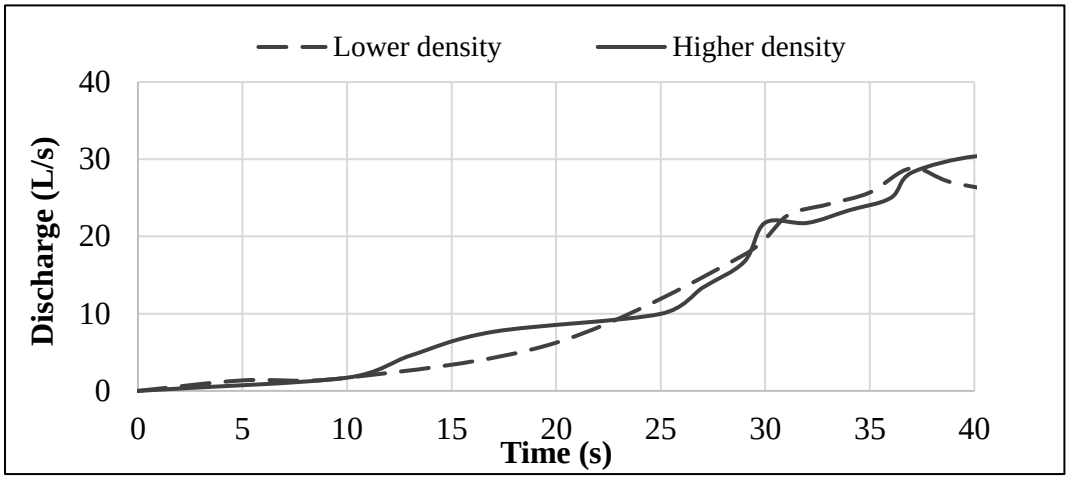

Figure 5.58. The temporal breach discharges together with the lower density and higher density dams

The time-varied upstream breach velocities, calculated by using Equation 4.2, together with the lower density and higher density dams are presented in Figure 5.59.

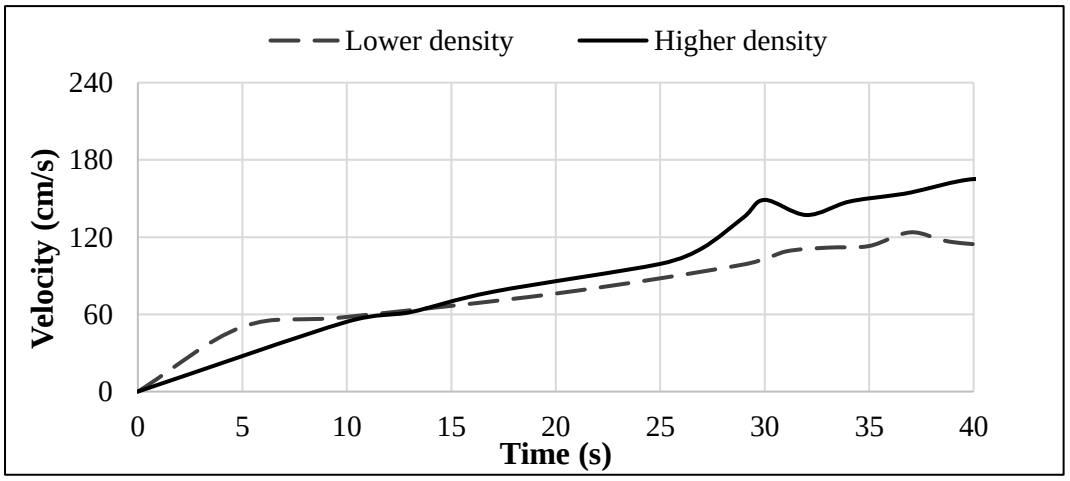

Figure 5.59. The time-varied upstream breach velocities together with the lower density and higher density dams

5.6. Results and Discussions

The experimental findings are commented on by taking into consideration the values corresponding to the interval where the initial water level decreased at most 10 % ($t_{10\%}$). The so-obtained comparative results are given in Table 5.2. In this table, $Area_{down10\%}$ and $Area_{up10\%}$ are the areas at downstream and upstream sides, respectively. $Wet_{down10\%}$ and $Wet_{up10\%}$ denote the wetted areas at downstream and upstream sides, respectively. $Q_{10\%}$ represents the flow rate through the breach. The velocities at downstream and upstream are denoted by $Velocity_{down10\%}$ and $Velocity_{up10\%}$, respectively.

Table 5.2. The so-obtained comparative results for at most 10 %

Findings	Experiment			
	1	2	3	4
$t_{10\%}$ (s)	19	37	37	33
$Area_{down10\%}$ (cm^2)	721	2711	-	1890
$Area_{up10\%}$ (cm^2)	365	452	1370	88.9
$Wet_{down10\%}$ (cm^2)	398	165	-	174
$Wet_{up10\%}$ (cm^2)	365	183	233	88.9
$Discharge_{10\%}$ (L/s)	28.6	28.3	28.8	24.2
$Velocity_{down10\%}$ (cm/s)	72	170	-	127
$Velocity_{up10\%}$ (cm/s)	78	155	124	248

The flow rates values corresponding to the times t=10 s, t=20 s, and t=30 s are given in Table 5.3

Table 5.3. The temporal discharges for different time intervals

Discharge (L/s)	Experiment			
	1	2	3	4
Q_{10}	12.5	1.7	1.7	2
Q_{20}	25.2	8.8	6.24	7.2
Q_{30}	30.5	21.8	22.6	19

The downstream and upstream breach areas corresponding to the times, t=10 s, t=20 s, and t=30 s are given in Table 5.4 and Table 5.5, respectively.

Table 5.4. The temporal breach developments at downstream for different time intervals

Downstream Breach Area (cm^2)	Experiment			
	1	2	3	4
$A_{down-10}$	551	1453	-	322
$A_{down-20}$	721	2145	-	1120
$A_{down-30}$	871	2406	-	1744

Table 5.5. The temporal breach developments at upstream for different time intervals

Upstream Breach Area (cm^2)	Experiment			
	1	2	3	4
A_{up-10}	144	58	118	27
A_{up-20}	365	148	553	54
A_{up-30}	753	290	703	81

The temporal variations of downstream and upstream breach-wetted areas corresponding to the times, t=10 s, t=20 s, and t=30 s are presented in Table 5.6 and Table 5.7, respectively.

Table 5.6. The temporal variations of downstream breach-wetted areas for different time intervals

Downstream Breach-wetted Area (cm^2)	Experiment			
	1	2	3	4
$Wetted_{downstream-10}$	242	124	-	60
$Wetted_{downstream-20}$	462	135	-	125
$Wetted_{downstream-30}$	441	152	-	152

Table 5.7. The temporal variations of upstream breach-wetted areas for different time intervals

Upstream Breach-wetted Area (cm^2)	Experiment			
	1	2	3	4
$Wetted_{upstream-10}$	144	32	29	27
$Wetted_{upstream-20}$	365	99	82	54
$Wetted_{upstream-30}$	451	146	207	81

The time-varied of downstream and upstream breach velocities corresponding to the times, t=10 s, t=20 s, and t=30 s are given in Table 5.6 and Table 5.7.

Table 5.8. The time-varied downstream breach velocities for different time intervals

Downstream Velocity (cm/s)	Experiment			
	1	2	3	4
$V_{down-10}$	52	14	-	34
$V_{down-20}$	58	64	-	57
$V_{down-30}$	64	143	-	152

Table 5.9. The time-varied upstream breach velocities for different time intervals

Upstream Velocity (cm/s)	Experiment			
	1	2	3	4
V_{up-10}	87	54	58	75
V_{up-20}	69	86	76	151
V_{up30}	68	149	108	226

The time interval corresponding to the decrease of the initial water by 10% was found to be nearly the same for the last three experiments, this time being nearly twice that of the first experiment.

The flow rates are found to be nearly equal.

In all experiments, the downstream areas were found to be greater than the upstream ones.

The orders of magnitude of the wetted areas were found to be similar for the dams of heigh 60 cm and 65 cm.

The temporal changes of downstream breach areas are likely linear.

The breach areas at upstream were influenced significantly by the compaction density, the compaction decreasing the breach areas.

It was revealed, the increase of the dam height and consequently the water head resulted in increase of the breach areas at downstream and upstream sides.

The wetted areas were found to be larger in the dam 60 cm high compared to those corresponding to the dam 65 cm high.

,

CHAPTER 6

3D FINITE ELEMENT ANALYSIS OF BREACHING OF HOMOGENOUS EARTH-FILL DAMS

Numerical simulations were performed using PLAXIS 3D to compare with the experimental findings.

The seepage forces can cause transportation according to the value of the hydraulic gradient, i, defined in Darcy's equation (V=k·i). The critical hydraulic gradient, i_{cr}, which causes the erosion is given in Equation 6.1.

$$i_{cr} = \frac{(\gamma_{sat} - \gamma_w).(1-n)}{\gamma_w} \tag{6.1}$$

where γ_{sat} is the saturated unit weight, γ_w is the unit weight of water, and n denotes the porosity.

6.1. Finite Element Method

6.1.1. Methodology

During the numerical analyses, after completing the dam geometry, mesh generation was accomplished by selecting as 0.4 for the relative element size and 0.4635 m for element dimension. Enhanced mesh options were utilized by arranging the global scale factor to 0.5 and the minimum element size factor to $5 \cdot 10^{-6}$ m.

The surface groundwater flow boundary condition (Surface GWFlowBC) was defined. The behavior was set as head option then the reference level was described as initial water level.

The general subtree in the staged construction tab was arranged to represent the experiment conditions. The water levels were arranged in steady-state calculation types when the levels remain unchanged. The fully coupled flow deformations option was used when the change in the water level occurred. For the simulations in time-dependent flow conditions, the temporal changes in water level in each scenario were transferred to the PLAXIS 3D as a table by assigning flow functions.

The flows within the dam body were obtained as a result of the simulations. To obtain the average velocity values, the relevant soil numbers at the upstream and downstream sides of the breach were considered. The values and corresponding soil numbers were reached as a table sheet in the output file.

The wetted areas were considered as flow distributions at the breach upstream and downstream sides and calculated by using Gauss's area method. The surface areas are calculated when hydraulic gradient values reach or exceed the threshold value at the dam.

Discharges at different time intervals are calculated by considering the wetted areas and the average velocity at the downstream and upstream sides of the breach. They calculated from Equation 4.2. The discharges are calculated for both downstream and upstream sides and the average values were determined. Since the bottom and the lateral sides of the dams were impermeable, the boundary conditions were selected as closed. Consequently, the boundary conditions were Z_{min}=Closed, Z_{max}=Open, Y_{min}=Y_{max}= Closed, and X_{min}=X_{max}= Open. The representation of wetted areas together with the phreatic level is given in Figure 6.1.

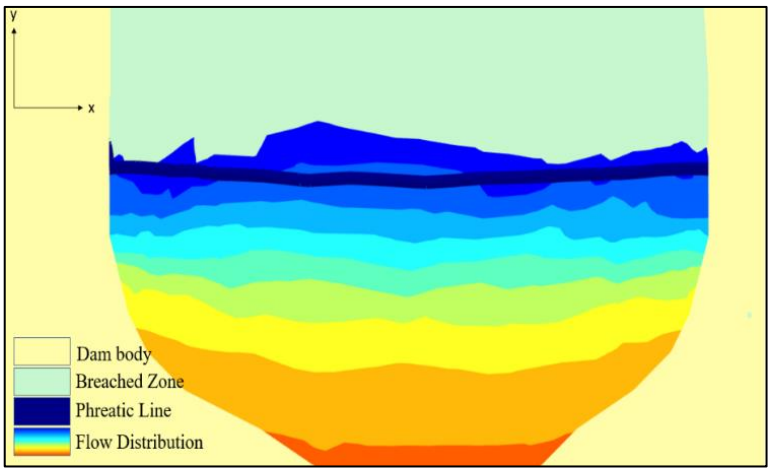

Figure 6.1. The representation of wetted area together with phreatic surface

The Root Mean Square Error (RMSE) and Mean Absolute Error (MAE), given in following equations, were used to evaluate the compatibility between experimental and numerical studies.

$$RMSE = \sqrt{\sum_{i=1}^{n} \frac{\left(Q_{experimental} - Q_{numerical}\right)^2}{n}} \tag{6.2}$$

$$MAE = \frac{1}{n}\sum_{i=1}^{n} \left|Q_{experimental} - Q_{numerical}\right| \tag{6.3}$$

where n is the number of data.

6.1.2. The Soil Properties

For the simulations, it is essential to define soil properties in each soil volume. The dam soil properties have been obtained from the soil mechanics tests (see Chapter 3.1). Since air parameters can not be defined, an estimation was performed to describe the properties of the weak zones such as hole or rock salt.

The H.S. Model-Undrained A model was used for the dam soil properties while the H.S. model-Undrained B model was chosen for the weak and breached zones model types.

The initial void ratio of the breach volume was selected as 0.9. Since the hole was considered as the filled by the air, the unsaturated ($\Upsilon_{unsat\text{-}weak}$) was taken as air density. When the hole was filled with water, the saturated unit weight ($\Upsilon_{sat\text{-}weak}$) was taken because of considering filled by the water. The undrained shear strength ($S_{u\text{-}weak}$) value was taken as 0.1 kN/m^2 to avoid numerical errors.

The oedometric modulus of deformation (E_{oed}) was obtained according to the consolidation test. As average values for various soil types, $E_{ur} = 3 \cdot E_{50}$ and $E_{oed} = E_{50}$ are suggested as default settings. (PLAXIS user manual, 2022).

The permeability coefficients in the breach were calibrated according to the first velocity measurement at the breach downstream. The permeability of the rock salt was

calibrated according to the first seepage discharge. When the erosion existed, the second calibration was performed to satisfy the next seepage discharge measurement. When the breached soil reached the upstream face, the third calibration was made to adjust the downstream velocity at the experiment.

The soil properties used in the numerical analyses are given in Table 6.1.

Table 6.1. The soil properties used in the finite element analyses

Input	Mixture 1	Mixture 2	Upper breach		Middle breach	Bottom breach	
			Upper-middle	Upper-corner	Breach zone	Breach zone	Rocksalt
Material	Hardening Soil						
Drainage type	UND-A		UND-B				
$\Upsilon unsat$ (kN/m^3)	20		0.012				1
Υsat (kN/m^3)	21.2		10				
e_{init}	0.469	0.488	0.9				
$E_{50, ref}$ (kN/m^2)	35,714	13,810	1000				
$E_{oed, ref}$ (kN/m^2)	35,714	13,810	1000				
$E_{ur, ref}$ (kN/m^2)	107,142	41,430	3000				
c' (kN/m^2)	15.33	11.68	-				
φ (º)	33.9	39.84	-				
S_u (kN/m^2)	-	-	0.1				
k (m/s)	$4.70 \cdot 10^{-7}$	$1.18 \cdot 10^{-6}$	0.47	0.32	1	0.054/1.1	0.022

6.1.3. Modelling of Piping Evolution

The critical hydraulic gradients, i_{cr}, for mixture 1 and mixture 2 were calculated from Equation 3.1 and found to be 0.76 and 0.74, respectively.

The locations where $i_s > i_{cr}$ were determined by means of a 3D python algorithm integrated with the Jupyter console after the manual calculation at time t=0. If the simulated hydraulic gradient reaches or exceeds the critical hydraulic threshold (i_{cr}), then localized piping is initiated and developed in these locations (Saliba et al., 2019).

The dam geometries were defined as 2 m in length, 0.6 m or 0.65 m in height, and 1 m in width. After setting the boundary and initial conditions, the first simulation is started manually, then the python algorithm takes over the analysis. After the determination of the coordinates of the region where $i_s = i_{cr}$, x coordinates are sorted by number starting from the downstream side with different intervals, dx, ranging from 5 to 10 cm. They were denoted by Xa, Xb, Xc… (Xa>Xb). Afterward, the y and z coordinates at each corresponding x coordinate are sorted to create surfaces.

Surfaces are created from the starting point (Ymin, Zmax) to the endpoint (Ymax, Zmax) in the counterclockwise direction to cover the higher hydraulic gradient values by obtaining Ymax and Ymin values at Zmin and Zmax and vice versa, respectively.

The simple and not scaled representation of the creation of breach surfaces is given in Figure 6.2.

.

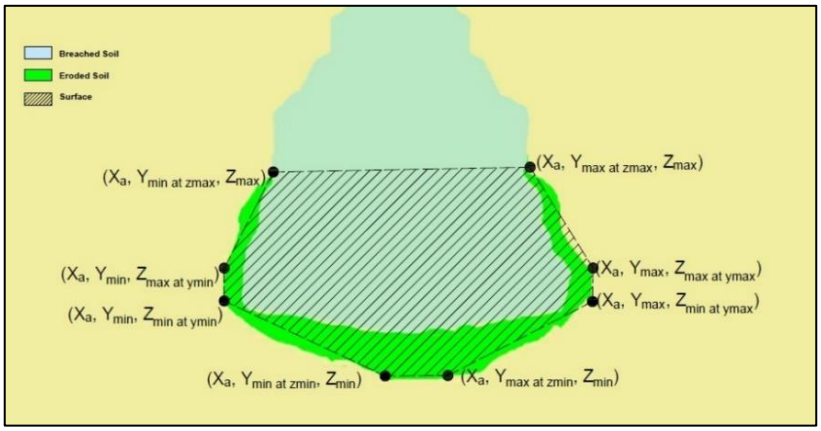

Figure 6.2. Not scaled representation of the creation of breach surfaces

The so obtained surfaces were linked to each other by extruding them in the x direction via the intersection and re-cluster command to create the breached soil volume. Since the created breached soil volumes have complex geometry, sometimes small or external distances appeared in the intersection zone. In such cases, “check the geometry” command was used to detect their locations. To do so, the locations partitioned with a closed box for isolating each partition to mesh generation (*Error When Generating 3D Mesh - GeoStudio | PLAXIS Wiki - GeoStudio | PLAXIS - Bentley Communities, 2019b*, accessed on December 4th, 2022). After the definition of the soil parameters into the breached soil volumes, the mesh generation was accomplished for the next time steps and the input files were saved.

The flow chart corresponding to the python algorithm is given in Figure 6.3. For the continuation of the simulation at new time steps, the initial flow boundary conditions were set. Therefore, the python algorithm completes the loops until the criteria was no longer satisfied.

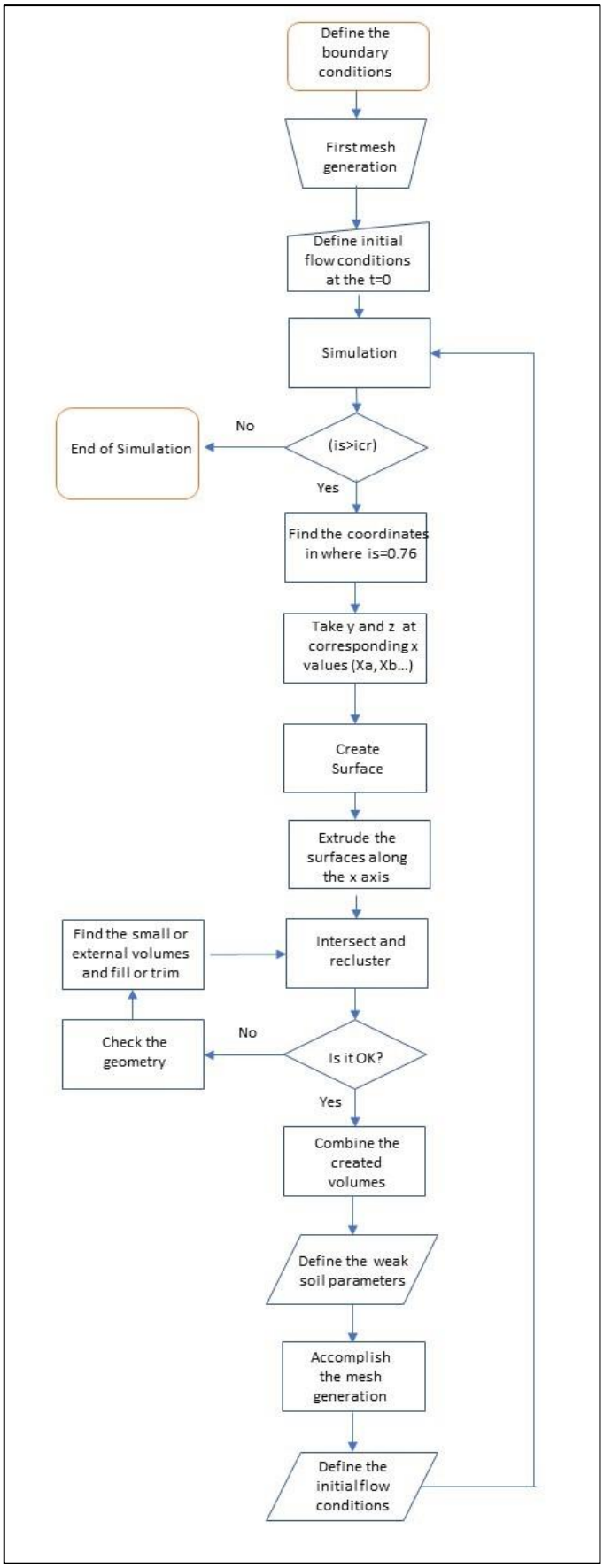

Figure 6.3. Flow chart of the applied 3D python algorithm

6.2. Numerical Simulation of the Experimented Dams

6.2.1. Numerical analysis corresponding to the first experiment

The details of the experiment are given in Chapter 5.1. The final geometry of the dam corresponding to the first experiment is given in Figure 6.4. The red color represents the weak zone.

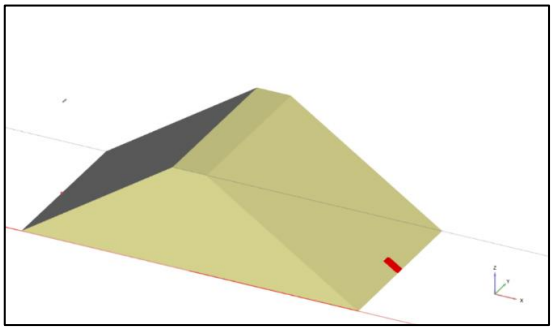

Figure 6.4. The final geometry of the first experiment

6.2.1.1. When the breach was not reached the upstream face

The experimental and numerical seepage discharges are given in Figure 6.5.

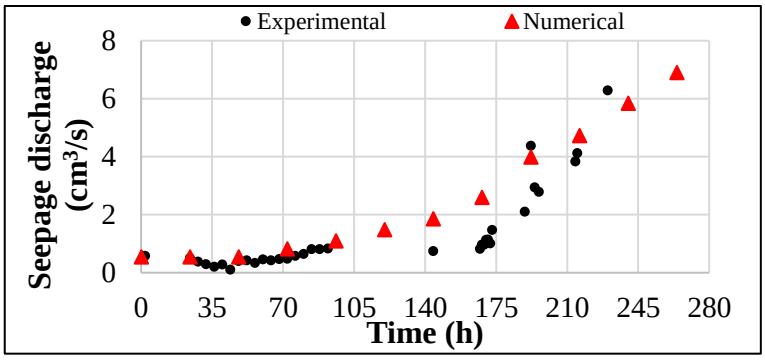

Figure 6.5. Experimental and numerical seepage discharges before the breach reached upstream face

The longitudinal views of the hydraulic gradient distributions together with cross sections when the breach did not reach the upstream are given in Figure 6.6.

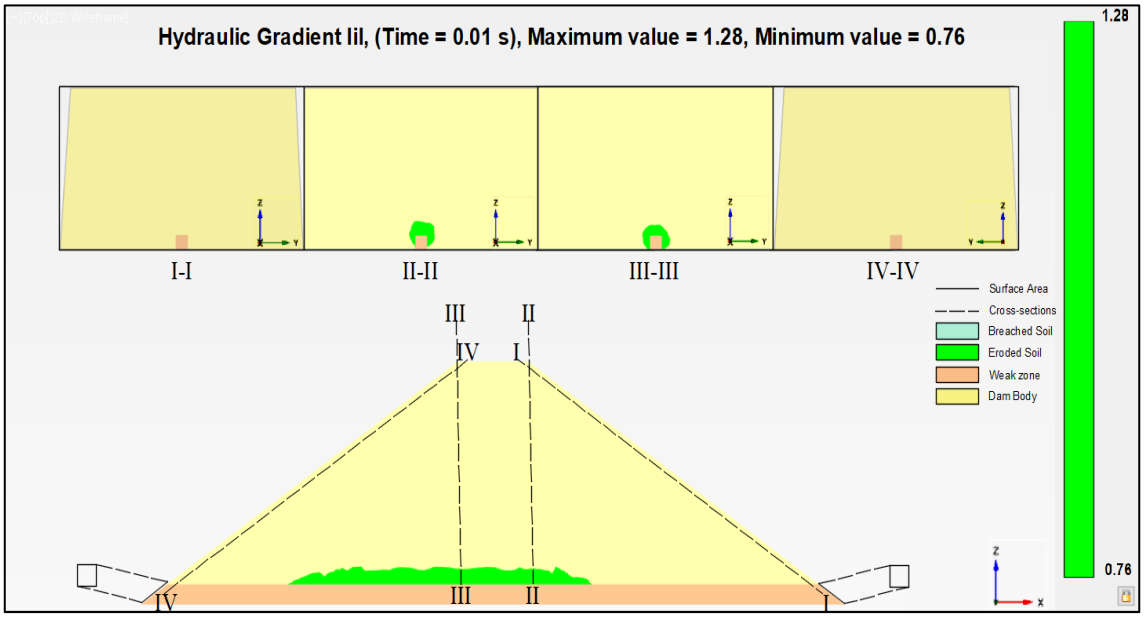

(a)

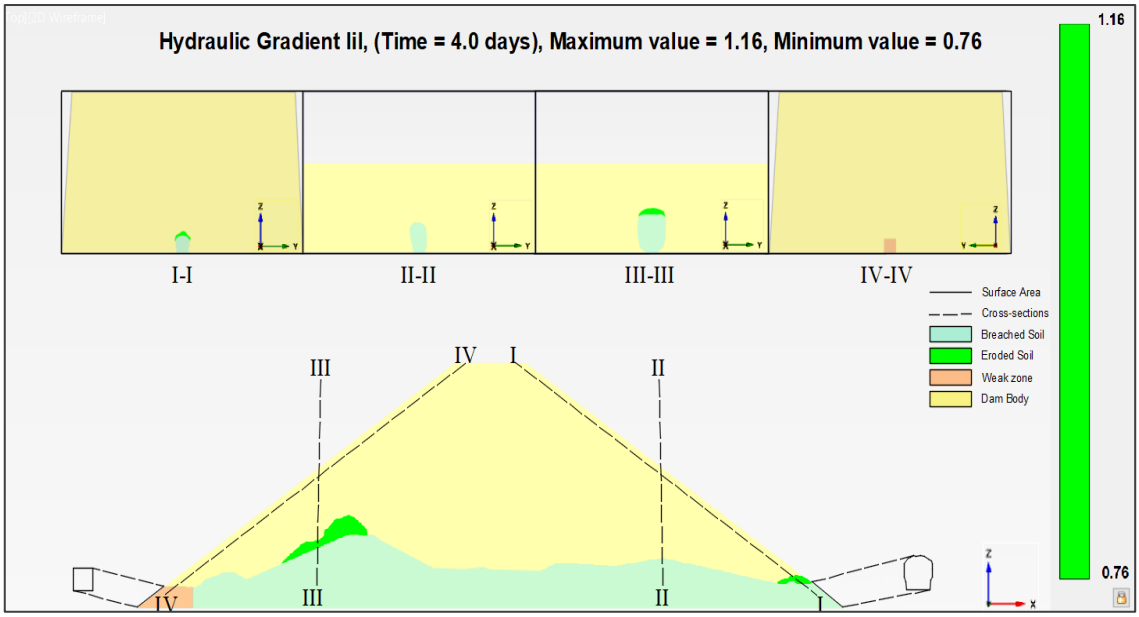

(b)

Figure 6.6. Hydraulic gradient distribution along the dam before the breach did not reach the upstream face for a) 0 days, b) 4 days

(cont. on next page)

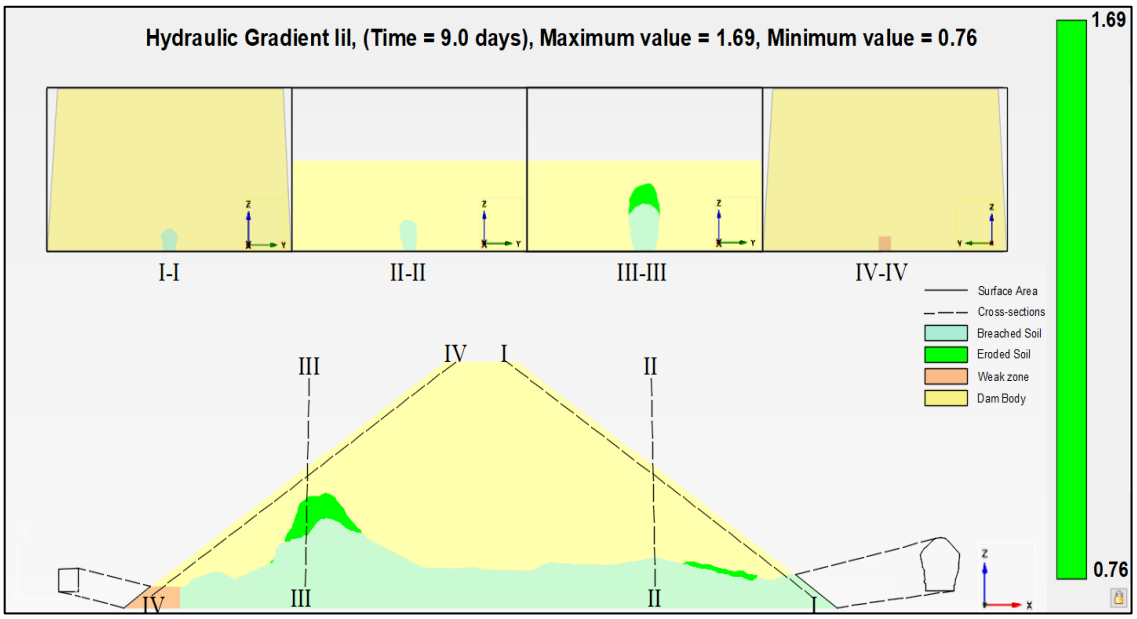

(c)

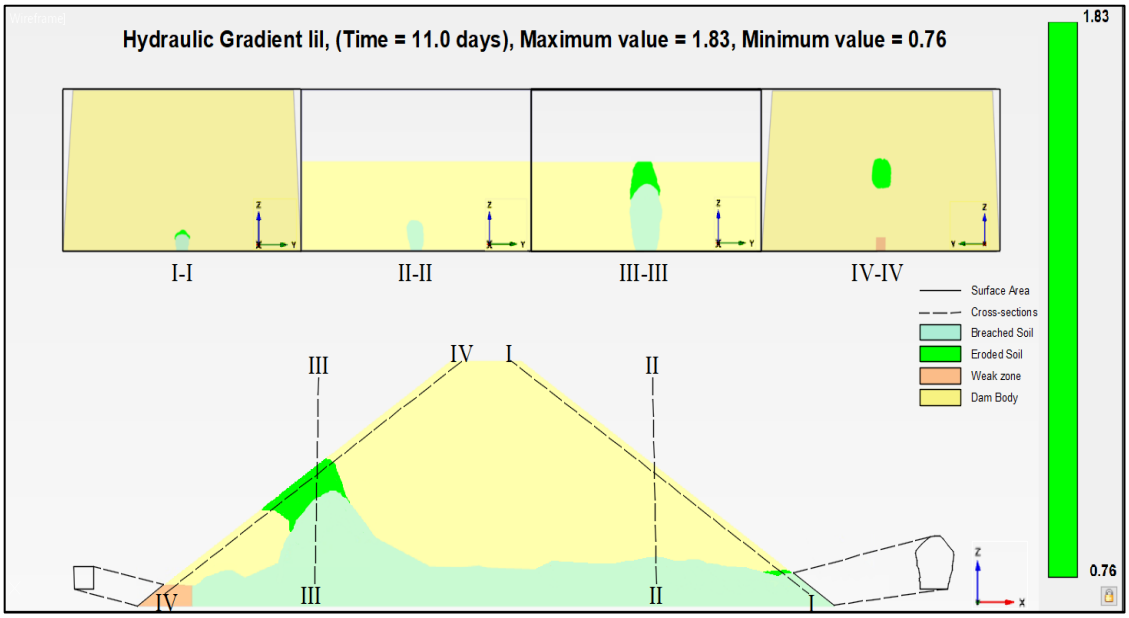

(d)

Figure 6.6. (cont.)

The numerical simulation was performed by considering the temporal changes in the water level in Figure 5.12 and defined as time-dependent flow conditions in fully coupled flow deformations.

6.2.1.2. When the breach reached the upstream face

When the breach reached the upstream side, the longitudinal hydraulic gradient distributions in color scale with maximum and minimum values are given in Figure 6.7.

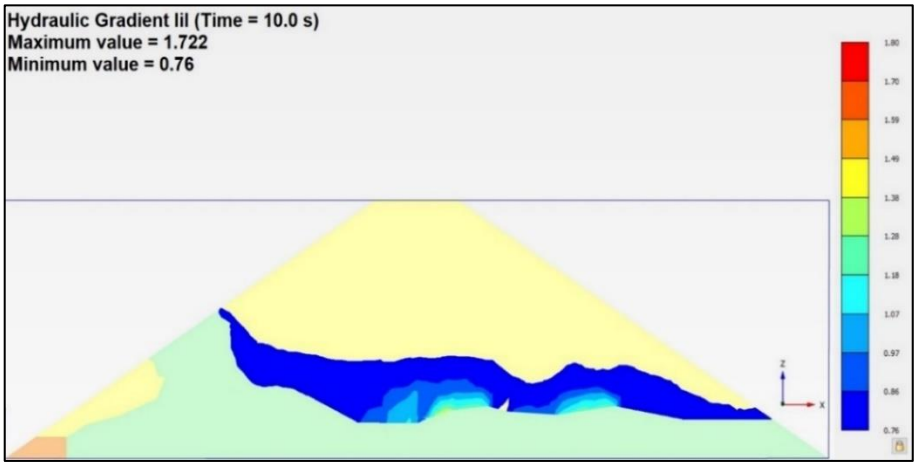

(a)

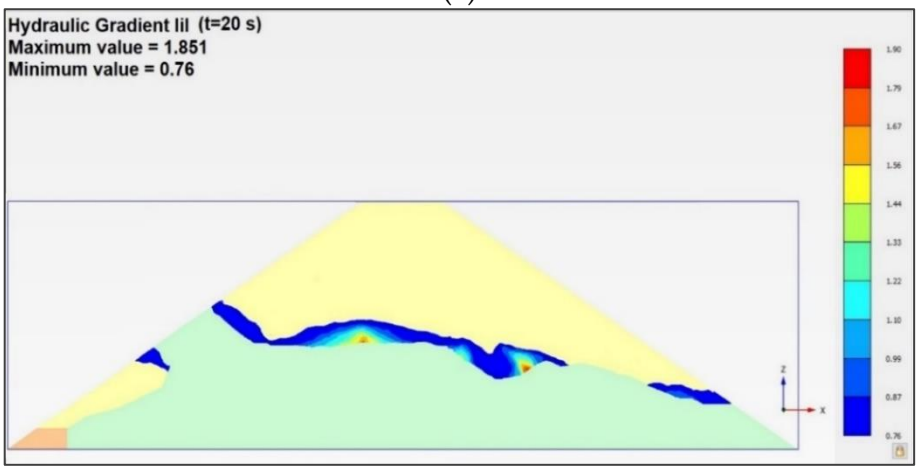

(b)

Figure 6.7. Hydraulic gradient distribution along the dam after the breach reached the upstream face for (a) 10 s (b) 20 (c) 30 s (d) 120

(cont. on next page)

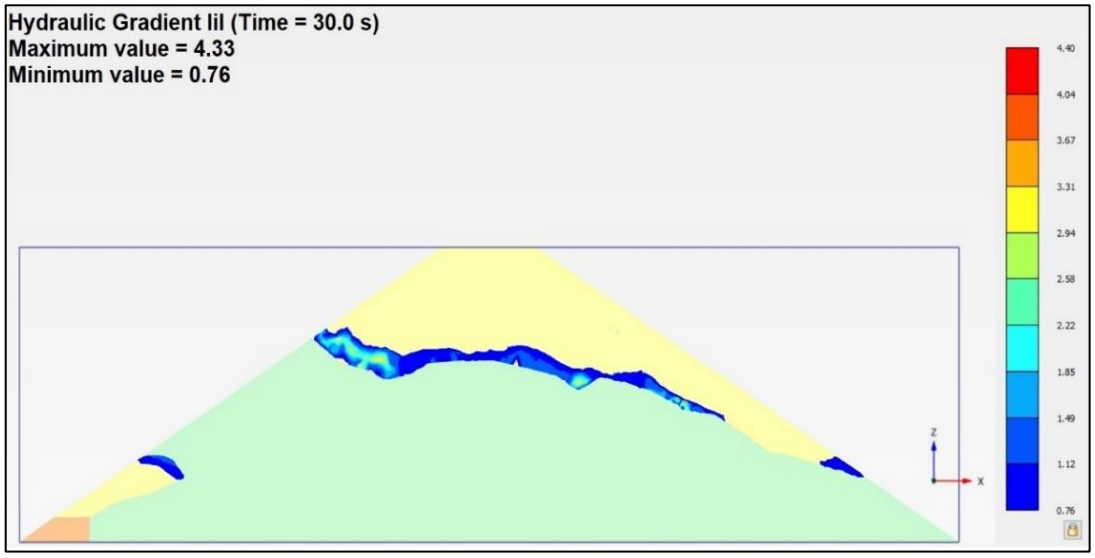

(c)

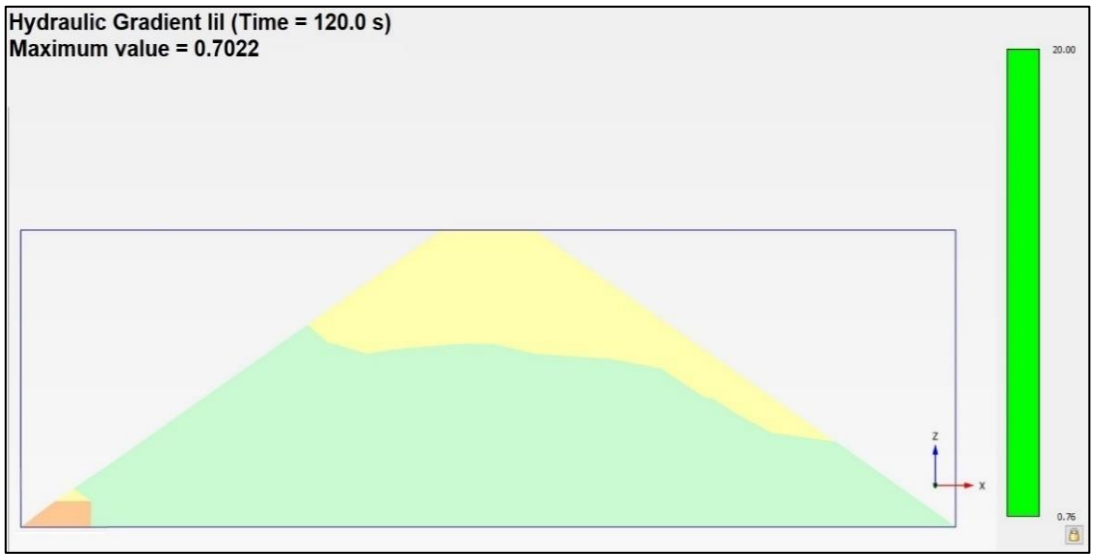

(d)

Figure 6.7. (cont.)

The flow through the breach together with upstream and downstream average values are given in Figure 6.8.

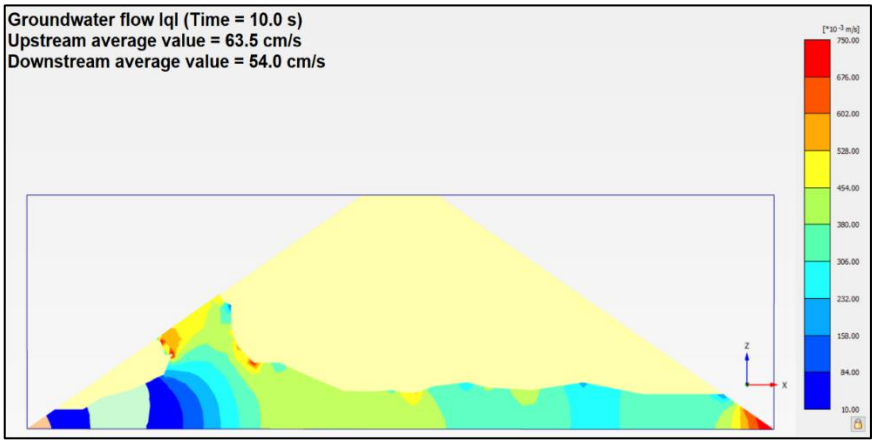

(a)

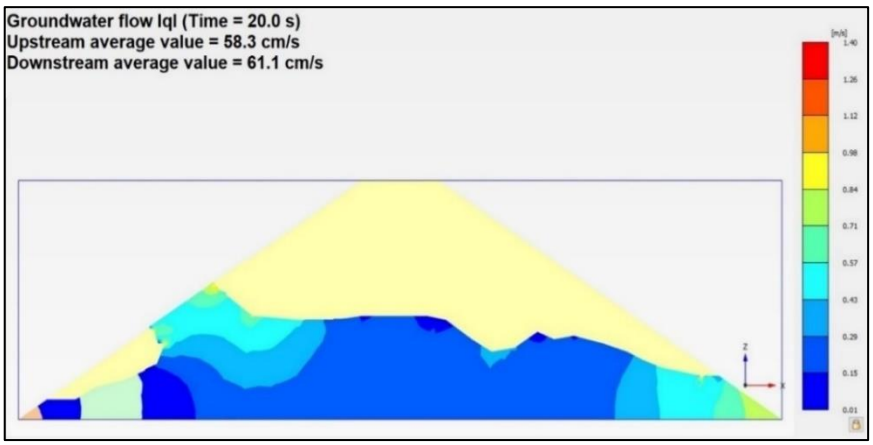

(b)

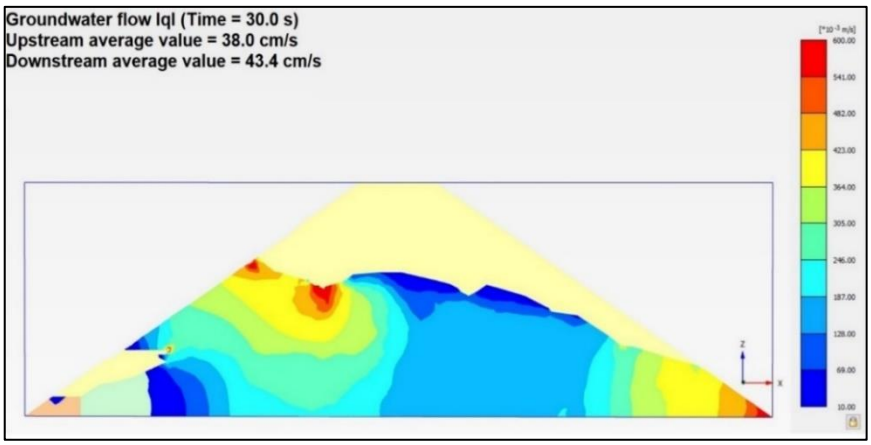

(c)

Figure 6.8. Flow distributions along the dam for a) 10 s (b) 20 s (c) 30 s (d) 120 s

(cont. on next page)

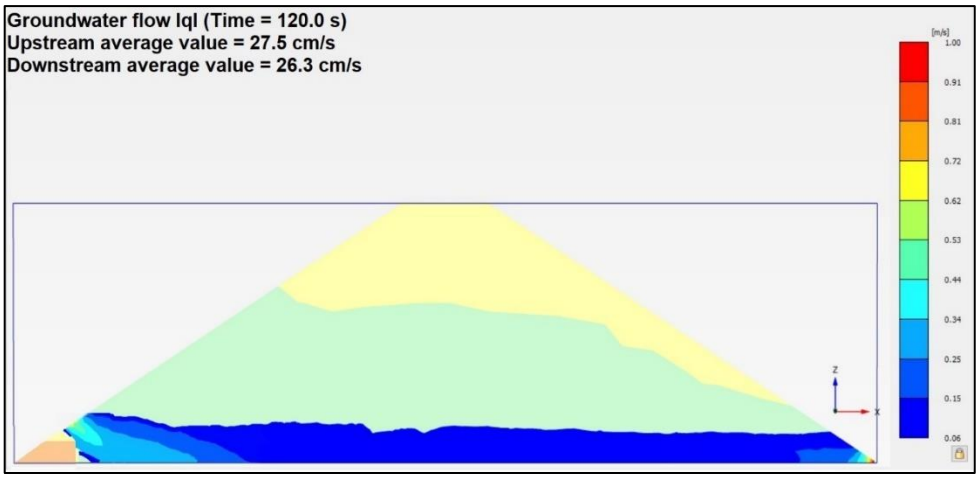

Figure 6.8. (cont.)

The downstream and upstream temporal breach developments in the experiment together with those obtained from the numerical analysis are given in Figure 6.9 and Figure 6.10, respectively. The time t=0 s indicates the initiation of seepage.

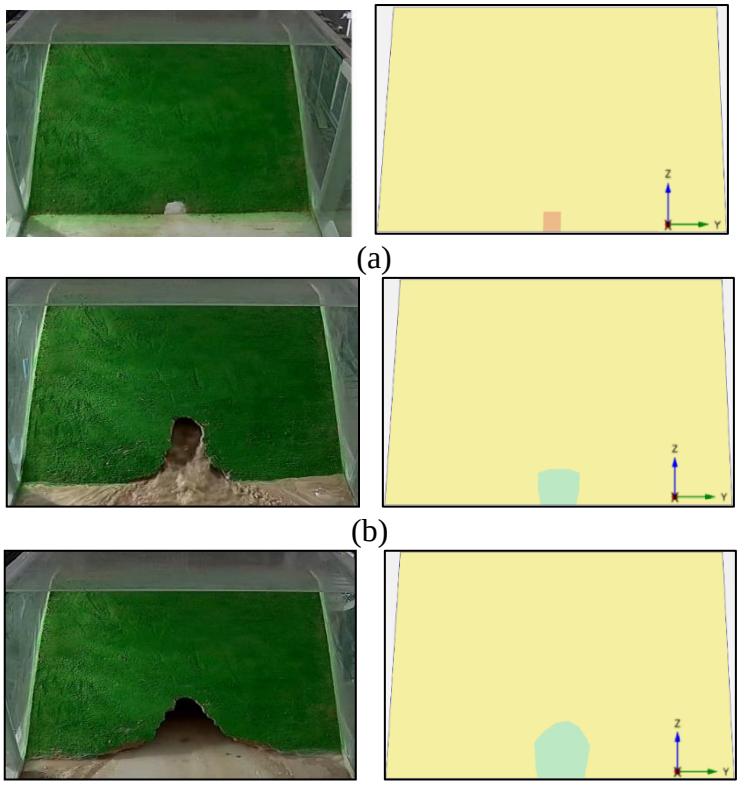

(a)

(b)

(c)

Figure 6.9. The downstream temporal breach developments a) 0 s, b) 10 s, c) 120 s

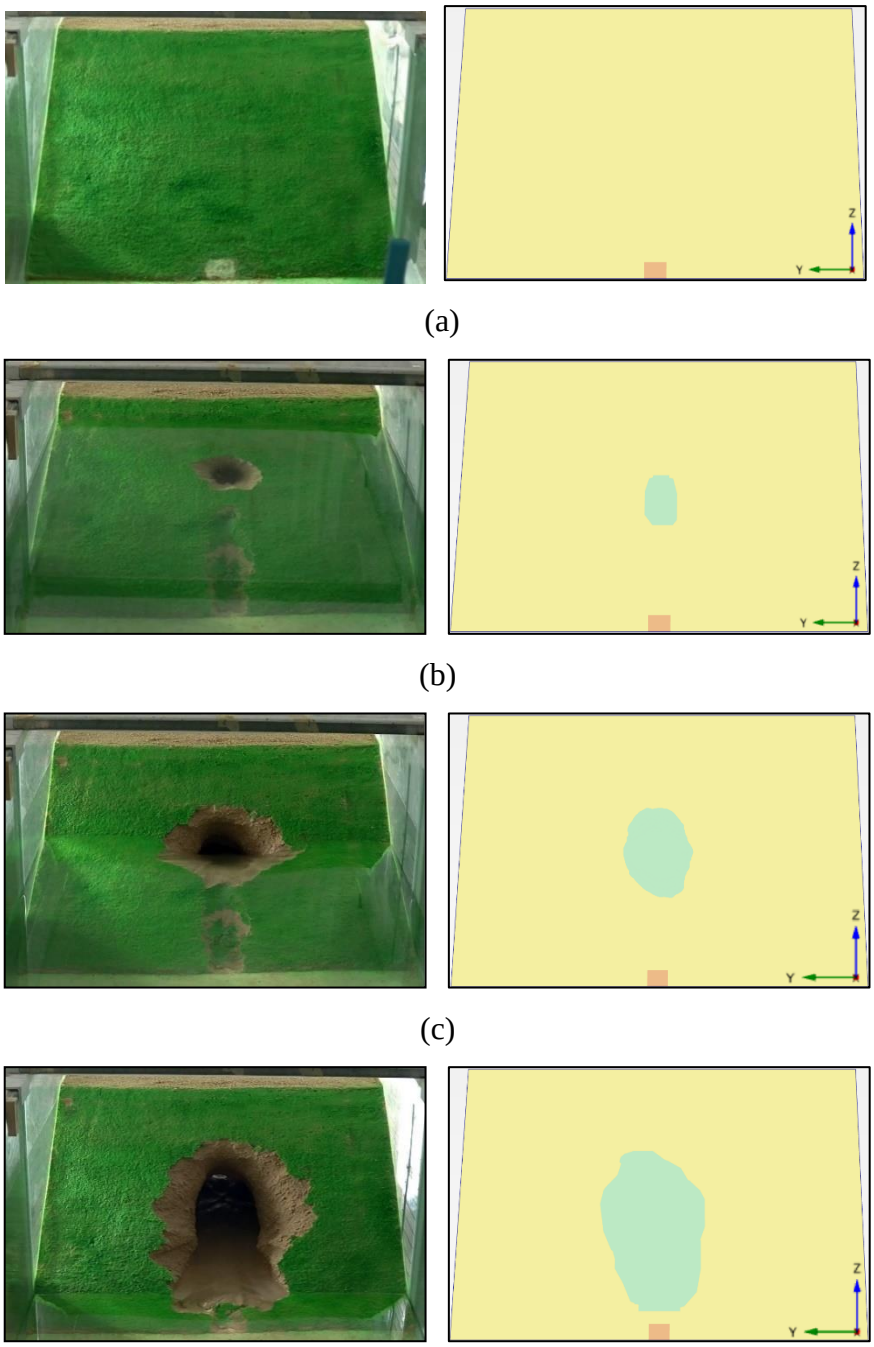

(a)

(b)

(c)

(d)

Figure 6.10. The upstream temporal breach developments a) 0 s, b) 10, c) 30 s, d) 120 s

The experimental and numerical temporal breach developments are presented in Figure 6.11 and Figure 6.12 for downstream and upstream, respectively.

The experimental and numerical time-varied breach velocities are presented in Figure 6.13 and Figure 6.14 for downstream and upstream, respectively.

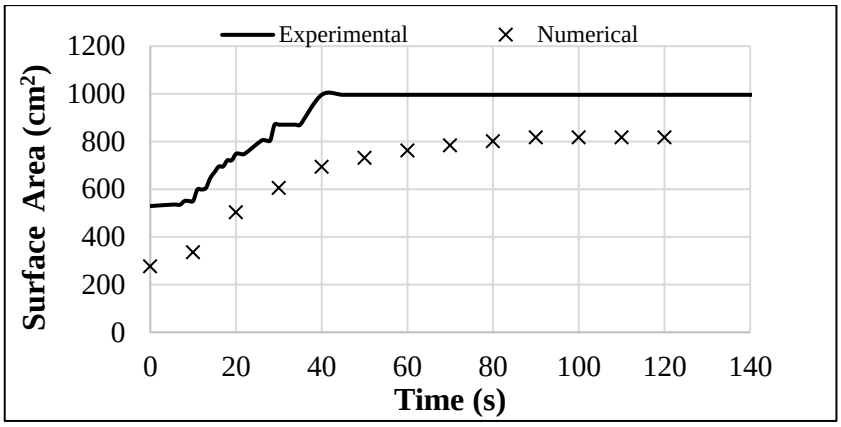

Figure 6.11. The downstream temporal breach developments together with experimental and numerical

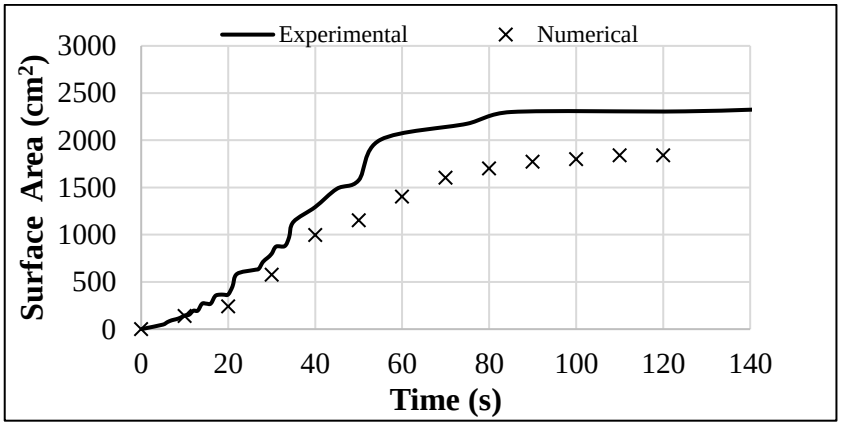

Figure 6.12. The upstream temporal breach developments together with experimental and numerical

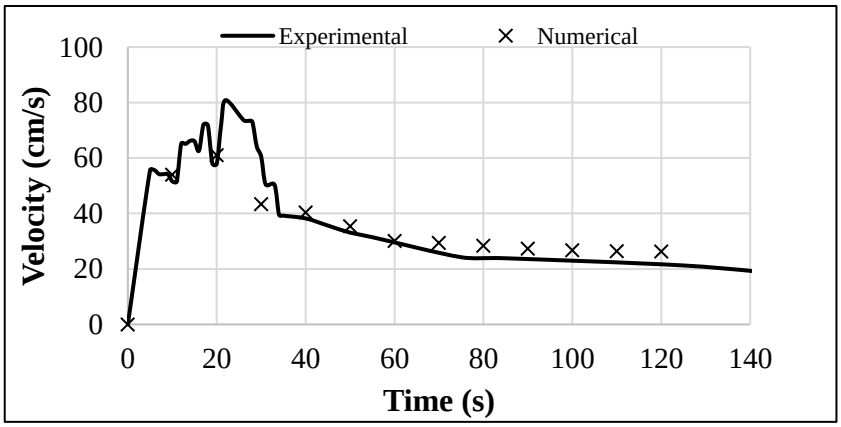

Figure 6.13. The time-varied downstream breach velocities together with experimental and numerical

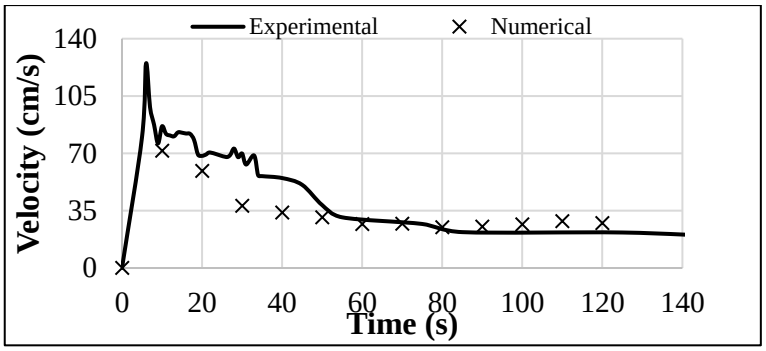

Figure 6.14. The time-varied upstream breach velocities together with experimental and numerical

The temporal variations of wetted areas for downstream and upstream together with experimental and numerical are given in Figure 6.15 and Figure 6.16, respectively.

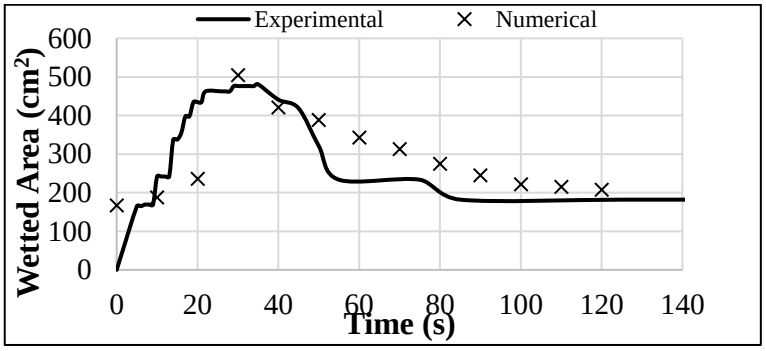

Figure 6.15. The temporal changes in downstream breach-wetted areas together with experimental and numerical

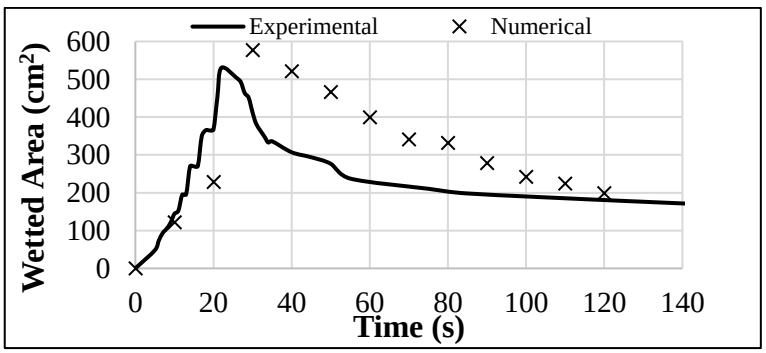

Figure 6.16. The temporal changes in upstream breach-wetted areas together with experimental and numerical

The calculated temporal discharge values together with experimental and numerical are given in Figure 6.17.

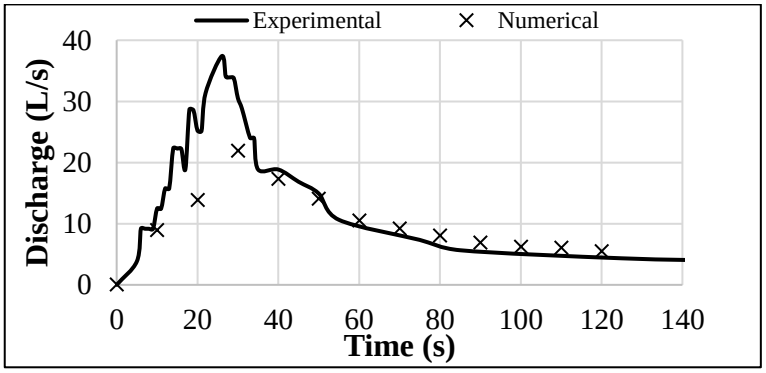

Figure 6.17. The temporal discharge values together with experimental and numerical

The calculated RMSE and MAE values to evaluate each error for each station are given in Table 6.2.

Table 6.2. RMSE and MAE values for each finding at the bottom-middle scenario

Findings	Unit	Root Mean Square Error (RMSE)	Mean Absolute Error (MAE)
$V_{downstream}$	(cm/s)	6.3	4.3
$V_{upstream}$	(cm/s)	13.8	9.8
$Wetted_{downstream}$	(cm^2)	101.8	84.3
$Wetted_{upstream}$	(cm^2)	127.3	107.1
$Surface_{downstream}$	(cm^2)	238.9	236.3
$Surface_{upstream}$	(cm^2)	398.9	330.1
Discharge	(L/s)	4.6	3.1

The RMSE and MAE values are calculated for each finding. For the middle-bottom part, RMSE and MAE values of the average value are calculated as 18.3% and 12.7% for $V_{downstream}$, 32.8% and 23.3% for $V_{upstream}$, 37.1% and 30.1% for $Wetted_{downstream}$, 54.6% and 45.9% for $Wetted_{upstream}$, 27.5% and 27.2% for $Surface_{downstream}$, 30.8% and 25.5% for $Surface_{upstream}$, 35.4% and 23.3% for discharge, respectively.

6.2.2. Numerical analysis corresponding to the fourth experiment

In the scope of this thesis, the middle-middle scenario was performed by building a dam 65 cm high, 200 cm long, and 5 cm crest by creating a 2x2 cm^2 weak zone at the middle center along the dam to investigate the temporal changes in breach and the breach discharge caused by piping.

The dam was constructed by mixture 2. The soil mechanics tests of mixture 2 and the experimental findings can be found in Chapter 3.1 and Chapter 5.4, respectively.

The final geometry of the middle-middle scenario is given in Figure 6.18.

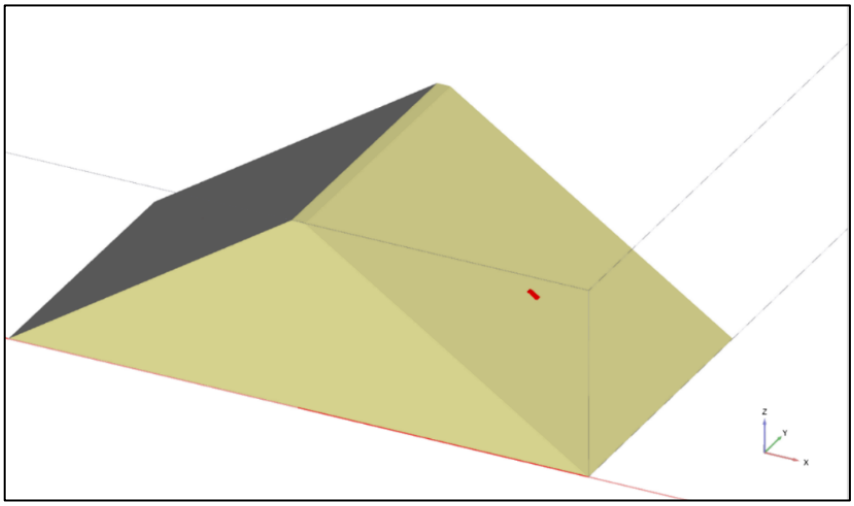

Figure 6.18. The final geometry of the middle-middle scenario

The defined dam body soil properties for the middle-middle part are given in Table 6.1. The numerical analysis was performed by defining the flow functions according to the temporal water depths in the experiment which was given in Figure 5.47.

During the numerical analysis, the first 10 s were performed as steady-state flow calculation types since the water level was continuous and it does not change on time. The rest of the analysis was performed as a time-dependent flow function by tabulating the water level table at each corresponding time.

After starting the simulation, the obtained longitudinal hydraulic gradient distributions in one color scale (green) with their maximum and minimum values are given in Figure 6.19.

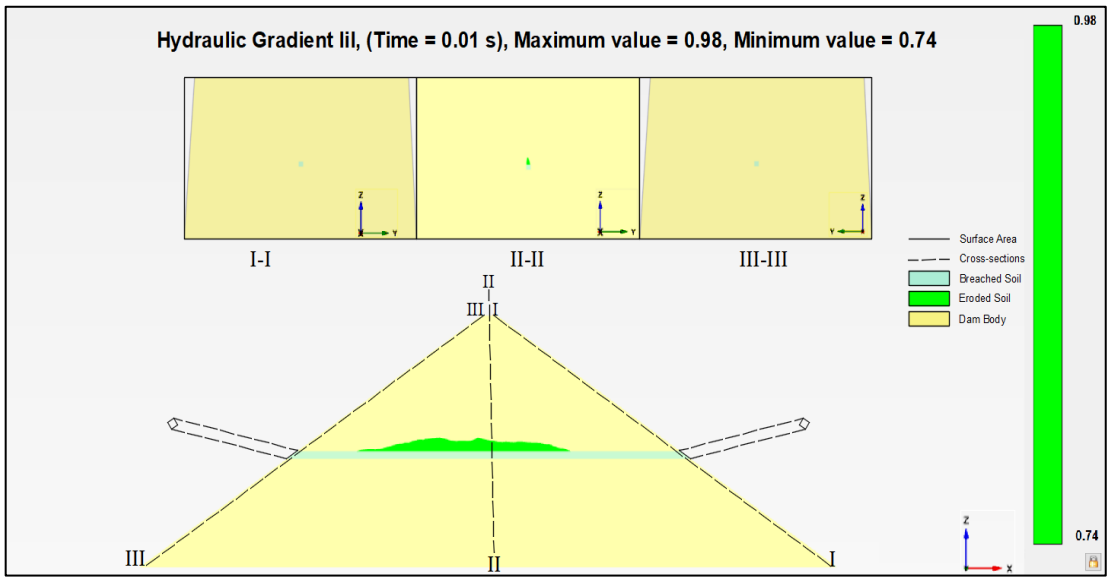

(a)

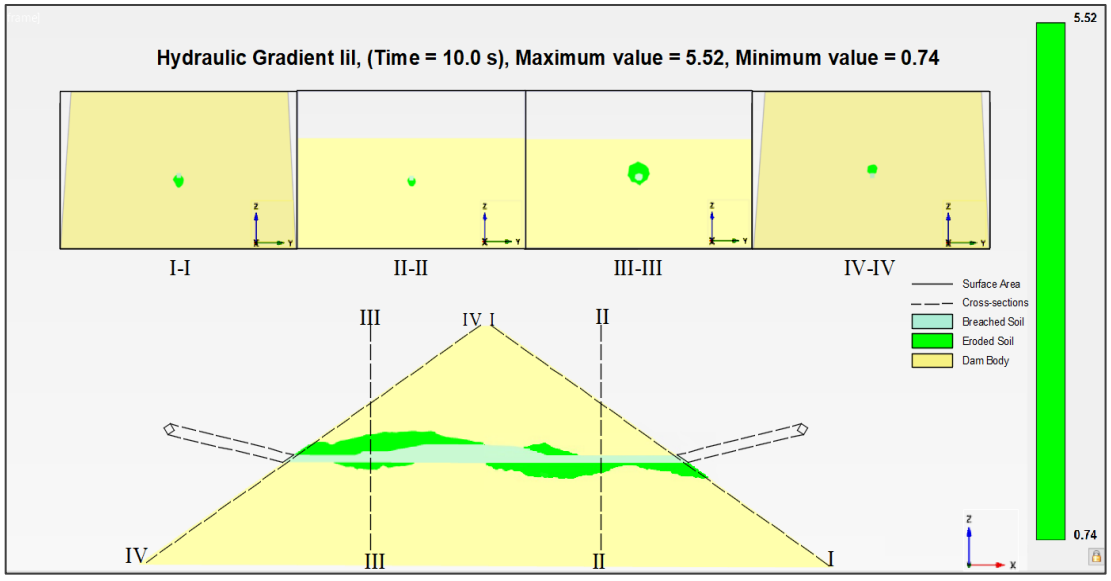

(b)

Figure 6.19. Hydraulic gradient distribution along the dam for (a) 0 s (b) 10 s (c) 40 s (d) 80 s

(cont. on next page)

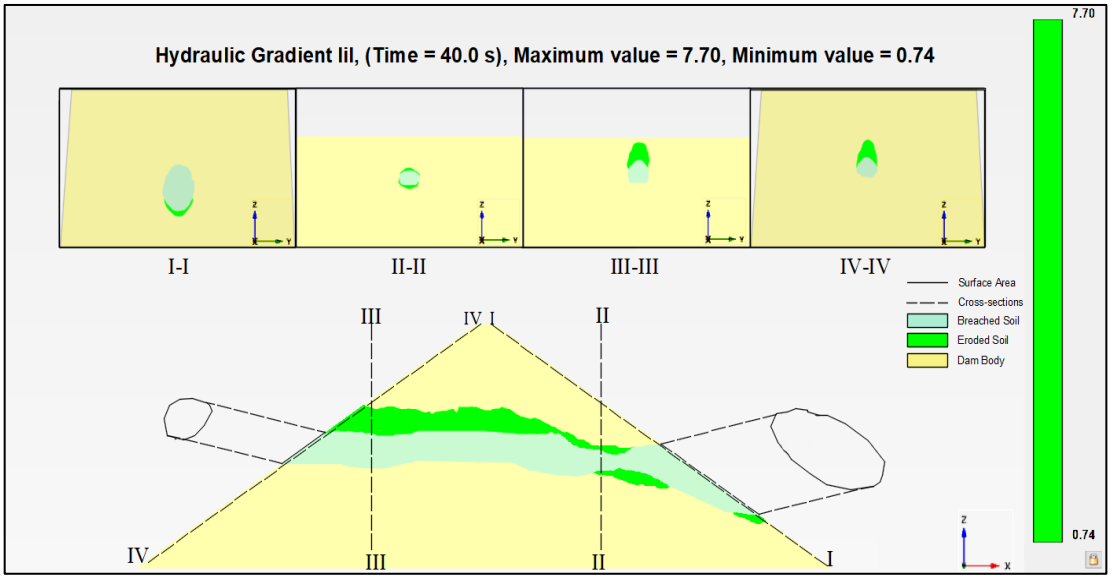

(c)

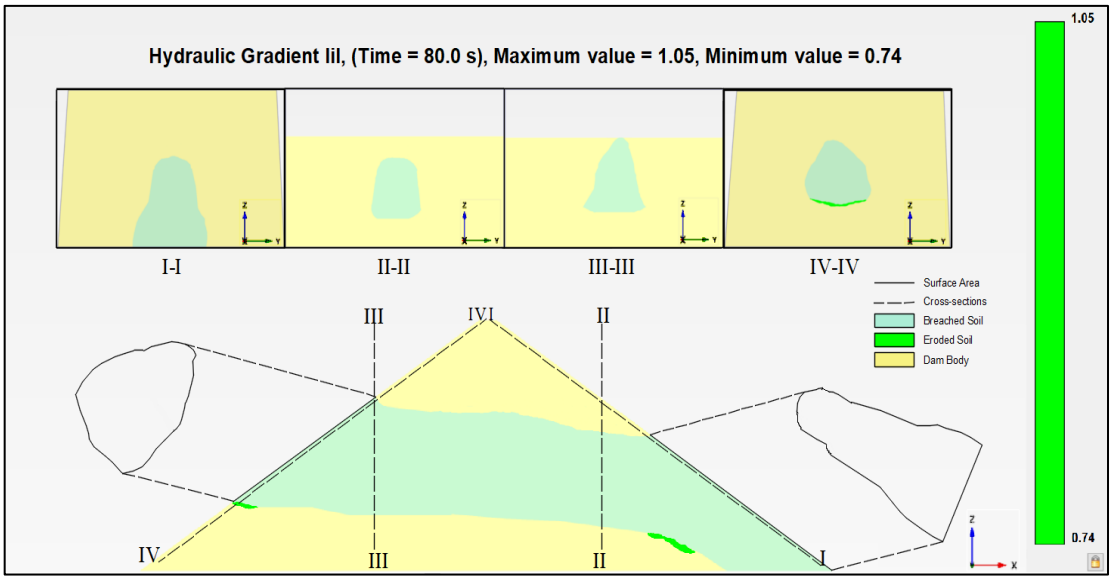

(d)

Figure 6.19. (cont.)

The flow through the breach together with upstream and downstream average values are given in Figure 6.20.

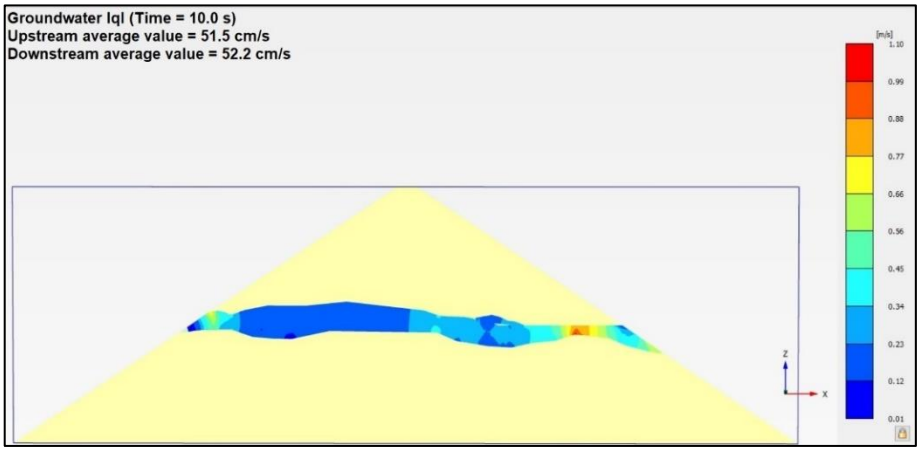

(a)

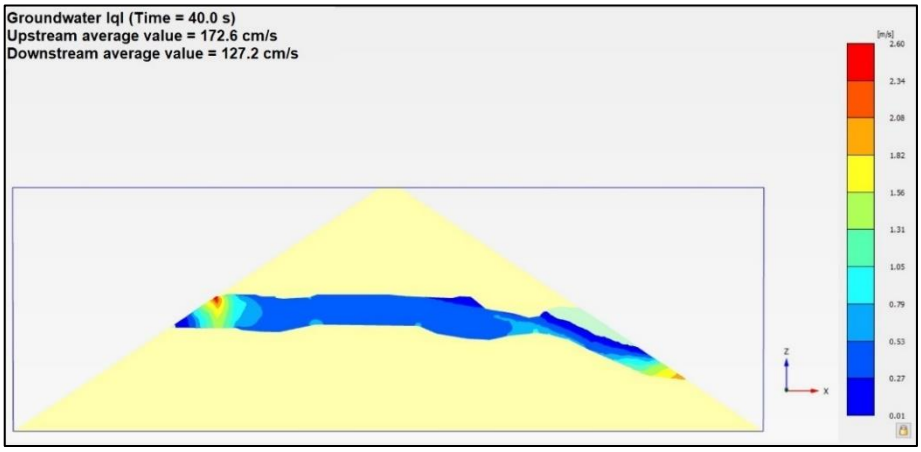

(b)

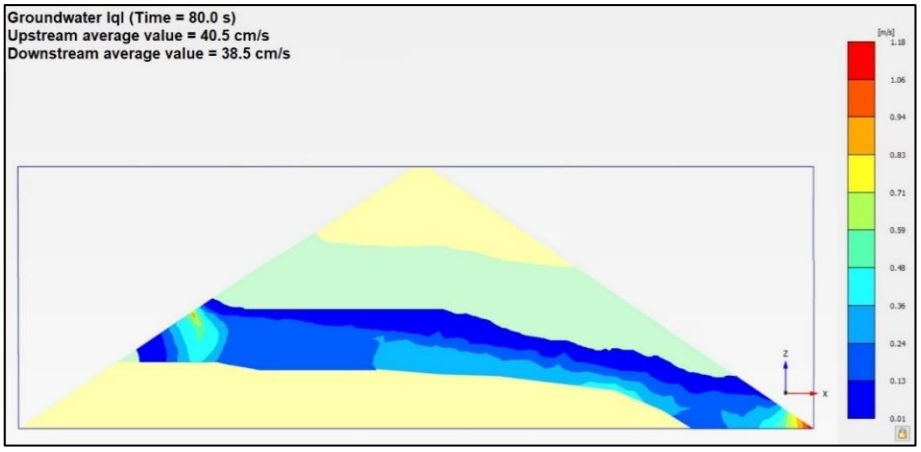

(c)

Figure 6.20. Flow through the breach a) 10 s, b) 40 s, c) 80 s

The downstream and upstream temporal breach developments in the experiment together with those obtained from the numerical analysis are given in Figure 6.21 and Figure 6.22, respectively. The time t=0 s indicates the initiation of seepage.

(a)

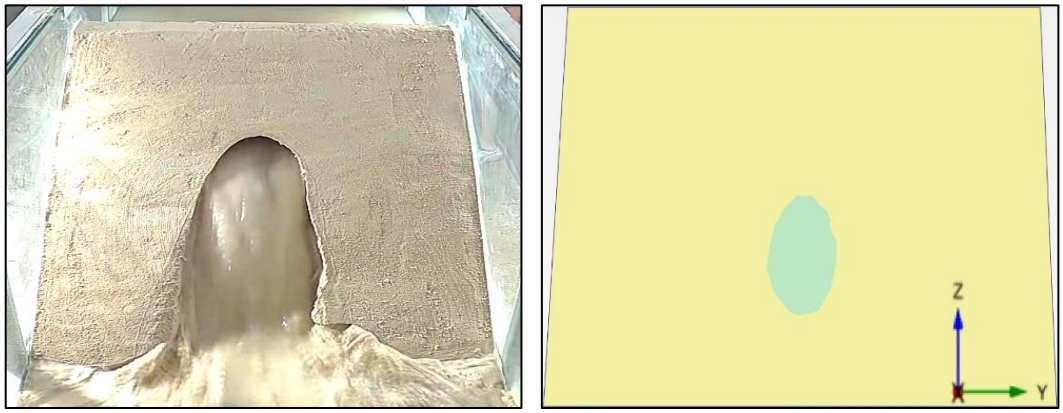

(b)

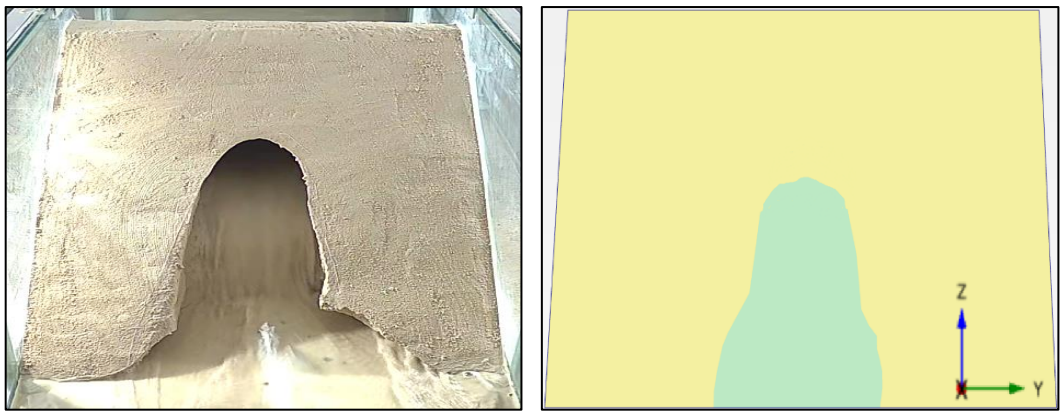

(c)

Figure 6.21. The downstream temporal breach developments a) 0 s, b) 40 s, c) 80 s

(a)

(b)

(c)

Figure 6.22. The upstream temporal breach developments a) 0 s, b) 40 s, c) 80 s

The numerical temporal breach developments together with experimental averaged values are presented in Figure 6.23 and Figure 6.24, respectively.

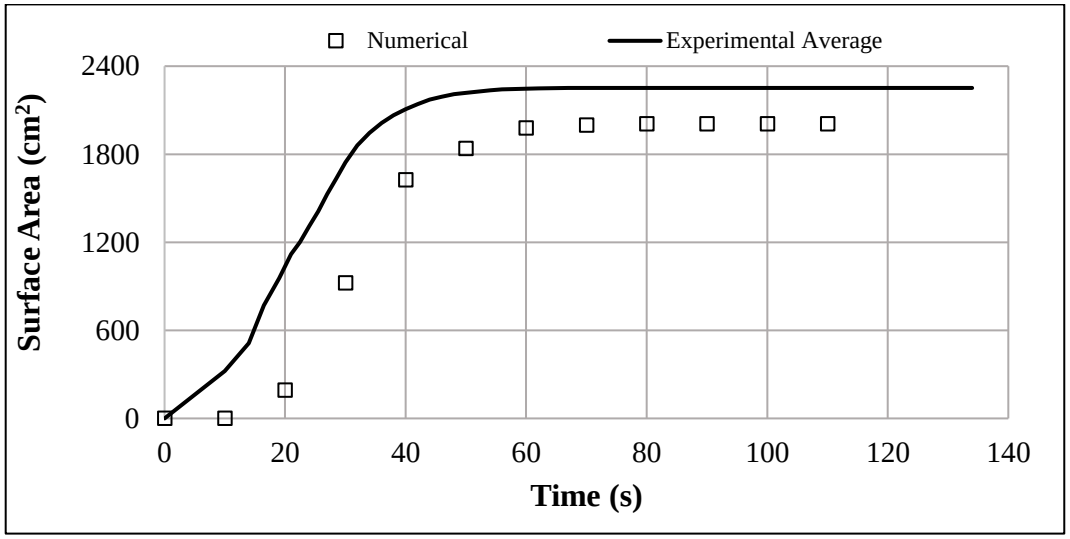

Figure 6.23. The downstream temporal breach developments together with experimental average and numerical

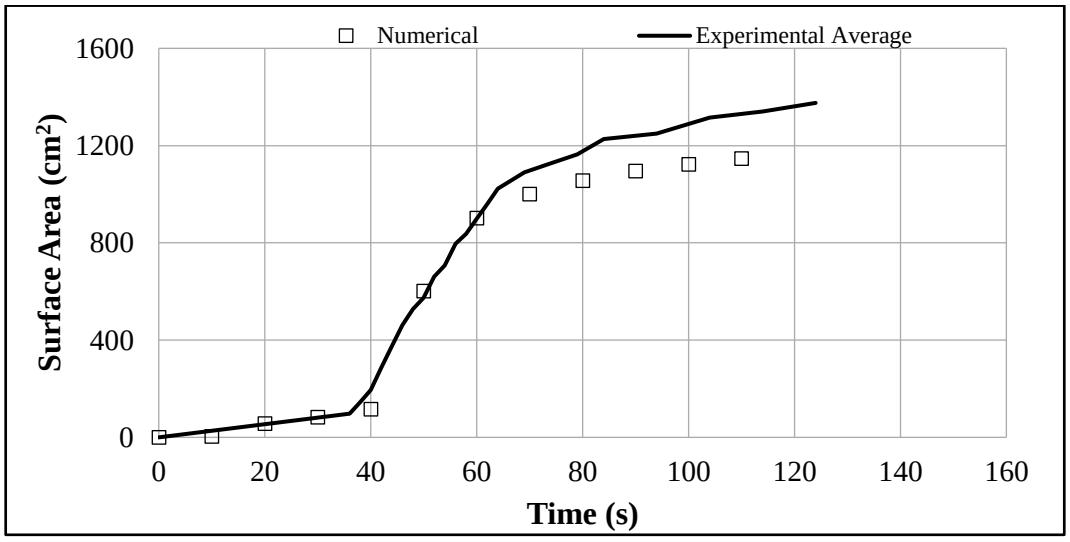

Figure 6.24. The upstream temporal breach developments together with experimental average and numerical

The experimental and numerical time-varied average velocities are presented Figure 6.25 and Figure 6.26 for downstream and upstream, respectively.

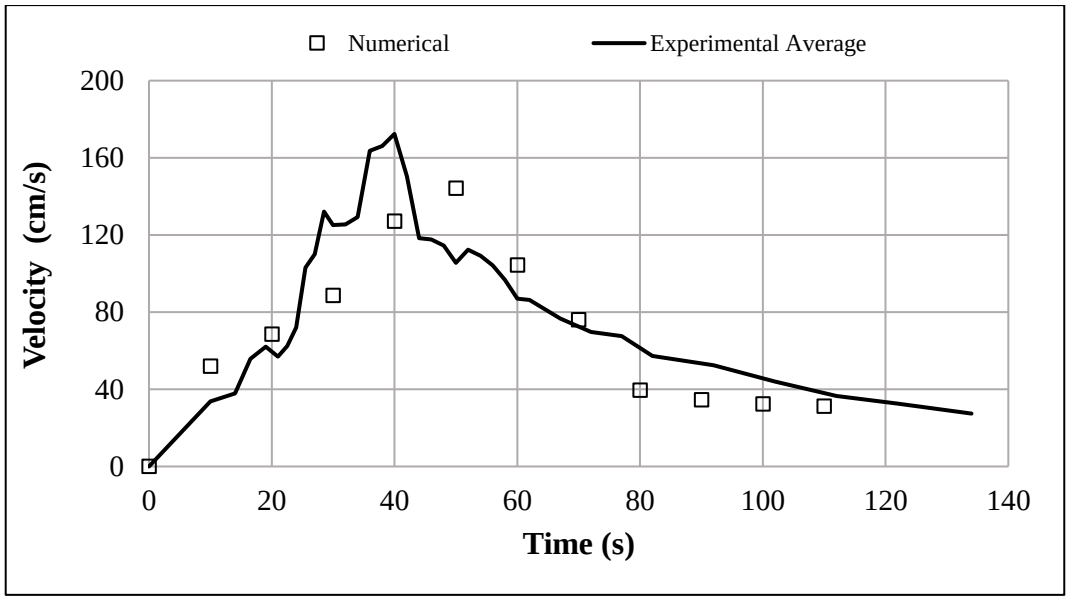

Figure 6.25. The time-varied downstream breach velocities together with experimental average and numerical

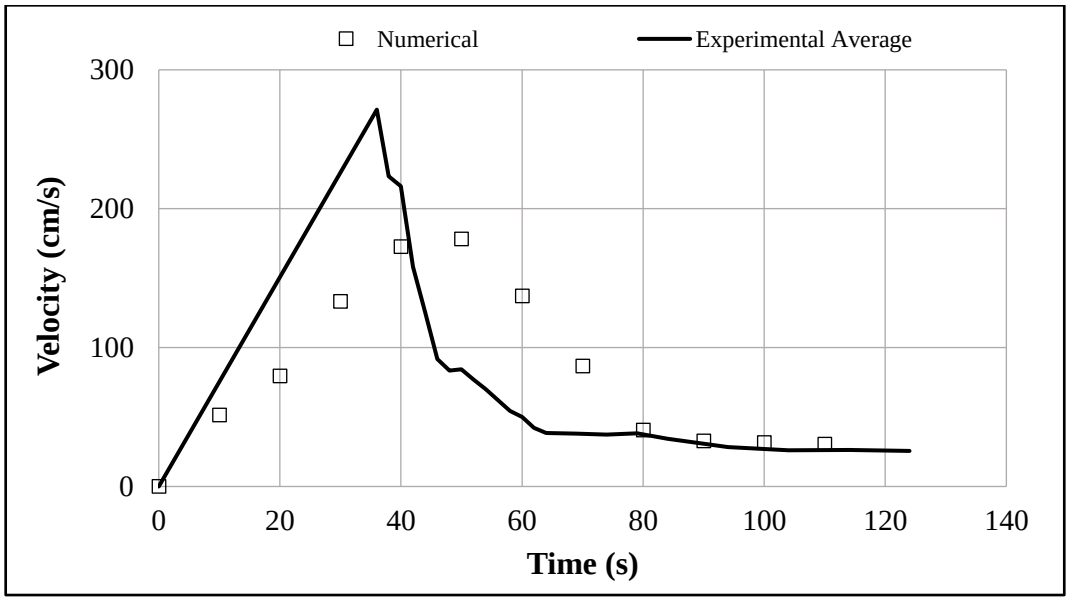

Figure 6.26. The time-varied upstream breach velocities together with experimental average and numerical

The temporal variations of the downstream and upstream wetted areas together with experimental average values and numerical are given in Figure 6.27 and Figure 6.28, respectively.

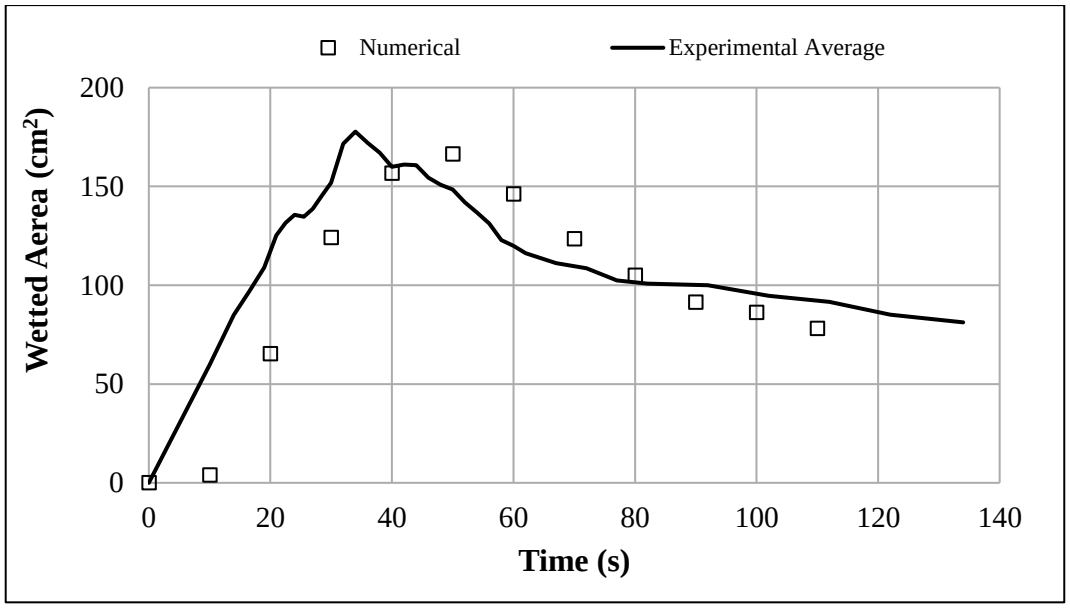

Figure 6.27. The temporal changes in downstream breach-wetted areas together with experimental and numerical

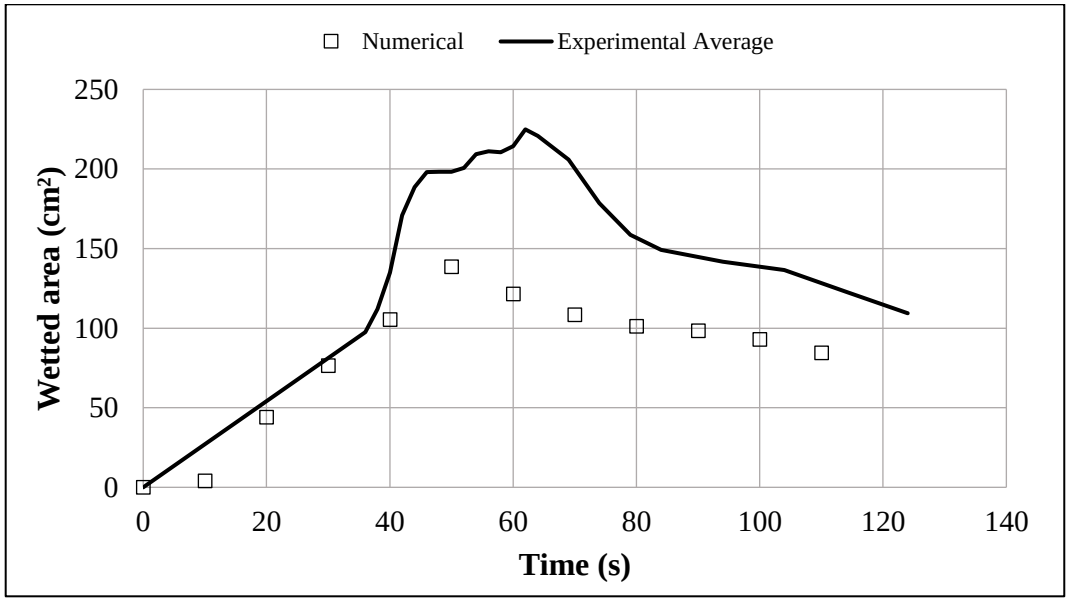

Figure 6.28. The temporal changes in upstream breach-wetted areas together with experimental and numerical

The average temporal discharge values for both the experimental and numerical are given in Figure 6.29.

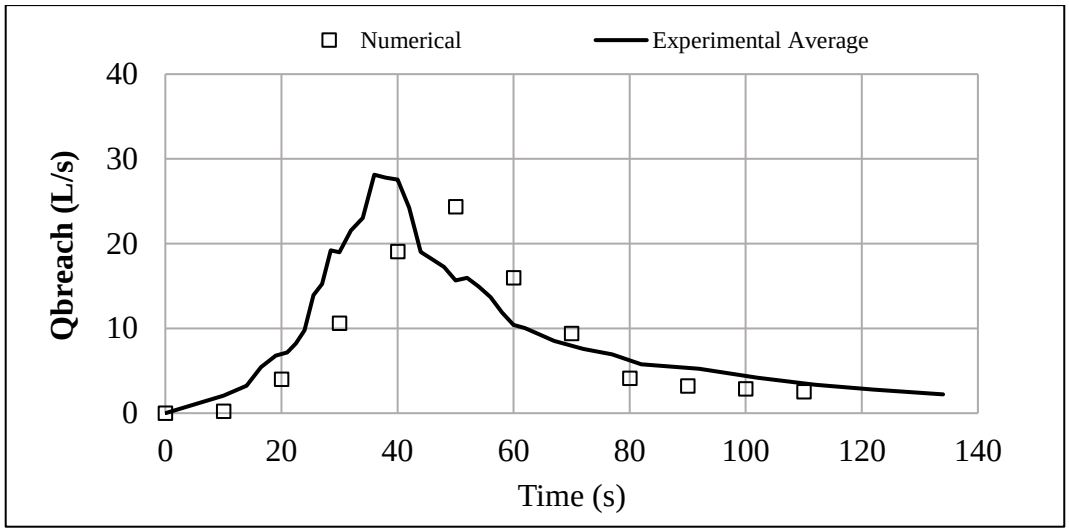

Figure 6.29. The average temporal discharge values together with experimental and numerical

The calculated and compared the RMSE and MAE values for each finding are given in Table 6.3.

Table 6.3. RMSE and MAE values for each finding at the middle-middle part

Findings	Unit	Root Mean Square Error (RMSE)	Mean Absolute Error (MAE)
$V_{downstream}$	(cm/s)	23.1	18.5
$V_{upstream}$	(cm/s)	43.9	30.7
$Wetted_{downstream}$	(cm^2)	27.0	20.1
$Wetted_{upstream}$	(cm^2)	51.2	40.9
$Surface_{downstream}$	(cm^2)	426.1	356.8
$Surface_{upstream}$	(cm^2)	102.1	71.8
Discharge	(L/s)	3.5	2.8

The RMSE and MAE values are calculated for each finding. For the middle-middle scenario, RMSE and MAE values of the average value are calculated as 30.0% and 24.0% for $V_{downstream}$, 58.4% and 40.8% for $V_{upstream}$, 23.2% and 17.2% for $Wetted_{downstream}$, 39.1% and 31.3% for $Wetted_{upstream}$, 22.5% and 18.8% for $Surface_{downstream}$, 14.1% and 9.9% for $Surface_{upstream}$, 36.0% and 28.2% for discharge, respectively.

6.2.3. Case 1: Seepage Starting at the Upper-Middle

In the scope of the project TUBITAK 119M609, (Guney et al., 2022a and Okan, 2022) performed an experiment by building a 60 cm in height, 200 cm in length, and 20 cm in crest width dam. A tunnel of 2 cm diameter located 6 cm below the crest to investigate temporal breach developments and the discharge through the breach caused by piping.

6.1.1.1. Construction procedures and Experiment

During the construction of the earth-fill dam, the bulk density was used as 2 g/cm^3 and in 12.5% optimum water content by the standard proctor test from Figure 3.2. The construction stages of the upper-middle scenario are given in Figure 6.30.

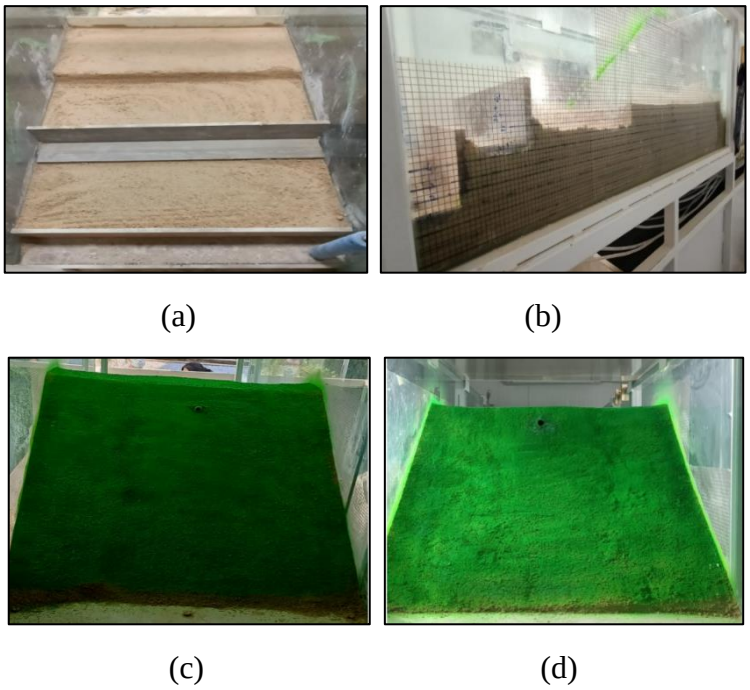

(a) (b)

(c) (d)

Figure 6.30. The construction stages of the upper-middle scenario (a) Top view of the third layer during construction, (b) Left view of the third layer during construction, (c) final upstream view, (d) final downstream view (Guney et al., 2022a and Okan, 2022)

The experimental processes of the upper-middle scenario are given in Figure 6.31.

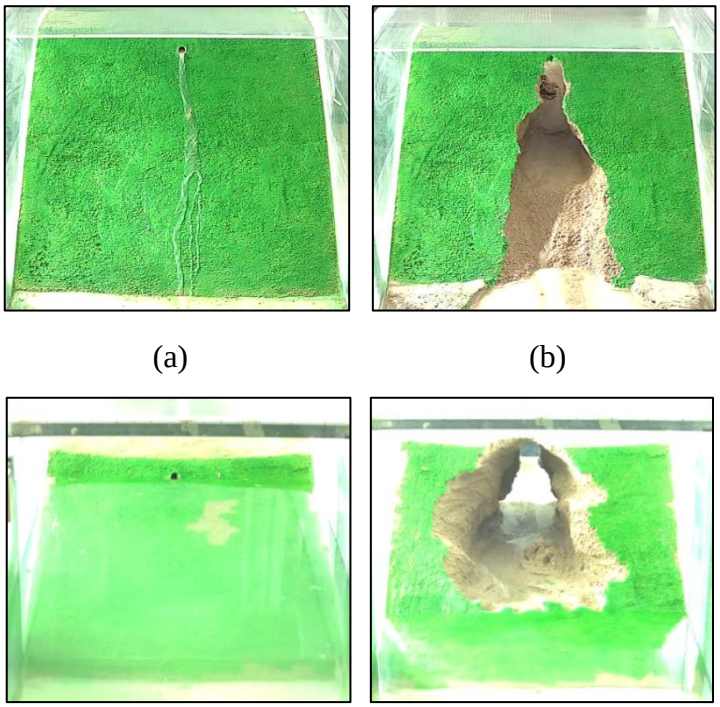

(a) (b)

(c) (d)

Figure 6.31. The experiment process for the upper-middle scenario (a) downstream beginning, (b) downstream ending, (c) upstream beginning, (d) upstream ending (Guney et al., 2022a and Okan, 2022)

The temporal water depth is given in Figure 6.32.

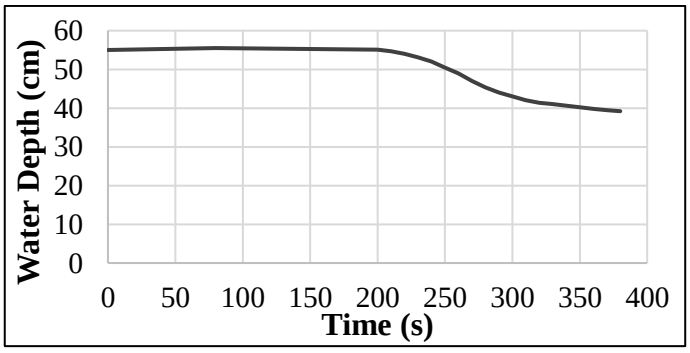

Figure 6.32. The temporal water depths of the upper-middle scenario (Guney et al., 2022a and Okan, 2022)

The numerical analysis was performed by defining the flow functions according to the temporal water depths corresponding to the experiment in the laboratory. During the numerical analysis, the first 200 s are performed as steady-state flow calculation type. The rest of the 200 s parts were performed as a time-dependent flow function by tabulating the water level table at each corresponding time. The geometry of the upper-middle scenario in PLAXIS 3D is given in Figure 6.33.

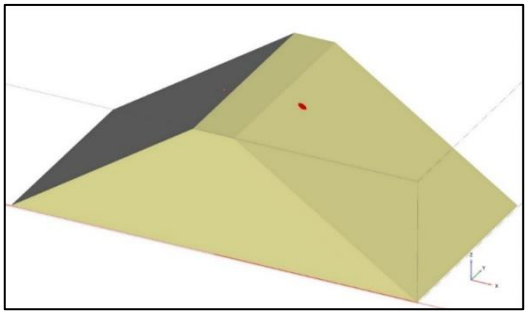

Figure 6.33. The final geometry of the upper-middle scenario

The longitudinal one-color scale (green) hydraulic gradient distributions at y=0.5 m together with four cross-sectional views at different time steps are given in Figure 6.34.

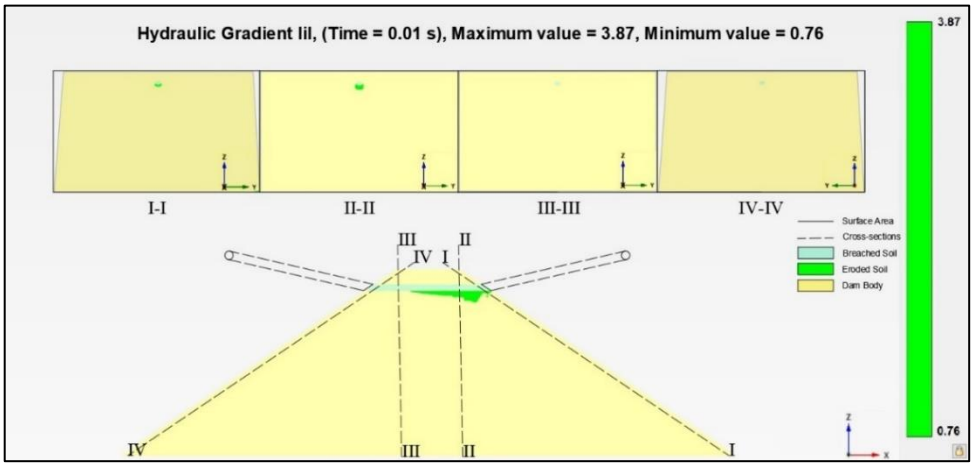

(a)

Figure 6.34. Hydraulic gradient distribution along the dam (a) 0 s (b) 40 s (c) 160 s (d) 240 s (e) 380 s

(cont. on next page)

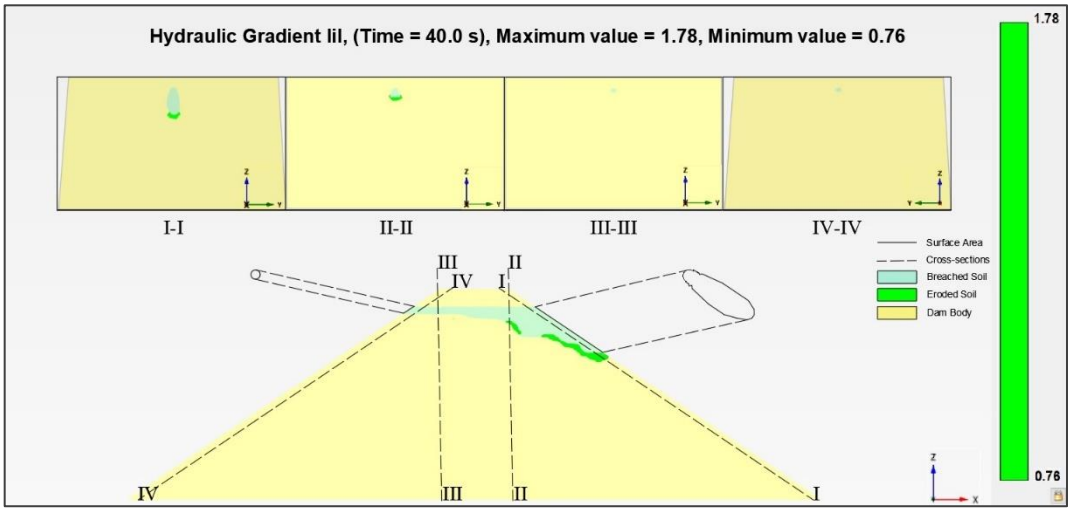

(b)

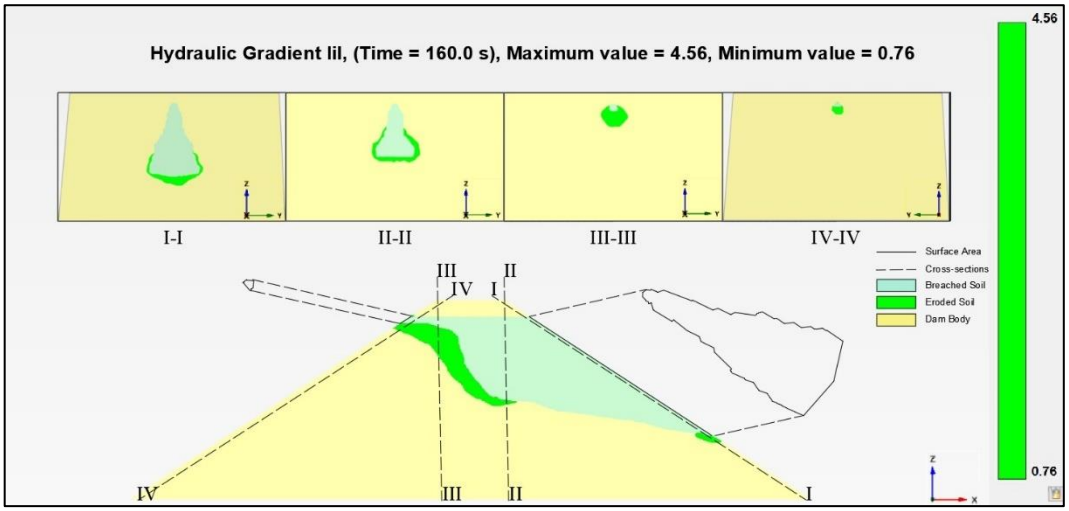

(c)

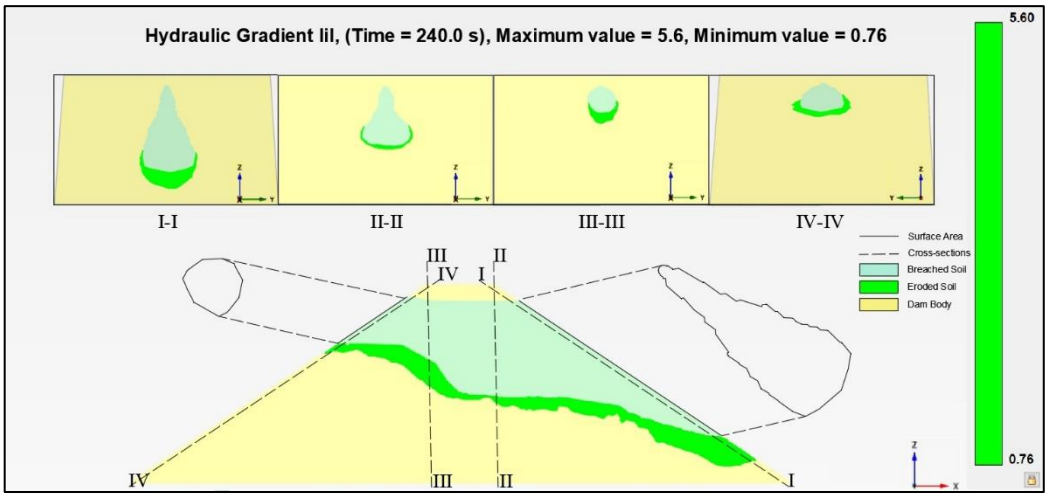

(d)

(cont. on next page)

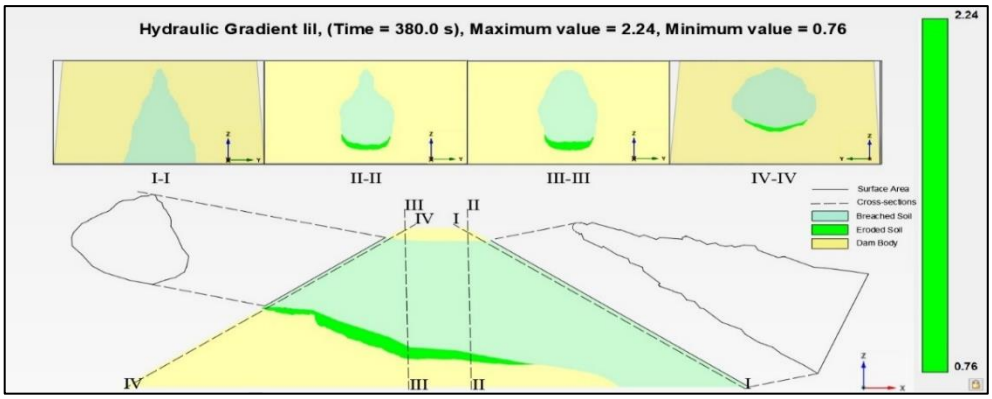

(e)

Figure 6.34. (cont.)

The flow through the breach together with upstream and downstream average values are given in Figure 6.35.

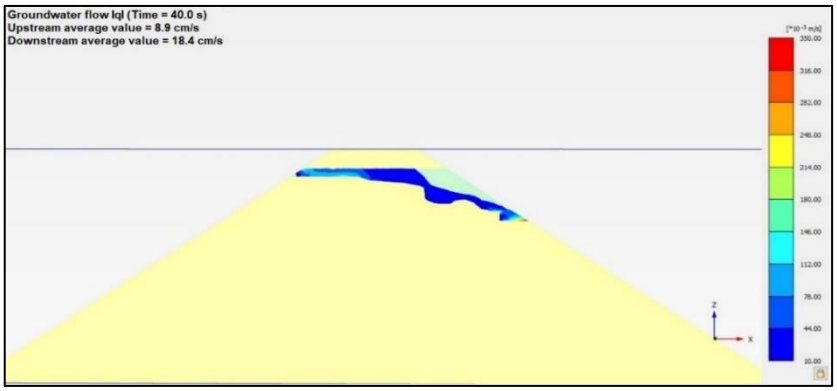

(a)

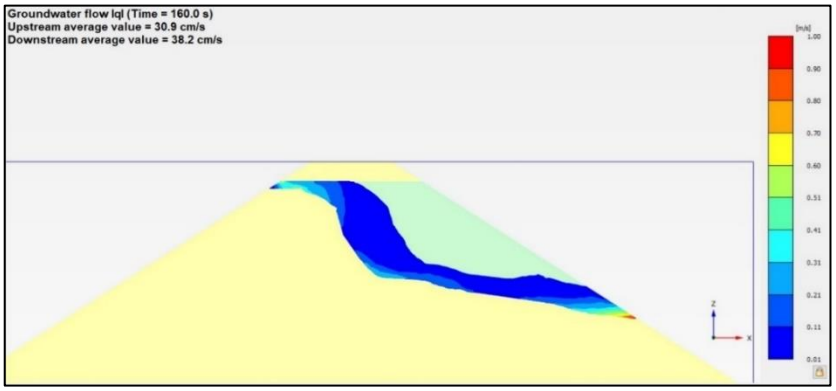

(b)

Figure 6.35. Flow through the breach a) 40 s, b) 160 s, c) 240 s

(cont. on next page)

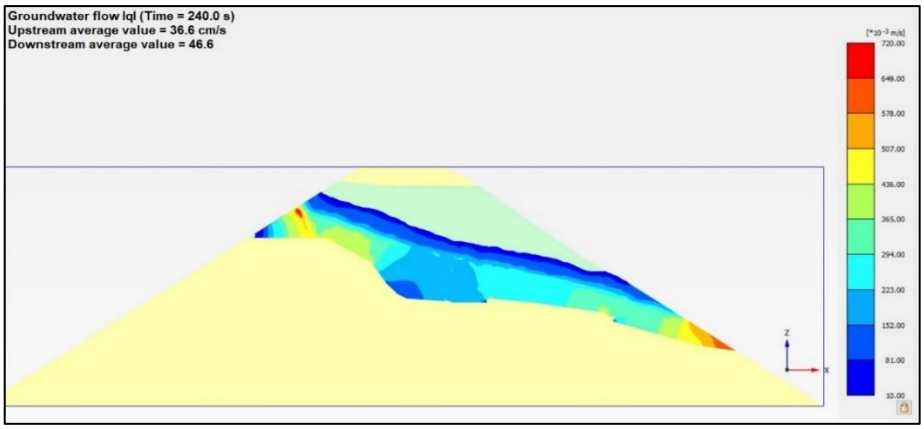

(c)

Figure 6.35. (cont.)

The downstream and upstream temporal breach developments in the experiment together with those obtained from the numerical analysis are given in Figure 6.36 and Figure 6.37, respectively. The time t=0 s indicates the initiation of seepage.

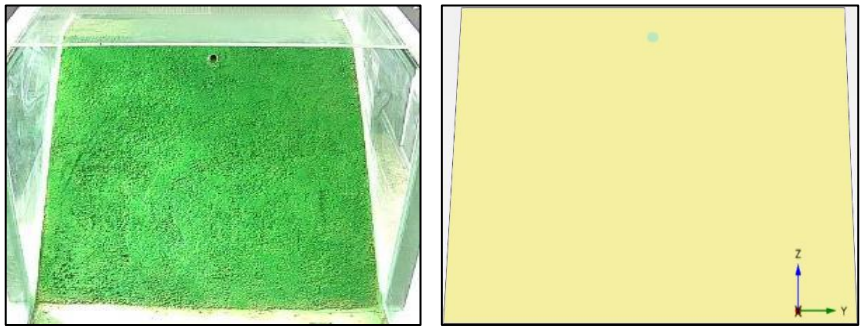

(a)

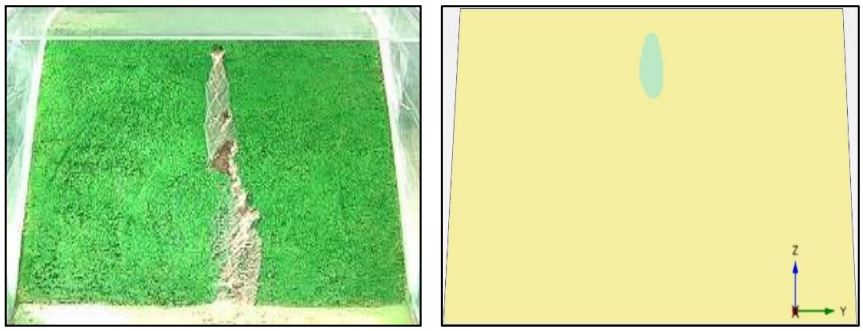

(b)

Figure 6.36. The downstream temporal breach developments (a) 0 s, b) 40 s, c) 240 s, d) 380

(cont. on next page)

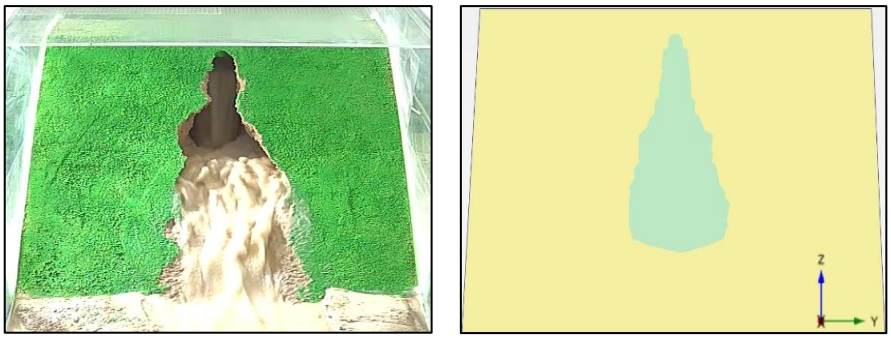

(c)

(d)

Figure 6.36. (cont.)

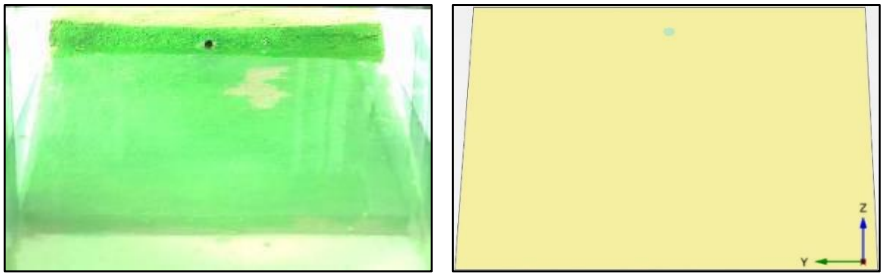

(a)

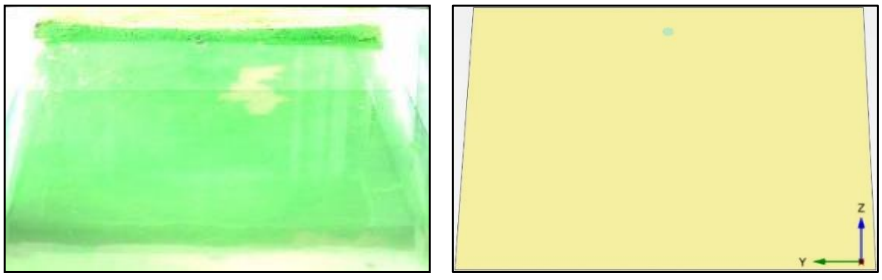

(b)

Figure 6.37. The upstream temporal breach developments (a) 0 s, (b) 40, (c) 240 s, (d) 380 s

(cont. on next page)

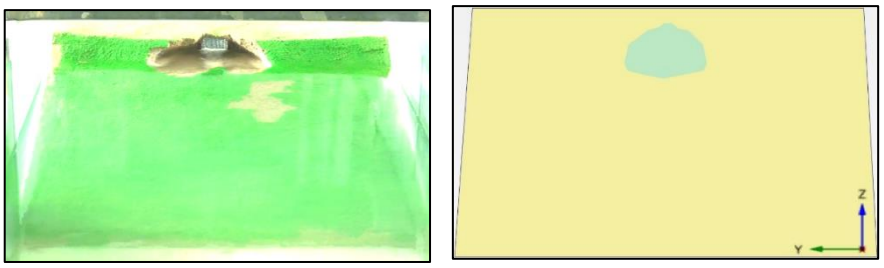

(c)

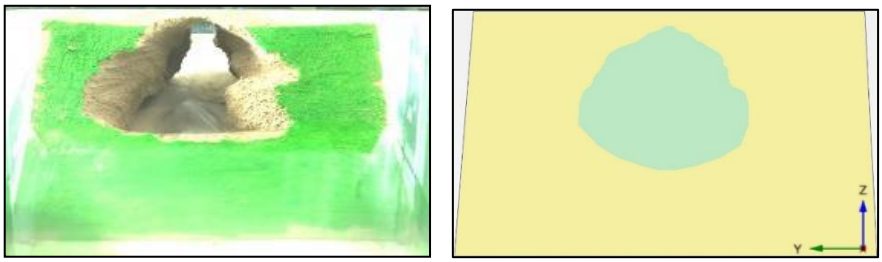

(d)

Figure 6.37. (cont.)

The numerical temporal breach developments together with experimental averaged values are presented in Figure 6.38 and Figure 6.39 for the downstream and the upstream sides, respectively.

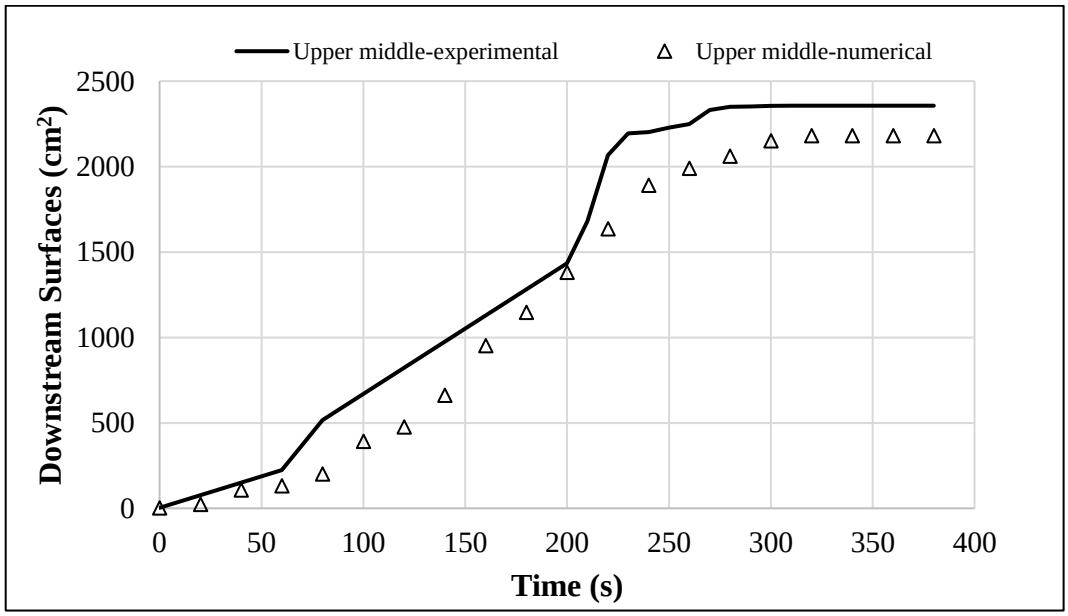

Figure 6.38. The downstream temporal breach developments together with experimental and numerical

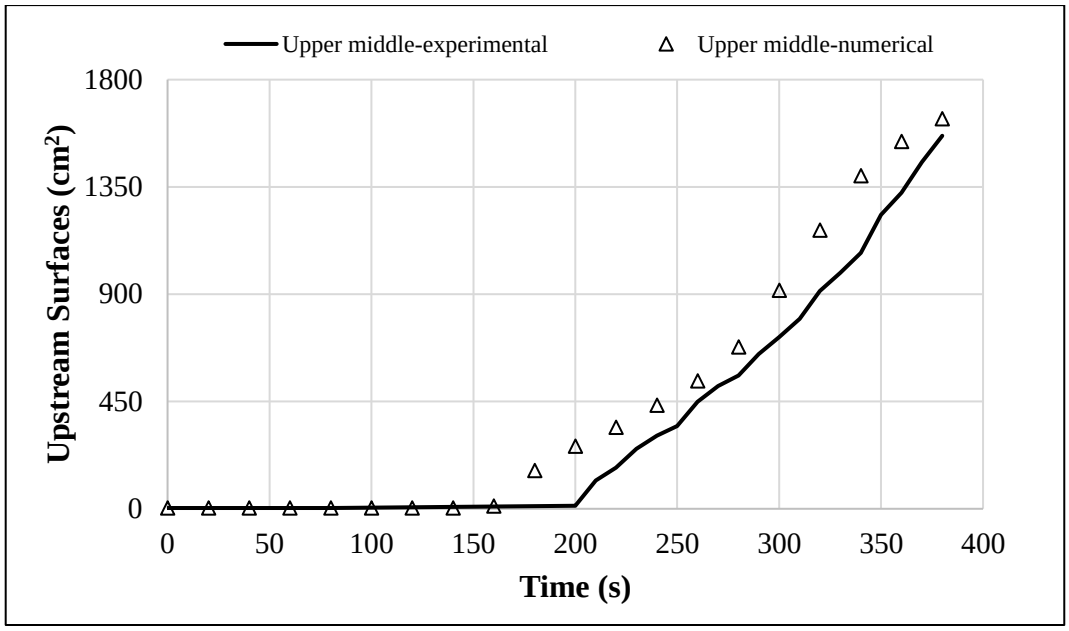

Figure 6.39. The upstream temporal breach developments together with experimental and numerical

The experimental and numerical time-varied average velocities are presented in Figure 6.40 and Figure 6.41 for downstream and upstream, respectively.

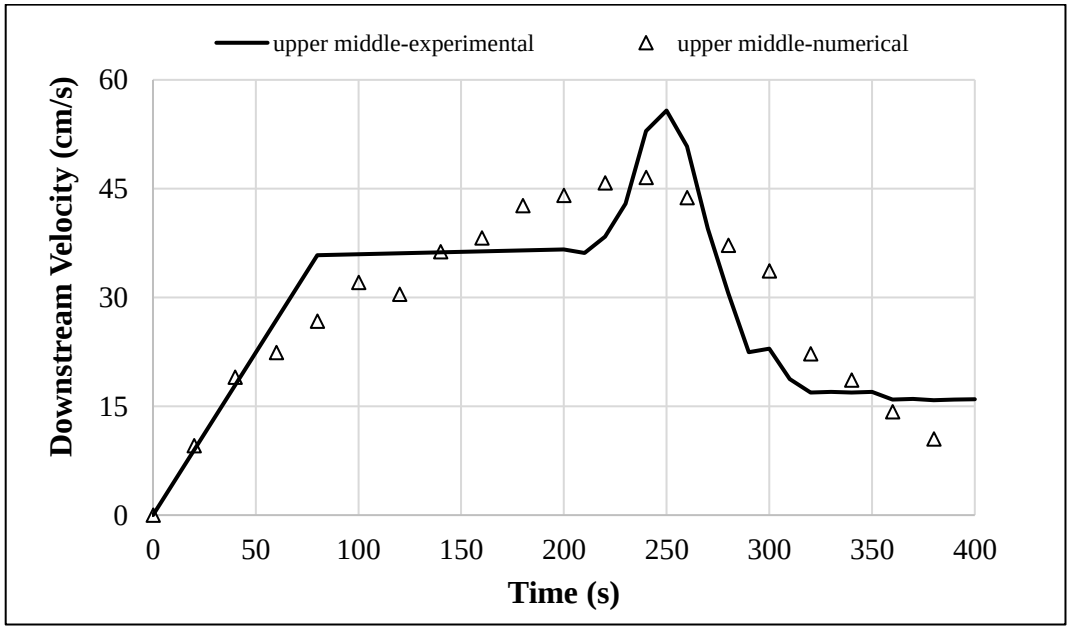

Figure 6.40. The time-varied downstream breach velocities together with experimental and numerical

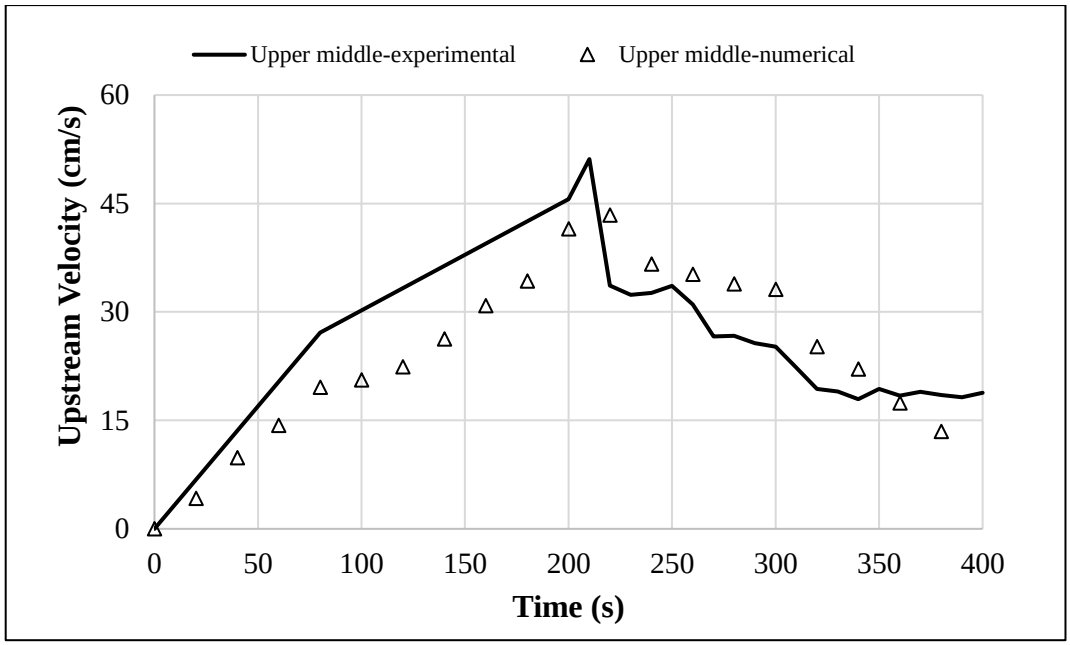

Figure 6.41. The time-varied upstream breach velocities together with experimental and numerical

The temporal variations of downstream and upstream wetted areas together with experimental and numerical are given in Figure 6.42 and Figure 6.43 respectively.

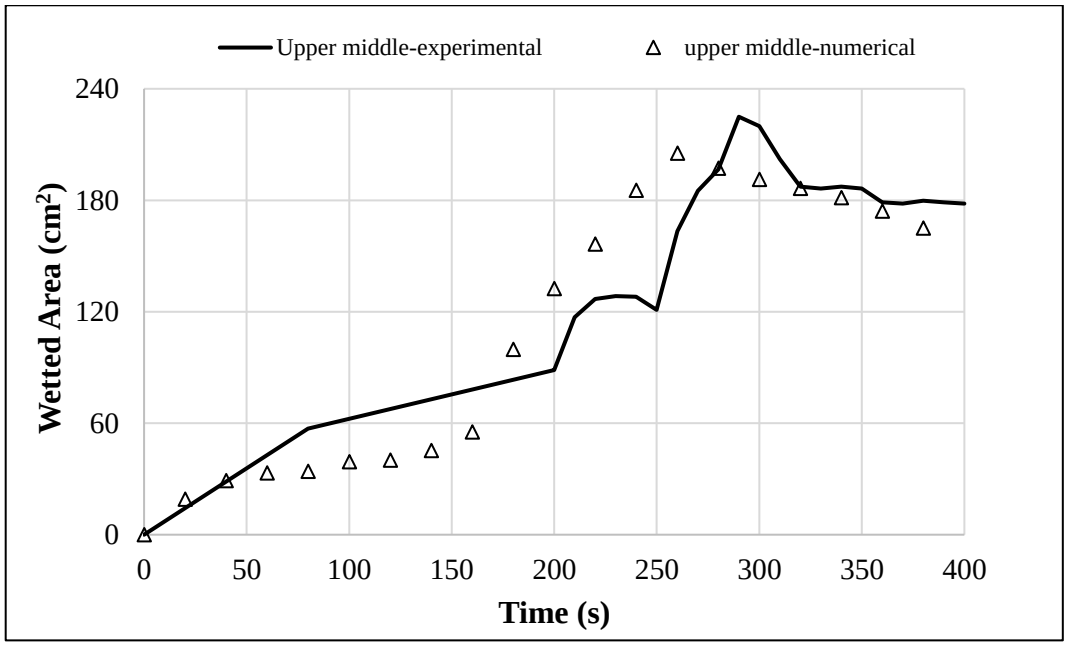

Figure 6.42. The temporal variations of downstream wetted areas together with experimental and numerical

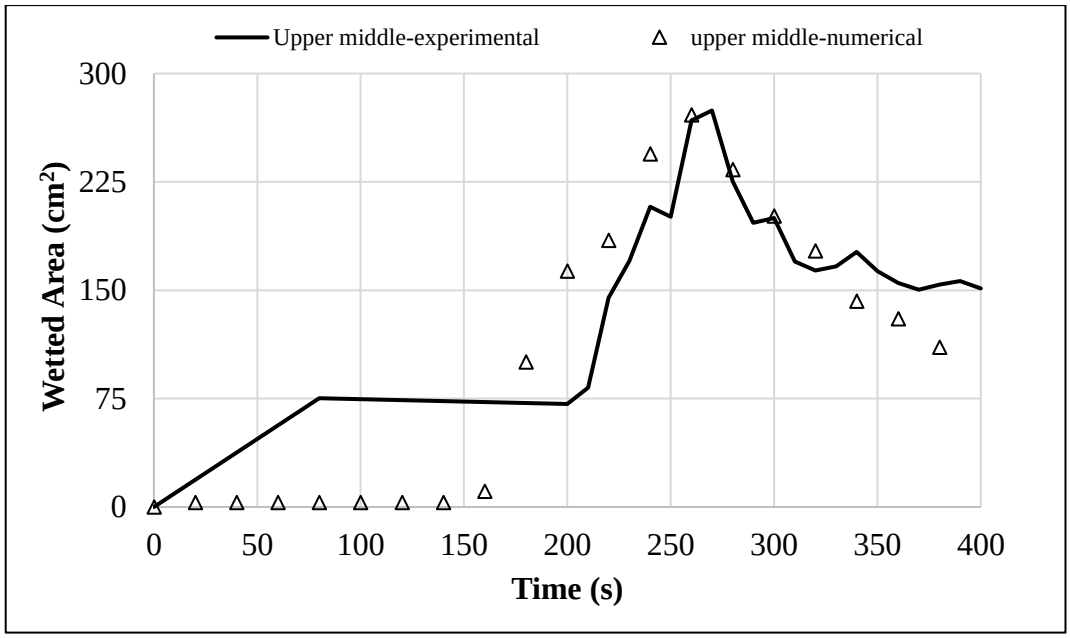

Figure 6.43. The temporal variations of upstream wetted areas together with experimental and numerical

The average temporal discharge values for both the experimental and numerical are given in Figure 6.44.

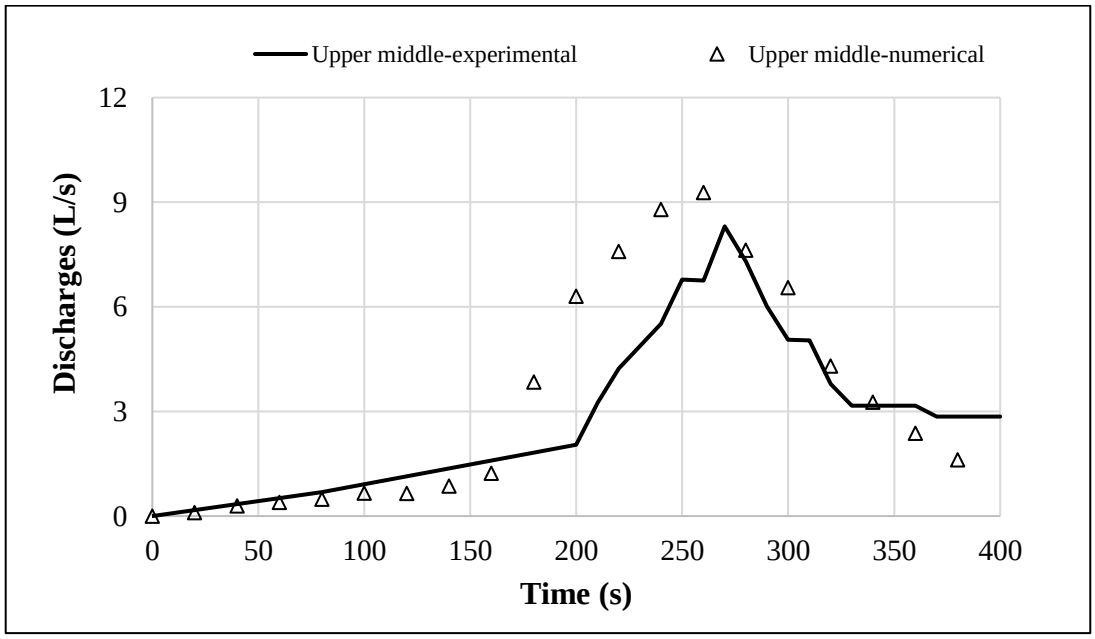

Figure 6.44. The temporal discharges together with experimental and numerical

The calculated RMSE and MAE values for each finding are given in Table 6.4.

Table 6.4. RMSE and MAE values for each finding at the upper-middle part

Findings	Unit	Root Mean Square Error (RMSE)	Mean Absolute Error (MAE)
$V_{downstream}$	(cm/s)	5.6	4.7
$V_{upstream}$	(cm/s)	6.7	6.0
$Wetted_{downstream}$	(cm^2)	24.9	19.1
$Wetted_{upstream}$	(cm^2)	41.8	32.5
$Surface_{downstream}$	(cm^2)	316.8	224.8
$Surface_{upstream}$	(cm^2)	143.6	100.6
Discharge	(L/s)	1.7	1.2

The RMSE and MAE values are calculated for each finding. For the upper-middle part, RMSE and MAE values of the average value are calculated as 19.7% and 16.6% for $V_{downstream}$, 25.9% and 23.2% for $V_{upstream}$, 23.0% and 17.7% for $Wetted_{downstream}$, %36.0 and 28.1% for $Wetted_{upstream}$, 27.4% and 19.4% for $Surface_{downstream}$, 31.2% and 26.1% for $Surface_{upstream}$, 59.6% and 42.1% for discharge, respectively.

6.2.4. Case 2: Seepage Starting at the Upper-Corner

In the scope of the project TUBITAK 119M609, (Guney et al., 2022b and Okan, 2022) experimented by building a 60 cm in height, 200 cm in length, and 20 cm in crest width dam which has a tunnel of 2 cm diameter located 6 cm below the crest corner to investigate temporal breach developments and the discharge through the breach caused by piping.

6.1.1.2. Construction procedures and Experiment

During the construction of the earth-fill dam, the bulk density was used as 2 g/cm^3 and in 12.5% optimum water content by the standard proctor test from Figure 3.2.

The construction stages of the upper-corner section are given in Figure 6.45.

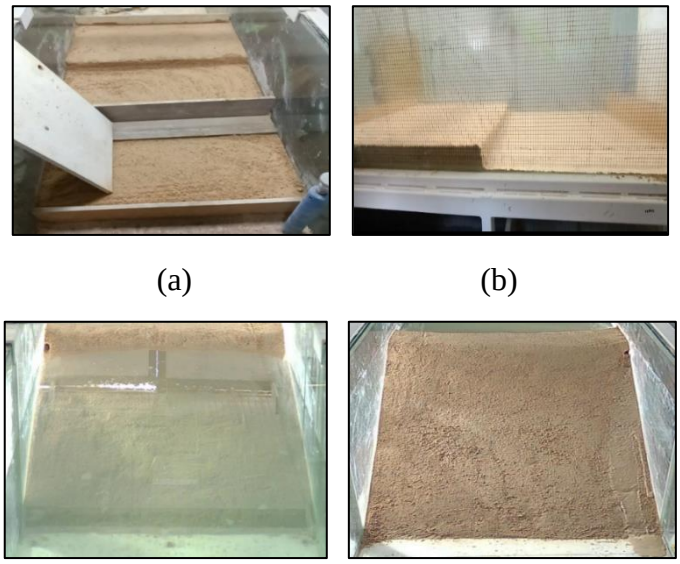

(a) (b)

(c) (d)

Figure 6.45. The constructions of the upper-corner scenario (a) the first layer from top view (b) the first layer from left view (c) final upstream view (d) final downstream view (Guney et al., 2022b and Okan, 2022)

The experimental processes of the upper-corner scenario for the downstream, right side, and upstream are given in Figure 6.46, respectively.

(a) (b)

Figure 6.46. The experiment process for the upper-corner scenario (a) downstream beginning (b) downstream ending (c) right side beginning (d) right side ending (e) upstream beginning (f) upstream ending

(cont. on next page)

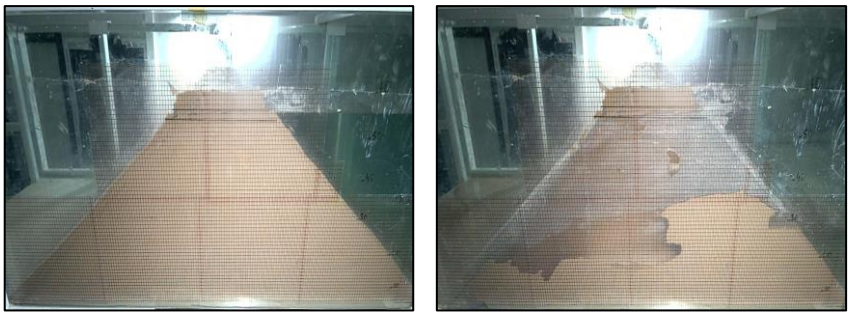

(c) (d)

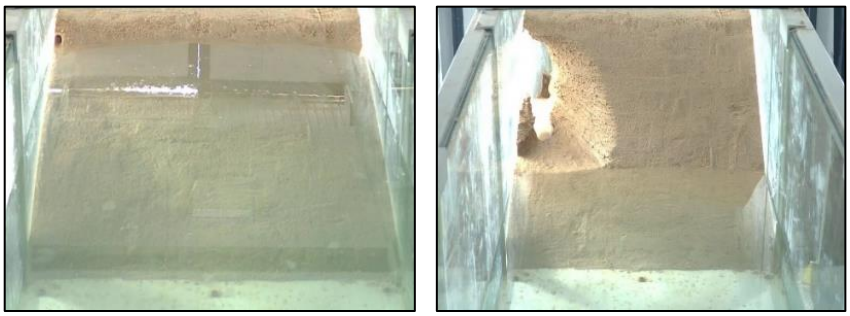

(e) (f)

Figure 6.46. (cont.)

Once the dam geometry was defined, a 2 cm diameter hole was created by using the poly curve at 6 cm below the dam crest corner. The final geometry of the upper-corner scenario in PLAXIS 3D is given in Figure 6.47.

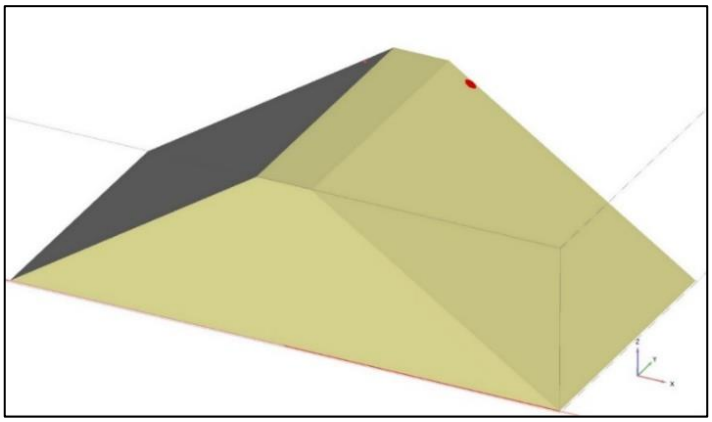

Figure 6.47. The final geometry of the upper-corner scenario

The numerical analysis was performed by defining the flow functions according to the temporal water depths corresponding to the experiment in the laboratory which is

given in Figure 6.48. The first 230 seconds were simulated steady-state flow calculation types while the rest of the analysis was simulated time-dependent.

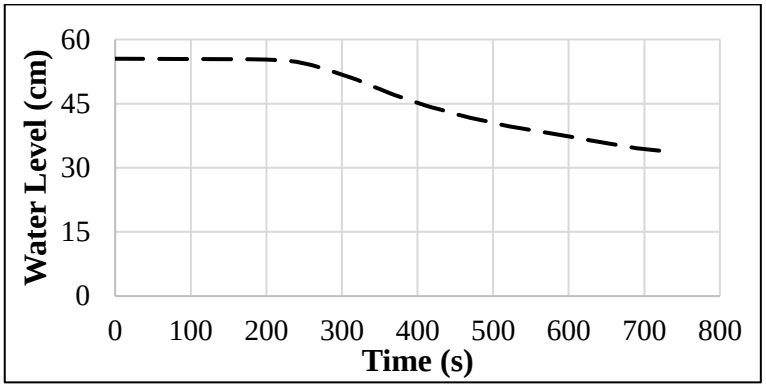

Figure 6.48. The changes in water level in time for the upper-corner scenario (Guney et al., 2022b and Okan, 2022)

The longitudinal one-color scale (green) hydraulic gradient distributions at y=0.98 m together with four cross-sectional views at different time steps are given in Figure 6.49.

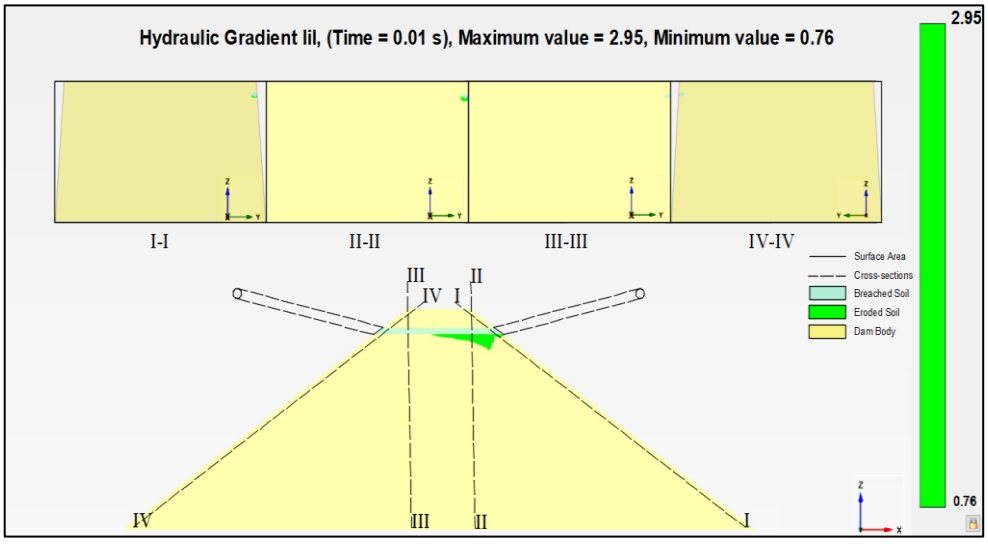

(a)

Figure 6.49. Hydraulic gradient distribution along the dam for a) 0 s, b) 40 s, c) 160 s, d) 500 s, e) 640 s

(cont. on next page)

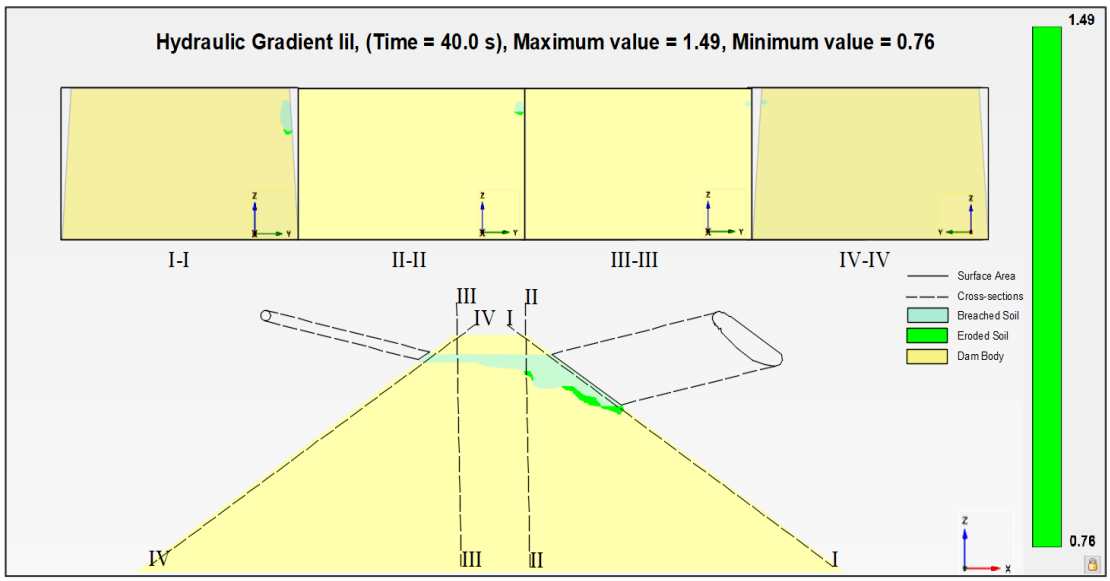

(b)

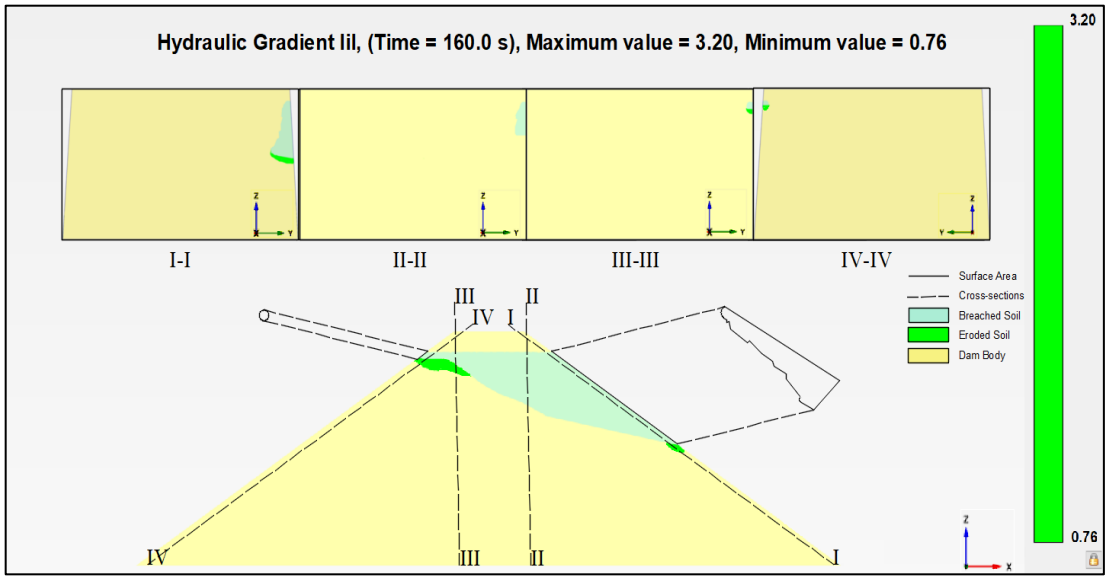

(c)

(cont. on next page)

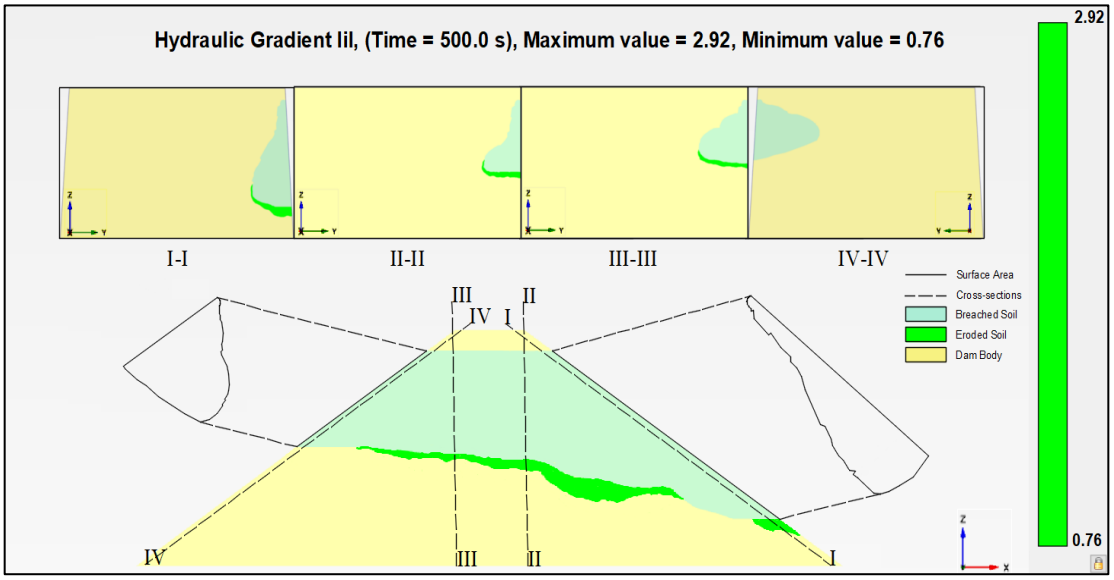

(d)

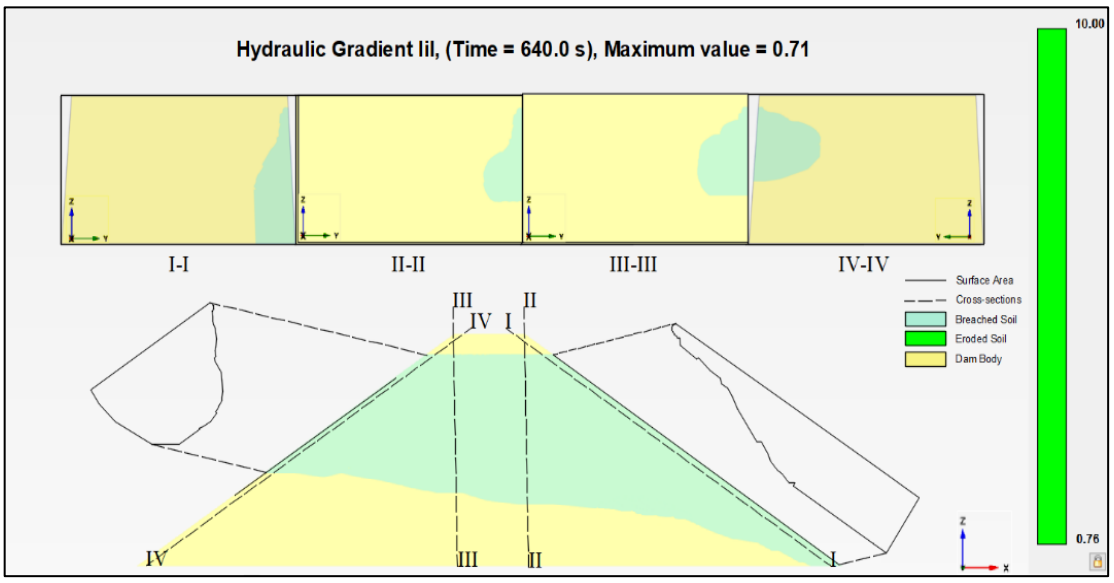

(e)

Figure 6.49. (cont.)

The flow through the breach is given in Figure 6.50.

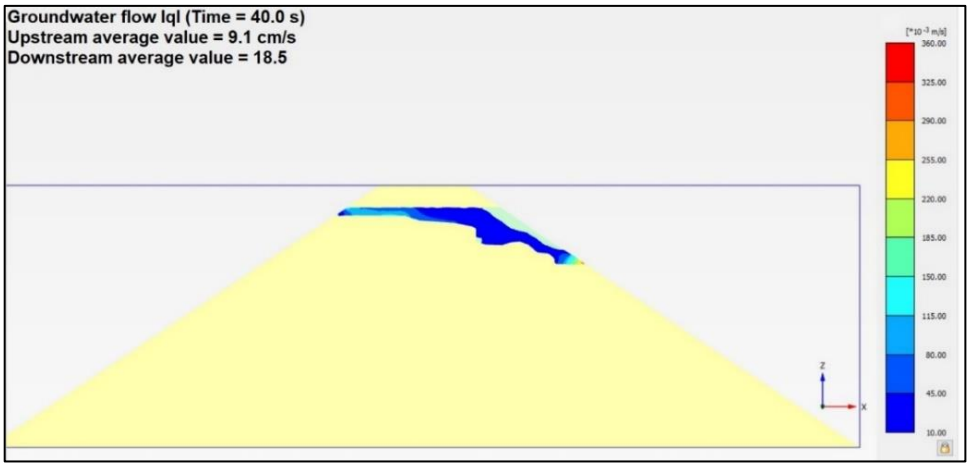

(a)

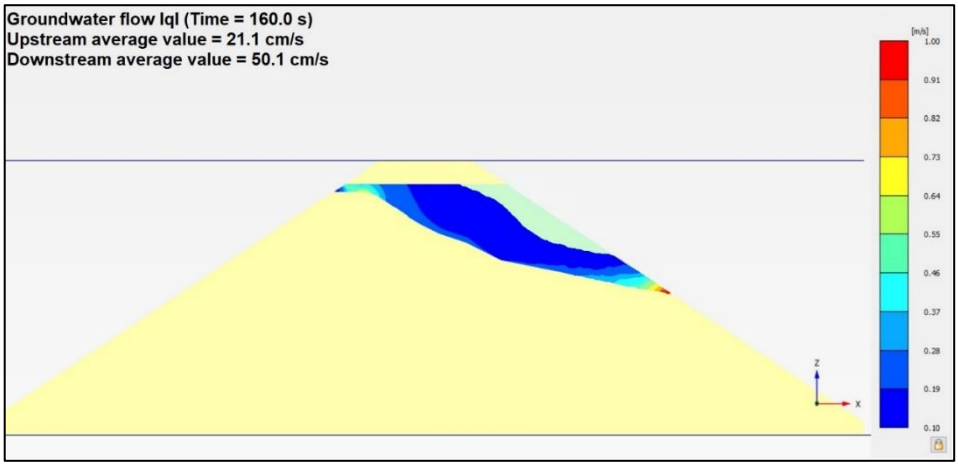

(b)

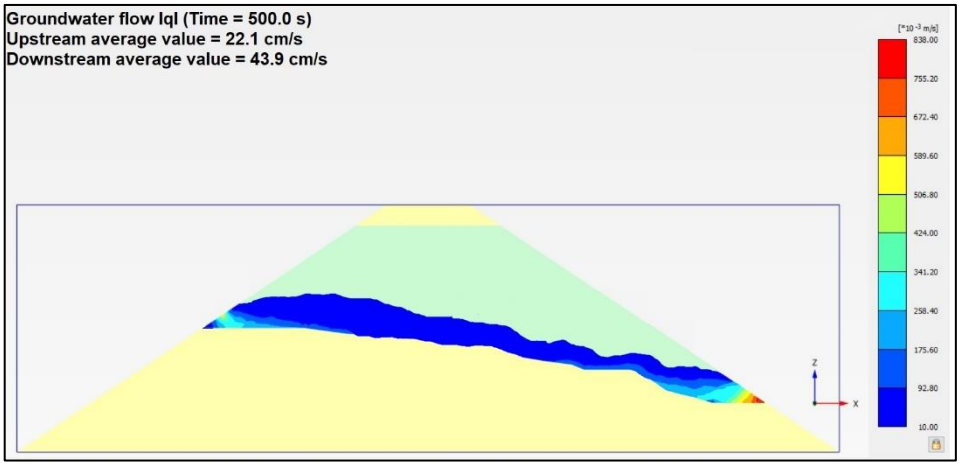

(c)

Figure 6.50**.** Flow through the breach a) 40 s a) 40 s, b) 160 s, c) 500

The downstream and upstream temporal breach developments in the experiment together with those obtained from the numerical analysis are given in Figure 6.51 and Figure 6.52, respectively. The time t=0 s indicates the initiation of seepage.

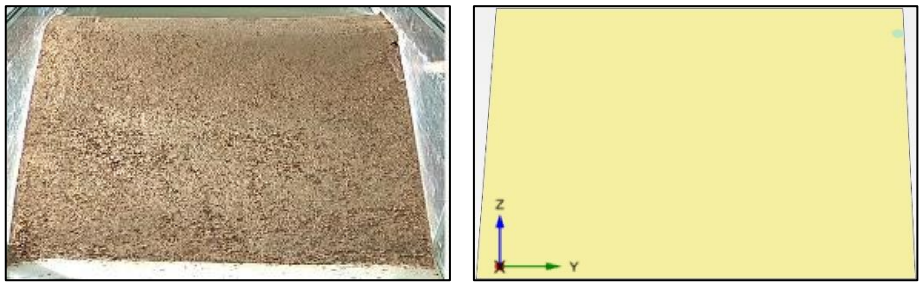

(a)

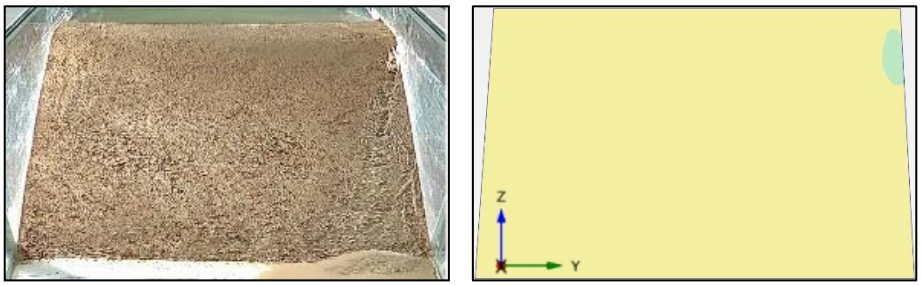

(b)

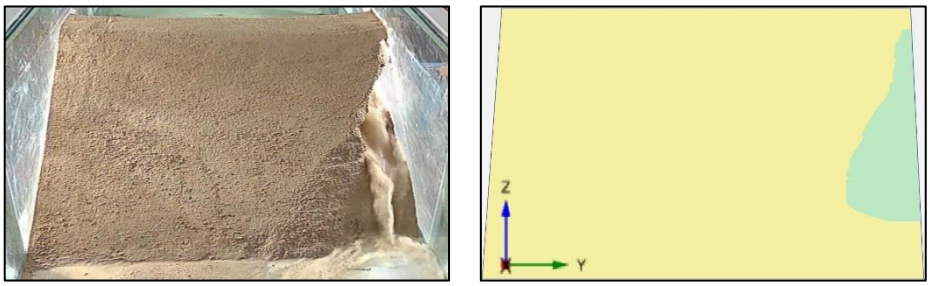

(c)

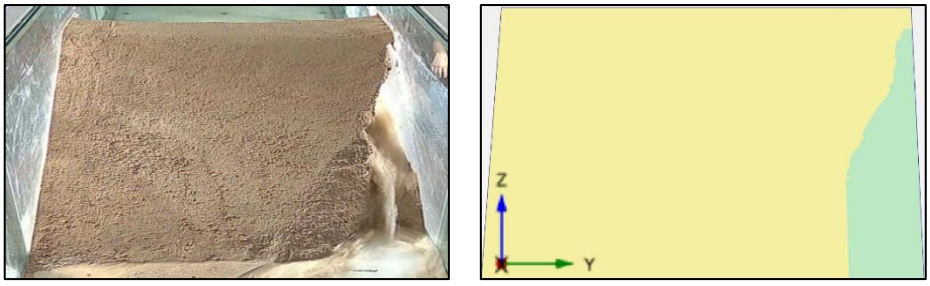

(d)

Figure 6.51. The downstream temporal breach developments a) 0 s, b) 40 s, c) 500 s, d) 640 s

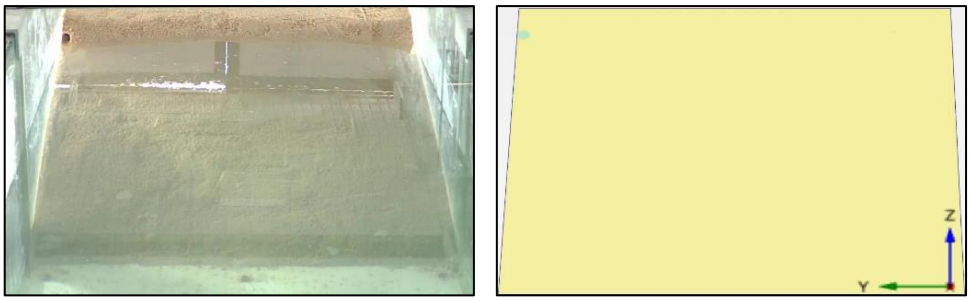

(a)

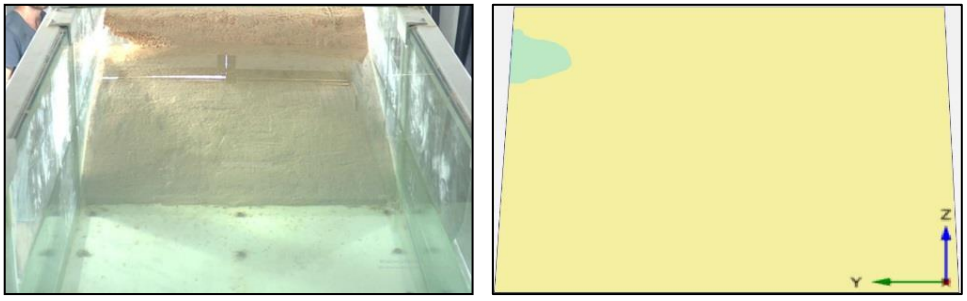

(b)

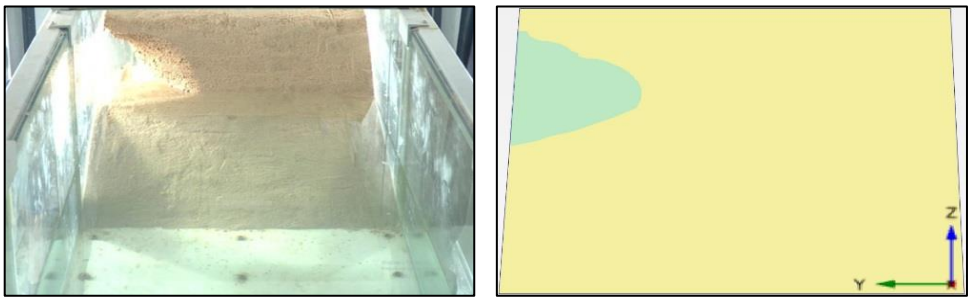

(c)

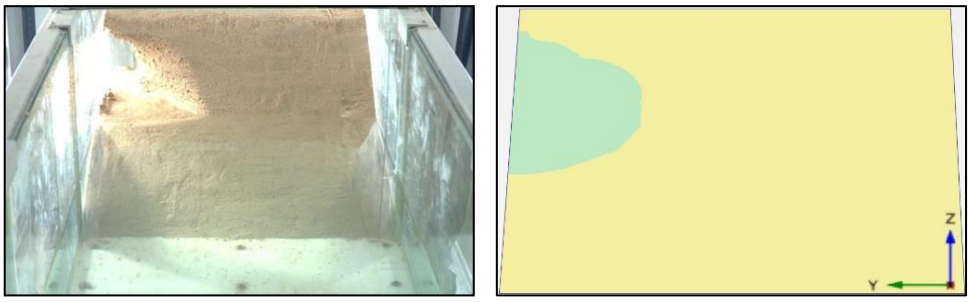

(d)

Figure 6.52**.** The upstream temporal breach developments (a) 0 s (b) 300 (c) 500 s (d) 640 s

The numerical temporal breach developments together with experimental are presented Figure 6.53 and Figure 6.54 for the downstream and the upstream sides, respectively.

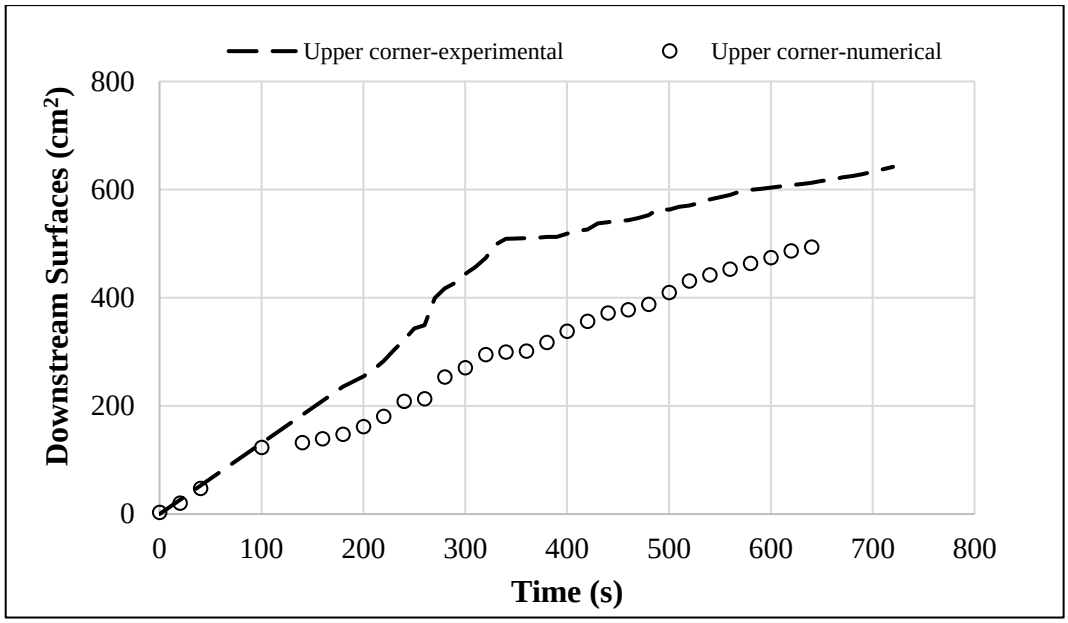

Figure 6.53. The downstream temporal breach developments together with experimental and numerical

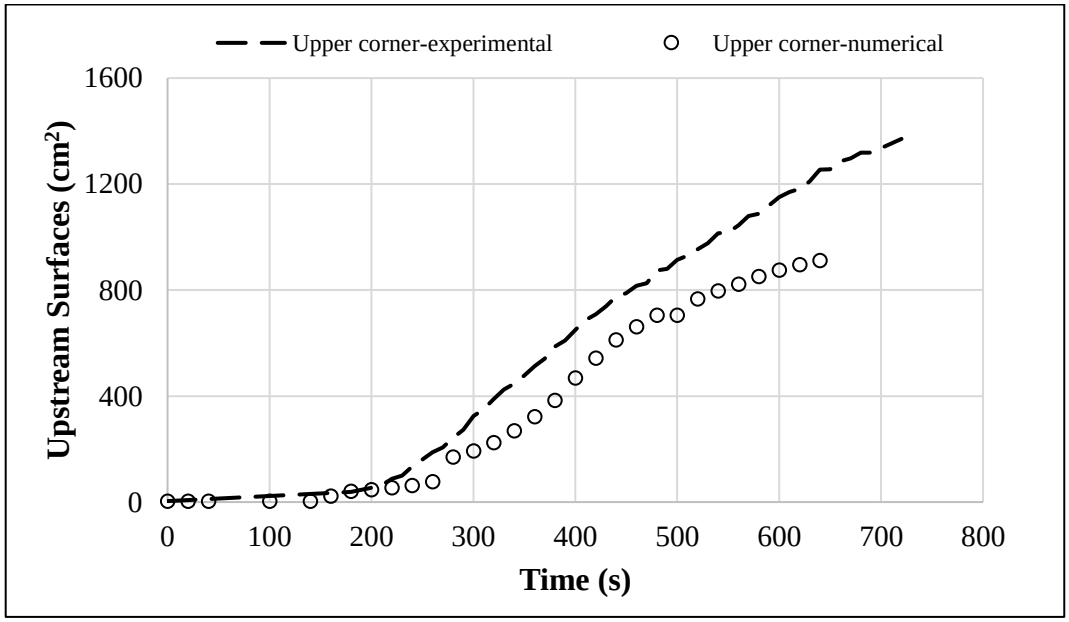

Figure 6.54. The upstream temporal breach developments together with experimental and numerical

The experimental and numerical time-varied average velocities are presented Figure 6.55 and Figure 6.56 for downstream and upstream, respectively.

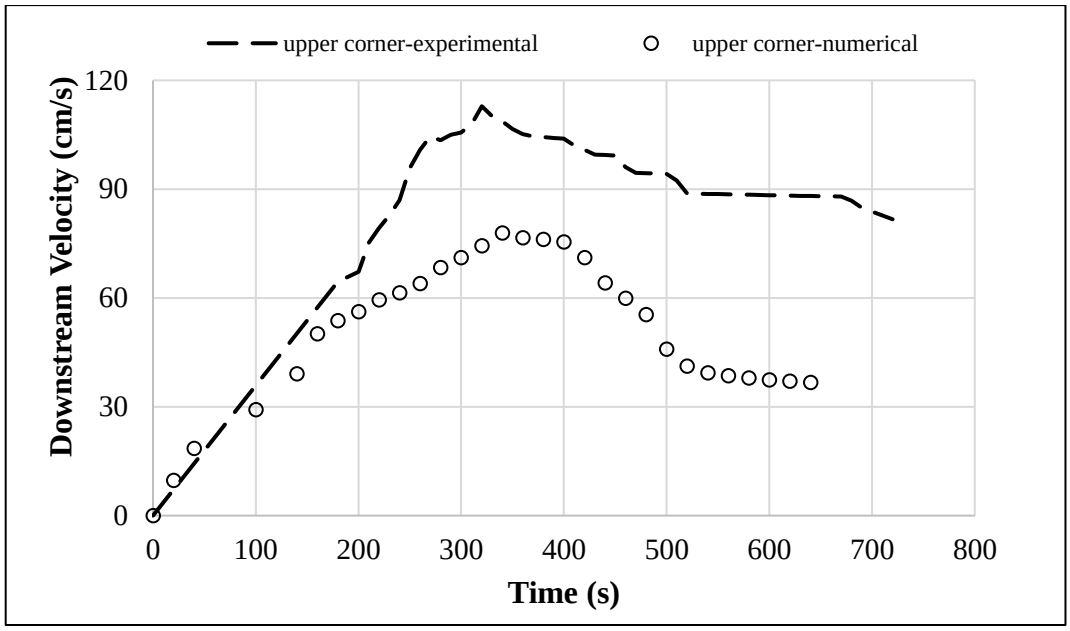

Figure 6.55. The time-varied downstream breach velocities together with experimental and numerical

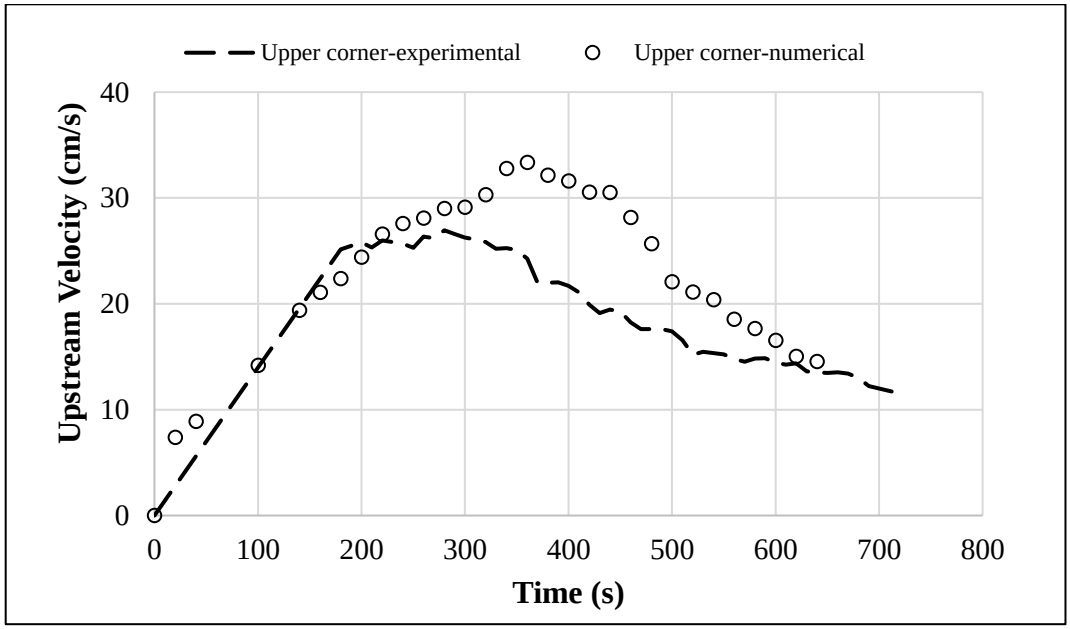

Figure 6.56. The time-varied upstream breach velocities together with experimental and numerical

The temporal variations of the downstream and upstream wetted areas together with experimental and numerical are given Figure 6.57 and Figure 6.58, respectively.

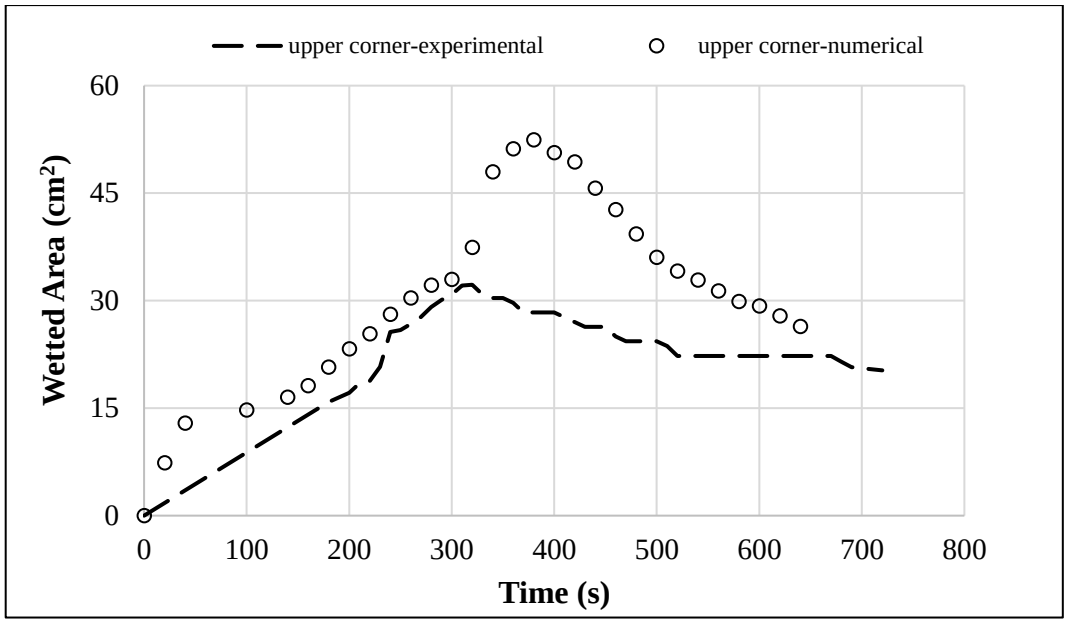

Figure 6.57. The temporal variations of the downstream wetted areas together with experimental and numerical

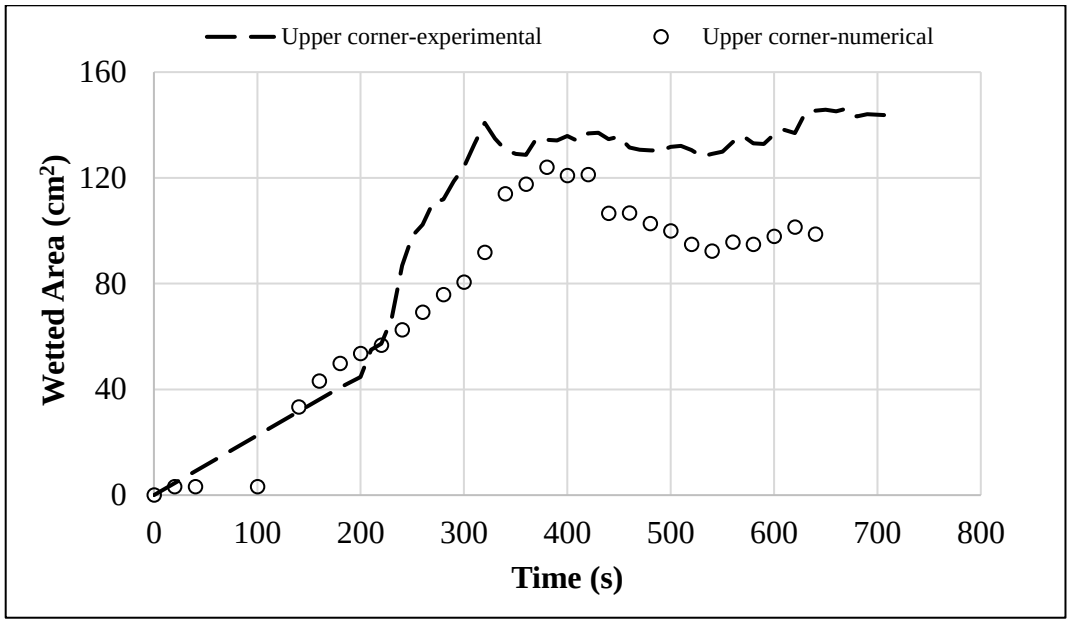

Figure 6.58. The temporal variations of the upstream wetted areas together with experimental and numerical

The average temporal discharge values for both the experimental and numerical are given in Figure 6.59.

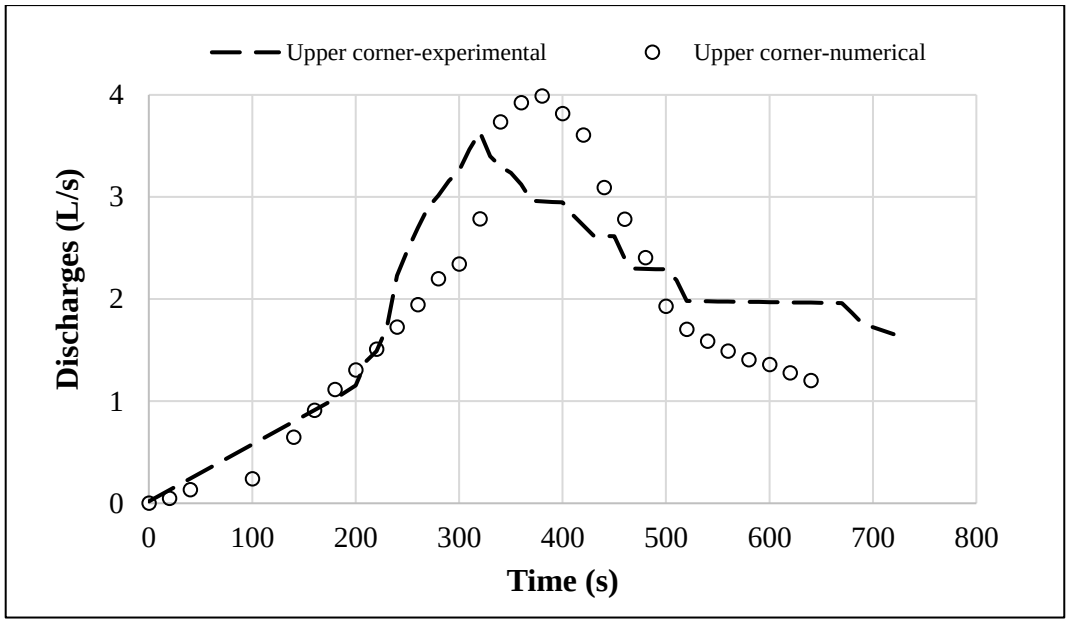

Figure 6.59. The temporal discharges together with experimental and numerical

The calculated RMSE and MAE values for each finding are given in Table 6.5.

Table 6.5. RMSE and MAE values for each finding at the upper-corner part

Findings		Root Mean Square Error (RMSE)	Mean Absolute Error (MAE)
$V_{downstream}$	(cm/s)	27.5	25.2
$V_{upstream}$	(cm/s)	5.2	3.9
$Wetted_{downstream}$	(cm^2)	5.2	4.5
$Wetted_{upstream}$	(cm^2)	31.1	26.3
$Surface_{downstream}$	(cm^2)	136.2	124.2
$Surface_{upstream}$	(cm^2)	198.8	160.6
Discharge	(L/s)	0.5	0.4

For the upper corner scenario RMSE and MAE values of the average value are calculated as 36.9% and 34.1% for $V_{downstream}$, 29.2% and 21.5% for $V_{upstream}$, 24.5% and 21.2% for $Wetted_{downstream}$, %30.0 and 25.4% for $Wetted_{upstream}$, 31.0% and 28.5% for $Surface_{downstream}$, 32.4% and 26.2% for $Surface_{upstream}$, 27.5% and 21.9% for discharge.

6.3. Results and Discussions

The numerical analyses were performed to realize the experimental conditions. In the simulation of the first experiment, the piping process was started at the interaction zone with the rock salt and the dam body, and it was continued to both sides, upstream and downstream, respectively. The breached soil zone headed upstream side in t=4 days and reached the upstream face after 11 days at 27 cm below the water surface. However, the process took about 9 days and 16 cm below the water surfaces in the experiments.

The temporal discharge values were underestimated during the first 30 seconds then, they decreased to the close parallel with the experiments. The time-dependent upstream and downstream wetted areas were continued closely parallel to the experiments, then it was overestimated during the numerical analysis. The time-related velocities were underestimated for the first 50 seconds then they continued to closely parallel the experiments. The downstream and upstream breach developments were underestimated during the numerical analysis. The minimum error was found for the downstream velocity while the maximum error was found for the wetted area upstream.

In the simulation of the fourth experiment, a similar breach formation was observed. The piping was initiated at the interaction zone, and it continued and progressed on both sides.

The temporal discharge values were calculated, and they were underestimated until they reached their peak value of 24.35 cm^3/s at t=50 s then the values were continued closely in accord with the experiments. The changes in upstream breach-wetted areas were underestimated during the analysis. However, the downstream sides continued closely with the experimental findings. The downstream time-varied velocity values were found close to the experiments while the upstream velocities were found to be underestimated. The upstream temporal breach developments were found to be fairly in accord with the experiment, however, the downstream sides were obtained as totally underestimated.

The breach mechanism in the upper simulations were found to be similar for the first t=160 s. In both simulations, the breach appeared on the upstream face at the same interval. Then the peak discharges were occurred. In the upper-middle simulation, the downstream temporal breach developments, downstream breach-wetted areas, and downstream breach velocities are found the lowest errors, while the highest was found in

the temporal breach discharges. In the upper-corner simulation, The minimum error was found in downstream wetted areas, while the maximum error was found to be downstream velocities.

CHAPTER 7

CONCLUSION AND RECOMMENDATIONS

In the scope of this thesis, homogenous earth-fill dams 0.6 m high having a bottom width of 2 m and side slopes 1 vertical to 1.5 horizontal were constructed in a rectangular flume 1 m wide, 6.14 m long, and 0.81 m high, in the laboratory of the Izmir University of Economics. Experimental and numerical investigation related to piping and resulting breaches in the homogenous earth-fill dams were realized with different experiments. A mixture consisting of 85 % sand and 15 % clay was used in the construction of the dams. The piping was generated by locating weak layers at different locations of the dams. Three experiments were performed by placing a weak layer of cross-section 5x5 cm^2 at the bottom of the dam along the centerline. One scenario was performed by locating a weak layer of 2x2 cm^2, 28 cm above the dam bottom. To facilitate the piping, each weak layer consisted of rock salt.

The breaches started at the weak zone and progressed and continued backward, as expected. The backward erosion within the first dam body was slower compared to other experiments. The weak zones were located at the dam bottom during the first three experiments while the fourth experiment was performed by placing the weak zone 28 cm above the dam bottom.

The first two dams were constructed with a mixture of bulk density of 2 g/cm^3.

The first dam height was 60 cm, and the water level in the channel was 55.5 cm. The experiment took about 9 days for the breach to reach the upstream face, approximately 16 cm below the water surface. In the first scenario, since the breach appeared under the water, the upstream surface area increased equally with the wetted area until the water level decreased. For these reasons, the obtained wetted areas in the first experiment for the first t=20 s were found to be the greatest relative to the other scenarios.

The second dam height was 65 cm, and the water level in the channel was 61 cm. The experiment took about 8 hours for the breach to reach the upstream face. The

experiment took about 8 hours for the breach to reach the upstream face at water surface, and the complete failure of the dam was observed.

The third dam was constructed with a mixture of bulk density of 1.7 g/cm^3. The dam height was 65 cm, and the water level in the channel was 61 cm. The soil erosion was initiated at different locations of the downstream face. The experiment lasted approximately 42 minutes and collapsed the dam crest, and the complete failure of the dam was observed.

For the second and third scenarios, the first 37 seconds were compared. The upstream breach area was eroded greater than in the second scenario. In conclusion, as the compaction density decreases, the upstream breach erodes more rapidly.

The fourth dam height was 65 cm and the water level in the channel was 61 cm. The experiment lasted approximately 2 minutes, being the experiment of the shorter duration.

The simulations were performed by commercial software, PLAXIS 3D. The use of the software by incorporating the python algorithm and the Jupyter console provided the satisfactory compatibility between experimental findings and the numerical results. The RMSE and MAE error parameters justified the accord between experimental findings and numerical results.

The backward erosion piping was observed in numerical analysis as well as experimental studies.

In the simulation of the first and fourth experiments, the piping initiated the interaction between the weak zone and the dam body.

The numerical analyses were performed by using constant soil parameters such as unit weights, void ratio, internal friction angle, oedometric modulus, permeability.

It is known that geotechnical parameters are affected by soil erosion resulting from the piping. More realistic results can be obtained by performing numerical analyses with time-dependent properties of geotechnical parameters.

.

REFERENCES

Shaikh, A., James, F. R., and Steven, R. 1988. “Erosion Rate of Compacted NA-Montmorillonite Soils.” *Journal of Geotechnical Engineering*, 114(3), 296–305. https://doi.org/10.1061/(asce)0733-9410(1988)114:3(296).

Al-Janabi, A. M. S., Ghazali, A. H., Ghazaw, Y. M., Afan, H. A., Al-Ansari, N., and Yaseen, Z. M. 2020. “Experimental and Numerical Analysis for Earth-Fill Dam Seepage.” *Sustainability*, *12*(6), 2490. https://doi.org/10.3390/su12062490.

Al-Mansori, N. J. H., Al-Fatlawi, T. A. F. J. M., Othman, N. Y., and Al-Zubaidi, L. S. A. 2020. “Numerical Analysis of Seepage in Earth-Fill Dams.” *Civil Engineering Journal*, *6*(7), 1336–1348. https://doi.org/10.28991/cej-2020-03091552.

Arulanandan, K., and Perry, E. B. 1983. “Erosion in Relation to Filter Design Criteria in Earth Dams.” *Journal of Geotechnical Engineering*, *109*(5), 682–698. https://doi.org/10.1061/(asce)0733-9410(1983)109:5(682).

ASLAN, T. A., and TEMEL, B. 2022. “Finite element analysis of the seepage problem in the dam body and foundation based on the Galerkin’s approach.” *European Mechanical Science*, *6*(2), 143–151. https://doi.org/10.26701/ems.1024266.

Athani, S. S., Shivamanth, Solanki, C., and Dodagoudar, G. 2015. “Seepage and Stability Analyses of Earth Dam Using Finite Element Method.” *Aquatic Procedia*, *4*, 876–883. https://doi.org/10.1016/j.aqpro.2015.02.110.

Borragan, V. 2014. “Modelling Internal Erosion Within An Embankment Dam Prior To Breaching”. [Master’s Dissertation].

Ojha, C. S. P., Singh, V. P., and Adrian, D. D. 2003. “Determination of Critical Head in Soil Piping.” *Journal of Hydraulic Engineering*, *129*(7), 511–518. https://doi.org/10.1061/(asce)0733-9429(2003)129:7(511).

Chen, S. S., Zhong, Q. M., & Shen, G. Z. 2019. “Numerical modeling of earthen dam breach due to piping failure.” *Water Science and Engineering*, *12*(3), 169–178. https://doi.org/10.1016/j.wse.2019.08.001.

Costa, J. 1985. “Floods from dam failures.” *Open-File Report*. https://doi.org/10.3133/ofr85560.

Error when generating 3D mesh - GeoStudio | PLAXIS Wiki - GeoStudio | PLAXIS - Bentley Communities. (2019, December 18). https://communities.bentley.com/products/geotech-analysis/w/wiki/45545/error-when-generating-3d-mesh.

Fisher, W. D., Camp, T. K., and Krzhizhanovskaya, V. V. 2017. “Anomaly detection in earth dam and levee passive seismic data using support vector machines and automatic feature selection.” *Journal of Computational Science*, *20*, 143–153. https://doi.org/10.1016/j.jocs.2016.11.016.

Foster, M. and Fell, R. 1999. “A framework for estimating the probability of failure of embankment dams by internal erosion and piping using event tree methods.” *UNICIV Report No. R-377*, University of New South Wales, Australia.

Foster, M., Fell, R., and Spannagle, M. 2000a. “The statistics of embankment dam failures and accidents.” *Canadian Geotechnical Journal*, *37*(5), 1000–1024. https://doi.org/10.1139/t00-030.

Foster, M., Fell, R., & Spannagle, M. 2000b. A method for assessing the relative likelihood of failure of embankment dams by piping. *Canadian Geotechnical Journal*, *37*(5), 1025–1061. https://doi.org/10.1139/t00-029.

Gattinoni, P., and Francani, V. 2009. “A Tool for Modeling Slope Instability Triggered by Piping.” *World Academy of Science, Engineering and Technology, International Journal of Geological and Environmental Engineering*, *3*(8), 238–244. https://publications.waset.org/3999/pdf.

Ghonim, M. T., Mowafy, M. H., Salem, M. N., and Jatwary, A. 2022. “Investigating the peak outflow through a spatial embankment dam breach.” *Ain Shams Engineering Journal*, 13(6), 101799. https://doi.org/10.1016/j.asej.2022.101799.

Guney, M. S., Dumlu, E., Okan, M., Bor, A., Aklık, P., and Tayfur, G. 2022a. “Experimental Study of the Evolution of the Breach and the Temporal breach discharges Resulting from Piping due to Seepage at the Earth-Fill Dam Bottom.” *Proceedings of the 7th International Conference on Civil, Structural and Transportation Engineering (ICCSTE’22)*. https://doi.org/10.11159/iccste22.215.

Guney, M. S., Dumlu, E., Okan, M., Bor, A., Aklık, P., and Tayfur, G. 2022b. “Experimental Study of the Evolution of the Breach and the Temporal breach discharges Resulting from Piping due to Seepage at the Earth-Fill Dam Top.” *Proceedings of the 39th IAHR World Congress (Granada, 2022)*. https://doi.org/10.3850/IAHR-39WC2521711920221298.

Guney, M. S., Dumlu, E., Okan M., Tayfur, G. 2022c. “Experimental Study of Breach Evolution and Discharge through Breach Resulting from Piping due to Seepage at the Upper Corner of in an Earth-fill Dam.” *Proceedings of 14th International Conference on Hydroscience and Engineering*.

Hanson, G., Ronald R. T., Sherry H., and Darrel T. 2010. “Internal Erosion and Impact of Erosion Resistance.” I*n Proceedings of the 30th U.S. Society on Dams Annual Meeting and Conference.* April 12-16, 2010, 773–84. Sacramento, California.

Hinderlider, M. C. 1914. “Failure of Horse Creek Earth Dam.” *Engineering News Record,* vol. 71, No. 16, April 16, 828-830.

ICOLD. 2017. “Internal Erosion of Existing Dams, Levees and Dikes, and Their Foundations.”

Ke, L., and Takahashi, A. 2012. “Strength reduction of cohesionless soil due to internal erosion induced by one-dimensional upward seepage flow.” *Soils and Foundations*, 52(4), 698–711. https://doi.org/10.1016/j.sandf.2012.07.010.

Kermani, E., and Barani, G. 2012. “Seepage Analysis through Earth Dam Based on Finite Difference Method.” *J. Basic Appl. Sci. Res*., 2, 11621–11625.

Khilar, K.C., Fogler, H.S., and Gray, D.H. 1985. “Model for Piping-Plugging in Earthen Structures.” *Journal of Geotechnical Engineering*, 111, 833-846.

Lachouette, D., Golay, F., and Bonelli, S. 2008. “One-dimensional modeling of piping flow erosion.” *Comptes Rendus - Mecanique*, 336(9), 731–736. https://doi.org/10.1016/j.crme.2008.06.007.

Li, D. Y., Zheng, D. F., Wu, H., Shen, Y. Q., and Nian, T. K. 2021. “Numerical Simulation on the Longitudinal Breach Process of Landslide Dams Using an Improved Coupled DEM-CFD Method.” *Frontiers in Earth Science*, *9*. https://doi.org/10.3389/feart.2021.673249.

Meister, A. L. F. 1769. "Generalia de genesi figurarum planarum et inde pendentibus earum affectionibus.", *Nov. Com. Gött. (in Latin)*, 1: 144.

Elkholy, M., Sharif, Y. A., Chaudhry, M. H., and Imran, J. 2015. “Effect of soil composition on piping erosion of earthen levees.” *Journal of Hydraulic Research*, *53*(4), 478–487. https://doi.org/10.1080/00221686.2015.1026951.

Greco M., Pontillo M., Iervolino M., and Leopardi A. 2008. “2DH numerical simulation of breach evolution in an earth dam.” *River-flow2008*, vol. 1, pp. 661–667.

Morris, M., Hassan, M., Kortenhaus, A., Geisenhainer, P., Visser, P., and Zhu, Y. 2008. "Modelling breach initiation and growth." *Flood Risk Management: Research and Practice*, 581–591. https://doi.org/10.1201/9780203883020.ch67.

No Finger in the Dike Could Have Stopped It!. 2018. *Newspapers.com.* https://www.newspapers.com/clip/23922672/no-finger-in-the-dike-could-have/

Okan, M. 2022. "Experimental and Numerical Investigation of Piping in Uniform Embankment Dam with Weak Layer at the Upper Region [Master Thesis]." *Izmir Institute of Technology*.

Okeke, A. C., Wang, F., Sonoyama, T., and Mitani, Y. 2012. "Laboratory Experiments on Landslide Dam Failure Due to Piping: An Evaluation of 2011 Typhoon-Induced Landslide and Landslide Dam in Western Japan." *Environmental Science and Engineering*, 525–545. https://doi.org/10.1007/978-3-642-29107-4_30.

Perrow, C. 1984. "Normal Accidents." *New York: Basic Books*. ISBN 0-465-05144-8, pp.233–238.

PLAXIS. 2022. "PLAXIS material models manual 2022." *Tech. rep*., Delft, Netherlands, http://www.plaxis.nl/shop/135/info/manuals/.

Reisner, M. 1993. "Cadillac Desert." pp. 407. ISBN 978-0-14-017824-1.

Richards, K., and Reddy, K. 2012. "Experimental investigation of initiation of backward erosion piping in soils." *Géotechnique*, 62(10), 933–942. https://doi.org/10.1680/geot.11.p.058.

Saliba, F., Nassar, R. B., Khoury, N., and Maalouf, Y. 2019. "Internal Erosion and Piping Evolution in Earth Dams Using an Iterative Approach." *Geo-Congress 2019*. https://doi.org/10.1061/9780784482155.007.

Sazzad, M. M., Roy, and Rahman, M. M. 2015. “FEM based seepage analysis through earth dam.” *International Journal of Advances in Structural and Geotechnical Engineering*, 4(3), 158-164.

Sharif, Y. A. 2013. “Experimental Study On Piping Failure of Earthen Levee and Dams.” [Doctoral dissertation]. *The University of South Carolina*. Retrieved from https://scholarcommons.sc.edu/etd/2558.

Sharif, Y. A., Elkholy, M., Hanif Chaudhry, M., and Imran, J. 2015a. “Experimental Study on the Piping Erosion Process in Earthen Embankments.” *Journal of Hydraulic Engineering*, *141*(7). https://doi.org/10.1061/(asce)hy.1943-7900.0001019.

Sharif, Y. A., Elkholy, M., Hanif Chaudhry, M., and Imran, J. 2015b. “Experimental Study on the Piping Erosion Process in Earthen Embankments.” *Journal of Hydraulic Engineering*, 141(7). https://doi.org/10.1061/(asce)hy.1943-7900.0001019.

Shin, S., Park, S., and Kim, J. H. 2019. “Time-lapse electrical resistivity tomography characterization for piping detection in earthen dam model of a sandbox.” *Journal of Applied Geophysics*, 170, 103834. https://doi.org/10.1016/j.jappgeo.2019.103834.

Sills, G. L., Vroman, N. D., Wahl, R. E., and Schwanz, N. T. 2008. “Overview of New Orleans levee failures: Lessons learned and their impact on national levee design and assessment.” *J. Geotech. Geoenviron. Eng*., 134(5), 556–565.

Bonelli, S. 2013. “Erosion in geomechanics applied to dams and levees.” *ISTE, Wiley EBooks*.

Tao, H., Tao, J. 2017. “Quantitative analysis of piping erosion micro-mechanisms with coupled CFD and DEM method.” *Acta Geotech*. 12, 573–592. https://doi.org/10.1007/s11440-016-0516-y

Temple, D.M., Hanson, G.J., Neilsen, M.L., and Cook, K.R. 2005. “Simplified Breach Analysis Model for Homogeneous Embankments: Part I, Background and Model Components.” *In Proceedings of the 2005 U.S. Society on Dams Annual Meeting and Conference*, Salt Lake City, Utah, 151–61.

Van Beek, V. M., Van Essen, H. M., Vandenboer, K., & Bezuijen, A. 2015. “Developments in modelling of backward erosion piping.” *Géotechnique*, *65*(9), 740–754. https://doi.org/10.1680/geot.14.p.119.

Vandenboer, K., van Beek, V. M., and Bezuijen, A. 2014. “3D finite element method (FEM) simulation of groundwater flow during backward erosion piping.” *Frontiers of Structural and Civil Engineering*, 8(2), 160–166. https://doi.org/10.1007/s11709-014-0257-7.

Xu, T., and Zhang, L. 2013. “Simulation of Piping in Earth Dams Due to Concentrated Leak Erosion.” *Geo-Congress 2013*. https://doi.org/10.1061/9780784412787.110.

Zhenzhen, L. 2015. “Hydro-Mechanical Analysis of Breach Processes Due to Levee Failure.” [Master’s Dissertation]. *Université D’aix-Marseille École*.

Zhong, Q. M., Chen, S. S., Mei, S. A., and Cao, W. 2017. “Numerical simulation of landslide dam breaching due to overtopping.” *Landslides*, *15*(6), 1183–1192. https://doi.org/10.1007/s10346-017-0935-3.